Strong decay widths and mass spectra of the 1*D*, 2*P* and 2*S* singly bottom baryons

H. García-Tecocoatzi
INFN, Sezione di Genova, Via Dodecaneso 33, 16146 Genova, Italy

A. Giachino
Departamento de Física Teórica and IFIC, Centro Mixto Universidad de Valencia-CSIC, Institutos de Investigación de Paterna, 46071 Valencia, Spain

A. Ramirez-Morales
Tecnologico de Monterrey, Escuela de Ingenieria y Ciencias, General Ramon Corona 2514, Zapopan 45138, Mexico

Ailier Rivero-Acosta
Departamento de Física, DCI, Campus León, Universidad de Guanajuato, Loma del Bosque 103, Lomas del Campestre, C.P. 37150, León, Guanajuato, México; Dipartimento di Fisica, Università di Genova, Via Dodecaneso 33, 16146 Genova, Italy; and INFN, Sezione di Genova, Via Dodecaneso 33, 16146 Genova, Italy

E. Santopinto*
INFN, Sezione di Genova, Via Dodecaneso 33, 16146 Genova, Italy

Carlos Alberto Vaquera-Araujo
Consejo Nacional de Humanidades, Ciencias y Tecnologías, Avenida Insurgentes Sur 1582. Colonia Crédito Constructor, Del. Benito Juárez, C.P. 03940, Ciudad de México, México; Departamento de Física, DCI, Campus León, Universidad de Guanajuato, Loma del Bosque 103, Lomas del Campestre C.P. 37150, León, Guanajuato, México; and Dual CP Institute of High Energy Physics, C.P. 28045, Colima, México

(Received 6 July 2023; accepted 19 August 2024; published 2 December 2024)

We calculate the 1*D*, 2*P*, and 2*S* mass spectra of the singly bottom baryons and their strong decay widths. The calculations are performed within a harmonic oscillator quark model that incorporates the spin, spin-orbit, isospin, and flavor interactions. To obtain the model parameters, we conducted a fit using only 13 of the 22 experimentally observed states. Our predictions align well with the observed states, showing a root-mean-square deviation of 9.6 MeV. We calculate the three-quark strong decay widths within the $^3P_0$ model, which has only one free parameter, the pair creation strength γ_0; this is the first time that the $\Lambda_b\eta$, $\Sigma_b\rho$, $\Sigma_b^*\rho$, $\Lambda_b\eta'$, $\Lambda_b\omega$, Ξ_bK, $\Xi_b'K$, Ξ_b^*K, Ξ_bK^*, $\Xi_b'K^*$, and $\Xi_b^*K^*$ channels have been considered in the calculation of the strong decay widths of the excited Λ_b states; the $\Sigma_b\eta$, Ξ_bK, $\Sigma_b\rho$, $\Sigma_b^*\rho$, $\Lambda_b\rho$, $\Sigma_b^*\eta$, $\Sigma_b\eta'$, $\Sigma_b^*\eta'$, $\Xi_b'K$,Ξ_b^*K, Ξ_bK^*, $\Xi_b'K^*$, $\Xi_b^*K^*$, $\Sigma_b\omega$, $\Sigma_b^*\omega$, Σ_8B_s, ΔB, $N(1520)B$, $N(1535)B$, $N(1680)B$, and $N(1720)B$ channels in the calculation of the strong decay widths of the excited Σ_b states; the Λ_bK^*, $\Xi_b\rho$, $\Xi_b'\rho$, $\Xi_b^*\rho$, Σ_bK^*, $\Sigma_b^*K^*$, $\Xi_b\eta'$, $\Xi_b'\eta'$, $\Xi_b^*\eta'$, $\Xi_b\omega$, $\Xi_b'\omega$, $\Xi_b^*\omega$, $\Xi_b\phi$, $\Xi_b'\phi$, $\Xi_b^*\phi$, Ξ_8B_s, Σ_8B^*, and $\Sigma_{10}B$ channels in the calculation of the strong decay widths of the excited Ξ_b and Ξ_b' states; the Ξ_bK^*, $\Xi_b'K^*$, $\Xi_b^*K^*$, $\Omega_b\eta$, $\Omega_b^*\eta$, $\Omega_b\phi$, $\Omega_b^*\phi$, $\Omega_b\eta'$, $\Omega_b^*\eta'$, Ξ_8B, and $\Xi_{10}B$ channels in the calculation of the strong decay widths of the Ω_b states. Moreover, in Appendix D, we give the flavor couplings that can be useful for other articles. In Appendix E, our partial decay widths are reported for each open flavor channel; these may be useful to the LHCb, ATLAS, and CMS experimentalists in order to plan in which particular channels to look for missing bottom baryons. The experimental masses and widths of the discovered $\Lambda_b(6146)^0$ and $\Lambda_b(6152)^0$ states

*Contact author: elena.santopinto@ge.infn.it

are consistent with our mass and width predictions for the D_λ excitations with quantum numbers $\mathbf{J}^P = \frac{3}{2}^+$ and $\mathbf{J}^P = \frac{5}{2}^+$, respectively. Moreover, the masses and widths of the new $\Xi_b(6327)^0$ and $\Xi_b(6333)^0$ states agree with our calculations for the D_λ excitations with quantum numbers $\mathbf{J}^P = \frac{3}{2}^+$ and $\mathbf{J}^P = \frac{5}{2}^+$, respectively. Finally, we calculate the electromagnetic decay widths from P-wave states to ground states. We give the exact analytical expressions of the spin-flip and orbit-flip transition amplitudes, both of which are functions of the photon-transferred momentum. The electromagnetic decays are dominant when the strong decays are suppressed. A relevant case is the Ω_b^- missing spin excitation, with $\mathbf{J}^P = \frac{3}{2}^+$, which cannot decay strongly, but has a nonvanishing predicted electromagnetic decay width in the $\Omega_b^-\gamma$ channel. Therefore, we suggest the $\Omega_b^-\gamma$ electromagnetic decay channel as a golden channel in which to search for this state. In all of our calculations, we report the uncertainties related to the experimental and model errors by means of the Monte Carlo bootstrap method.

DOI: 10.1103/PhysRevD.110.114005

I. INTRODUCTION

To date, only a few singly bottom baryons have been discovered, even though if further discoveries are expected in the coming years. Currently, the Particle Data Group [1] lists 21 singly bottom baryons (25 if one considers the different charge states). None of their quantum numbers have been measured yet, so the isospin I, parity P, and angular momentum J reported by the PDG are based on quark model expectations. Most importantly, since we do not know the quantum numbers of those states, it is not yet possible to distinguish between three-quark and quark-diquark structures.

As there are many missing states, this sector is interesting. Therefore, the main aim of this study was to give predictions for the $1D$, $2P$, and $2S$ singly bottom baryons that are still waiting to be discovered, and in particular, to provide their partial strong decay widths by considering new decay channels (as will be explained later).

In 1981, the production of the Λ_b^0 baryon was first observed by the CERN-ISR experiment (R415) [2] (with a 6σ statistical significance). In 1991, this result was confirmed by the experiment R422 [3] and the UA1 Collaboration [4], which observed this state with a statistical significance of about 4σ and 5σ, respectively. In 2007, a bottom baryon with quark content dsb, namely a Ξ_b^-, was observed by the D0 [5] and CDF [6] Collaborations with 5.5σ and 7.7σ statistical significance, respectively. In the same year, the $\Sigma_b^\pm$ and $\Sigma_b^{*\pm}$ were discovered by the CDF Collaboration [7] (with a statistical significance greater than 5.2σ) and confirmed in [8]. In 2008, the D0 Collaboration [9] discovered the ground state Ω_b^- (ssb) (5.4σ), which was confirmed by CDF [10]. In 2011, the CDF Collaboration [11] observed the Ξ_b^0 ground state baryon (usb) (6.8σ). In 2012, CMS [12] discovered an excited state, most likely corresponding to the $J^P = 3/2^+$ partner of Ξ_b, denoted as Ξ_b^*, with a statistical significance exceeding 5σ. In the same year, two narrow P-wave Λ_b^0 baryons, denoted as $\Lambda_b(5912)^0$ and $\Lambda_b(5920)^0$, were discovered by the LHCb Collaboration [13], with 5.2σ and 10.2σ, respectively, and confirmed by the CDF Collaboration [14] one year later. In 2015, the $\Xi_b^{\prime-}$ was discovered and the Ξ_b^{*-} was confirmed by the LHCb Collaboration [15] with a statistical significance greater than 10σ. In 2018 the LHCb Collaboration reported the discovery of one excited Ξ_b state, $\Xi_b(6227)^-$ [16] (7.9σ), and two excited Σ_b states, $\Sigma_b(6097)^\pm$ [17] (12.6σ). In 2020, two D-wave Λ_b^0 candidates, $\Lambda_b(6146)^0$ and $\Lambda_b(6152)^0$, were discovered by LHCb in the $\Lambda_b^0\pi^+\pi^-$ spectrum [18]; both states were discovered with statistical significance exceeding six standard deviations. In the same year, the LHCb collaboration [19] reported the observation of four narrow peaks in the $\Xi_b^0 K^-$ invariant mass spectrum, $\Omega_b(6316)$, $\Omega_b(6330)$, $\Omega_b(6340)$, and $\Omega_b(6350)$, with 2.1σ, 2.6σ, 6.7σ, and 6.2σ statistical significance, respectively, and the CMS collaboration [20] reported evidence of a broad excess of events in the $\Lambda_b^0\pi^+\pi^-$ channel in the region of 6040–6100 MeV with 4σ; this was confirmed by LHCb [21] exceeding 7σ in the same decay channel and was called $\Lambda_b(6070)$. In 2021 the CMS collaboration discovered the $\Xi_b(6100)^-$ in the $\Xi_b^-\pi^+\pi^-$ invariant mass spectrum [22]. More recently, in 2021, the LHCb collaboration reported the discovery of two new Ξ_b states, namely $\Xi_b(6327)^0$ and $\Xi_b(6333)^0$, in the $\Lambda_b^0 K^-\pi^+$ channel, with a statistical significance larger than nine standard deviations [23]. In 2023, the LHCb [24] discovered the $\Xi_b(6087)^0$ and $\Xi_b(6095)^0$ states, which are not yet on the PDG. As will be discussed in Sec. V, $\Xi_b(6087)$ [24], will be associated by us with the $1P$ $1/2^-$ state, while $\Xi_b(6095)^0$ will be considered by us to be the neutral partner of $\Xi_b(6100)^-$ reported by the PDG; thus, according to our assignments, there are in total 22 discovered states.

The first theoretical predictions of the Λ_b and Σ_b baryon mass spectra within the quark model were published by Capstick and Isgur in their pioneering work in 1986 [25,26], using a three-quark string-like confinement plus an OGE-inspired potential. The first QCD spectral sum rule calculation for Σ_b and Λ_b baryons was performed by Bagan *et al.* [27] in 1992. Later in 1995, Roncaglia *et al.* used the Feynman-Hellmann theorem to estimate the ground state singly bottom baryon masses [28]. In 1996, Silvestre-Brac published the mass spectra for Λ_b, Σ_b, Ξ_b, Ξ_b', and Ω_b [29]

using a nonrelativistic model. The Λ_b, Σ_b, Ξ_b, Ξ_b', and Ω_b ground and excited states (up to 1 GeV excitation energy) were displayed in the figures with a large energy scale, but only the numerical values for the ground state were provided in a table, making it difficult to extract from the figures the precise numerical values for the excited state masses. In 1996, Bowler *et al.*, in the first exploratory lattice study [30], estimated the ground state singly bottom baryon masses by extrapolating the lattice data, first in the light quark masses and then in the heavy quark mass. Jenkins studied the ground state bottom baryon masses by using a combined expansion in $1/m_Q$, $1/N_c$ and $SU(3)$ flavor symmetry breaking of the heavy hadron masses in the heavy quark effective theory [31]. In the 2000s, Mathur *et al.* calculated the ground state singly bottom baryon masses by using quenched lattice nonrelativistic QCD [32]. In 2004, Albertus *et al.* used a variational method for the solution of the non-relativistic three-body problem for the ground state of the singly heavy baryons, considering the one-gluon exchange plus the pion and the σ meson exchange potential [33]. Later, in Refs. [34–36], this model was extended to include some exchange of K and η mesons, and was applied to the study of excited singly heavy baryon states. Ebert *et al.* developed a relativistic quark-diquark description [37,38]. Some examples of the recent wide literature on theoretical investigations of heavy baryon spectroscopy are: the non-relativistic quark model (NRQM) [39–41], the Regge phenomenology [42], the hypercentral constituent quark model [43–46], which has been used to study the excited Ω_b states [47], the QCD sum rules (QCDSR) [48–52], and the symmetry-preserving Schwinger-Dyson equation approach [53]. Further discussions involving other models can be found in Refs. [54–59]. For more references, see the review articles [60–65].

None of the previous three-quark theoretical articles calculated the possible states up to all the 1D, 2P, and 2S, but only a subset of them (as will be more evident in Tables VII–XI in which our three-quark model results are compared with those of the other three-quark models). We also observe that none of the previous theoretical articles discussed the constructions of the states up to the 1D, 2P, and 2S.

In addition to the mass spectrum, the decay properties are one of the main features in assigning consistent quantum numbers to hadrons. Matching experimental data with the predicted mass spectra and decay widths is a reliable method for identifying these states.

Only a few studies have addressed the strong decays of singly bottom baryons [66–82] and most have used the constituent quark model [66–78].

All the constituent quark model calculations of singly bottom baryon strong decays [66–78] use harmonic oscillator wave functions. This choice is not only because, otherwise, the calculations would be too difficult but also because, as observed by Kokoski and Isgur in 1985 [83], the excited hadrons are well described by harmonic oscillator wave functions. For these reasons, the use of harmonic oscillator wave functions is now a standard in hadron decay calculations. In 2010, the authors of Ref. [66] calculated the decay widths of the Ξ_b ground and P-wave excited states by using the masses from Karliner [40] and PDG, within the $^3P_0$ strong decay model with h.o. wave functions. In Refs. [67,68,70,77] the authors calculated the strong decay by using the nonrelativistic quark pseudoscalar meson coupling, also known as chiral strong decay model (χQM) or elementary emission model (EEM). In Refs. [67,68,70,77] the authors used the masses from the relativistic quark-diquark model by Ebert *et al.* [38], and they used three-quark baryon harmonic oscillator wave functions. Specifically, the authors of Refs. [67,68] studied the strong decays of the S- P- and D-wave singly heavy baryons with emission of π and K meson only. In Ref. [69], the two previous studies were extended to the P_ρ-mode excitations by using the masses from the three-quark model by Yoshida *et al.* [41]. In 2020, following the discovery of $\Sigma_b(6097)$ by LHCb [17], the strong decay widths of the P-wave Σ_b states were calculated in Ref. [70] within χQM, but the authors considered the pion emission only. In Refs. [71–76] the authors calculated the strong decay widths by using the Ebert *et al.* quark-diquark masses [38] within the $^3P_0$ model for the strong decays and the h.o. wave functions.

In particular, in Ref. [71] the authors calculated the P-wave Ω_b strong decay widths only. Later on, the same authors used the $^3P_0$ model to study the $\Lambda_b(6072)^0$ baryon decays [72]. In a subsequent study, [73], this analysis was further extended to the $\Xi_b^{(\prime)}$ strong decays up to the D-wave, but only the emission of pions or K mesons was considered. In Refs. [75,76], the authors calculated the $\Xi_b(6227)$ and $\Sigma_b(6097)$ decays with pion emission only. References [71–76] examined the λ-mode excitations only.

The $\Sigma_b^{(*)} \to \Lambda_b\pi$ strong decay widths were also calculated in Ref. [79] within the MIT model. The study of $\Sigma_b \to \Lambda_b\pi$ and $\Sigma_b \to \Lambda_b\pi$ decays also has been conducted using the partial conservation of the axial current in Ref. [80]. The P-wave Ω_b states were studied using light-cone sum rules within HQET in Ref. [81]. The strong decay widths of the Σ_b, Σ_b^*, Ξ_b', and Ξ_b^* ground states were studied within chiral effective theory in Ref. [82].

However, all these studies [66–82] did not include the decays into the bottom baryon-vector meson channels or the bottom meson-octet/decuplet baryon channels, which are the main focus of this article. Furthermore, a comprehensive investigation of the mass spectra that includes the strong decay width calculations for both ground and excited states up to the second shell within the same model has never been performed.

The main aim of this article is to study the strong decay channels that have never been investigated. Indeed, this is the first time that the $\Lambda_b\eta$, $\Sigma_b\rho$, $\Sigma_b^*\rho$, $\Lambda_b\eta'$, $\Lambda_b\omega$, Ξ_bK, $\Xi_b'K$, Ξ_b^*K, Ξ_bK^*, $\Xi_b'K^*$ and $\Xi_b^*K^*$ channels have been considered in the calculation of the strong decay widths of the

excited Λ_b states; the $\Sigma_b\eta$, Ξ_bK, $\Sigma_b\rho$, $\Sigma_b^*\rho$, $\Lambda_b\rho$, $\Sigma_b^*\eta$, $\Sigma_b\eta'$, $\Sigma_b^*\eta'$, $\Xi_b'K$, Ξ_b^*K, Ξ_bK^*, $\Xi_b'K^*$, $\Xi_b^*K^*$, $\Sigma_b\omega$, $\Sigma_b^*\omega$, Σ_8B_s, ΔB, $N(1520)B$, $N(1535)B$, $N(1680)B$, and $N(1720)B$ channels in the calculation of the strong decay widths of the excited Σ_b states; the Λ_bK^*, $\Xi_b\rho$, $\Xi_b'\rho$, $\Xi_b^*\rho$, Σ_bK^*, $\Sigma_b^*K^*$, $\Xi_b\eta'$, $\Xi_b'\eta'$, $\Xi_b^*\eta'$, $\Xi_b\omega$, $\Xi_b'\omega$, $\Xi_b^*\omega$, $\Xi_b\phi$, $\Xi_b'\phi$, $\Xi_b^*\phi$, Ξ_8B_s, Σ_8B^*, and $\Sigma_{10}B$ channels in the calculation of the strong decay widths of the excited Ξ_b and Ξ_b' states; and the Ξ_bK^*, $\Xi_b'K^*$, $\Xi_b^*K^*$, $\Omega_b\eta$, $\Omega_b^*\eta$, $\Omega_b\phi$, $\Omega_b^*\phi$, $\Omega_b\eta'$, $\Omega_b^*\eta'$, Ξ_8B, and $\Xi_{10}B$ channels in the calculation of the strong decay widths of the Ω_b states.

For the radiative transitions, a few articles have been dedicated to the radiative decays of singly heavy baryons, as evidenced by references using χQM [67,68], light-cone QCD [84–90], and chiral perturbation theory (χPT) [91–93]. Further results yielded by other models can be found in Refs. [94–97]. However, there are no available experimental data for the electromagnetic decays of singly bottom baryons to compare with the theoretical predictions.

In a previous study [98], prompted by the discovery of the five Ω_c baryons by LHCb [99], a harmonic oscillator three-quark model was developed (a mass formula), which will be used in the present article. This model in Ref. [98], was applied to the $1P$ Ω_c and Ω_b mass spectra, and to the $\Omega_{c/b}$ strong decay widths into the $\Xi_{c/b}^+K^-$ and $\Xi_{c/b}'^+K^-$ channels, using the $^3P_0$ strong decay model. It is noteworthy that the predictions for the masses and widths of $1P$ Ω_b states were subsequently confirmed by the LHCb experiment [19], which cited the paper [98].

Subsequently, the model of Ref. [98] was also applied to the Ξ_c, Ξ_c', Ξ_b, and Ξ_b' $1P$ mass spectra and strong decay widths in Ref. [100], without changing the previous parameters, and provided an accurate description of the LHCb data concerning $\Xi_c(2923)^0$, $\Xi_c(2939)^0$, and $\Xi_c(2965)^0$ for both masses and widths, as reported in Ref. [101]. In particular, in Ref. [100] the $1P$ $\Xi_{c/b}'$ strong partial decay widths into $^2\Sigma_{c/b}\bar{K}$, $^2\Xi_{c/b}'\pi$, $^4\Sigma_{c/b}\bar{K}$, $^4\Xi_{c/b}'\pi$, $\Lambda_{c/b}\bar{K}$, $\Xi_{c/b}\pi$, and $\Xi_{c/b}\eta$ were calculated, by using both the EEM and the $^3P_0$ model, and also the electromagnetic decay widths. In Ref. [102], a more systematic investigation was made, which involved a further application of the model of Ref. [98] to the cqq, cqs, and css singly charm baryon up to $1D$, $2P$, and $2S$. That study calculated the three-quark and quark-diquark mass spectra of the singly charm baryons and the decay widths of the ground and excited singly charm baryon states (ρ- and λ-mode excitations) into singly charm baryon-(vector/pseudoscalar) meson pairs and (octet/decuplet) light baryon-(pseudoscalar/vector) charmed meson pairs. It is worth noting that the experimental mass and decay widths of $\Omega_c(3327)$ states, which LHCb has recently observed [103], agree with the $1D_{3/2}$ predicted mass and decay widths of Ref. [102]. The reproduction of the masses and widths of the $\Xi_c(2923)^0$, $\Xi_c(2939)^0$, $\Xi_c(2965)^0$, $\Omega_c(3000)$, $\Omega_c(3050)$, $\Omega_c(3066)$, $\Omega_c(3090)$, $\Omega_c(3119)$, $\Omega_c(3327)$, $\Omega_b(6316)$, $\Omega_b(6330)$, $\Omega_b(6340)$, and $\Omega_b(6350)$ states is an indication of the predictive power of this model.

In Ref. [104], the mass formula of Ref. [98] was applied to the singly, doubly, and triply charm and bottom baryons up to the P-wave and only the electromagnetic decays were calculated.

In that study [104] the authors did not evaluate the exact expression of the orbit-flip operator, since they replaced $\mathbf{p}_\lambda$ with $im_\lambda \mathrm{k}_0\boldsymbol{\lambda}$ and $\mathbf{p}_\rho$ with $im_\rho \mathrm{k}_0\boldsymbol{\rho}$. Similarly to the approach taken in Ref. [102] for the charm sector, the aim of this article was to expand the application of the model presented in Ref. [98], in the bottom sector, to the $1D$, $2P$, and $2S$ states, in both the three-quark and quark-diquark schemes, and to study the strong decay widths within the $^3P_0$ model. This is the first time that the $\Lambda_b\eta$, $\Sigma_b\rho$, $\Sigma_b^*\rho$, $\Lambda_b\eta'$, $\Lambda_b\omega$, Ξ_bK, $\Xi_b'K$, Ξ_b^*K, Ξ_bK^*, $\Xi_b'K^*$, and $\Xi_b^*K^*$ channels have been considered in the calculation of the strong decay widths of the excited Λ_b states; the $\Sigma_b\eta$, Ξ_bK, $\Sigma_b\rho$, $\Sigma_b^*\rho$, $\Lambda_b\rho$, $\Sigma_b^*\eta$, $\Sigma_b\eta'$, $\Sigma_b^*\eta'$, $\Xi_b'K$, Ξ_b^*K, Ξ_bK^*, $\Xi_b'K^*$, $\Xi_b^*K^*$, $\Sigma_b\omega$, $\Sigma_b^*\omega$, Σ_8B_s, ΔB, $N(1520)B$, $N(1535)B$, $N(1680)B$, and $N(1720)B$ channels in the calculation of the strong decay widths of the excited Σ_b states; the Λ_bK^*, $\Xi_b\rho$, $\Xi_b'\rho$, $\Xi_b^*\rho$, Σ_bK^*, $\Sigma_b^*K^*$, $\Xi_b\eta'$, $\Xi_b'\eta'$, $\Xi_b^*\eta'$, $\Xi_b\omega$, $\Xi_b'\omega$, $\Xi_b^*\omega$, $\Xi_b\phi$, $\Xi_b'\phi$, $\Xi_b^*\phi$, Ξ_8B_s, Σ_8B^*, and $\Sigma_{10}B$ channels in the calculation of the strong decay widths of the excited Ξ_b and Ξ_b' states; the Ξ_bK^*, $\Xi_b'K^*$, $\Xi_b^*K^*$, $\Omega_b\eta$, $\Omega_b^*\eta$, $\Omega_b\phi$, $\Omega_b^*\phi$, $\Omega_b\eta'$, $\Omega_b^*\eta'$, Ξ_8B, and $\Xi_{10}B$ channels in the calculation of the strong decay widths of the Ω_b states. Moreover, in Appendix G, we calculate the electromagnetic decay widths of the S- and P-wave singly bottom baryons, and report the analytical expressions of the relevant matrix elements for the electromagnetic couplings. Finally, the uncertainties are propagated with the Monte Carlo bootstrap method [105], which is based on the estimation of the probability density functions of the fitted parameters.

II. MASS SPECTRA

The masses of the bottom baryon states are calculated as the eigenvalues of the Hamiltonian introduced in Ref. [98], which we report below for convenience

$$H = H_{\mathrm{h.o.}} + a_{\mathrm{S}}\mathbf{S}_{\mathrm{tot}}^2 + a_{\mathrm{SL}}\mathbf{S}_{\mathrm{tot}}\cdot\mathbf{L}_{\mathrm{tot}} + a_{\mathrm{I}}\mathbf{I}^2 + a_{\mathrm{F}}\hat{\mathbf{C}}_2, \qquad (1)$$

where $H_{\mathrm{h.o.}}$ corresponds to the sum of the constituent masses and the harmonic oscillator Hamiltonian. In Eq. (1) the symbols $\mathbf{S}_{\mathrm{tot}}, \mathbf{L}_{\mathrm{tot}}, \mathbf{I}$ and $\hat{\mathbf{C}}_2$ denote the spin, orbital angular momentum, isospin, and the $SU_f(3)$ Casimir operators, respectively, and they are weighted with the model parameters $a_{\mathrm{S}}, a_{\mathrm{SL}}, a_{\mathrm{I}}$, and a_{F}.

A. Mass spectra of the bottom baryons within three quark model

In the case where baryons are modeled as three-quark systems, the $H_{\mathrm{h.o.}}$ term of Eq. (1) can be expressed using

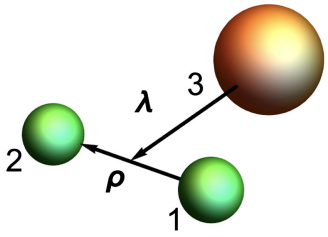

FIG. 1. The $\boldsymbol{\rho}$ coordinate describes the excitations within the light quark pair while the $\boldsymbol{\lambda}$ coordinate describes the excitations between the light quark pair and the bottom quark b.

the Jacobi coordinates $\boldsymbol{\rho} = (\boldsymbol{r}_1 - \boldsymbol{r}_2)/\sqrt{2}$ and $\boldsymbol{\lambda} = (\boldsymbol{r}_1 + \boldsymbol{r}_2 - 2\boldsymbol{r}_3)/\sqrt{6}$ and their conjugate momenta $\mathbf{p}_\rho$ and $\mathbf{p}_\lambda$ as

$$H^{3q}_{\text{h.o.}} = \sum_{i=1}^{3} m_i + \frac{\mathbf{p}_\rho^2}{2m_\rho} + \frac{\mathbf{p}_\lambda^2}{2m_\lambda} + \frac{1}{2} m_\rho \omega_\rho^2 \boldsymbol{\rho}^2 + \frac{1}{2} m_\lambda \omega_\lambda^2 \boldsymbol{\lambda}^2, \tag{2}$$

where m_i with $i = 1, 2$ are the light quark masses, m_3 is the bottom quark mass; $m_\rho = (m_1 + m_2)/2$, and $m_\lambda = 3m_\rho m_3/(2m_\rho + m_3)$. The ρ- and λ-oscillator frequencies are $\omega_{\rho(\lambda)} = \sqrt{\frac{3K_b}{m_{\rho(\lambda)}}}$, where K_b is the harmonic oscillator constant. Here the $\boldsymbol{\rho}$ coordinate describes the excitations within the light quark pair while the $\boldsymbol{\lambda}$ coordinate describes the excitations between the light quark pair and the bottom quark b, as depicted in Fig. 1.

The $H^{3q}_{\text{h.o.}}$ Hamiltonian described in Eq. (2) has the eigenstates given in Appendix A 1, see Eq. (A5), and its eigenvalues are

$$E^{3q}_{\text{h.o.}} = \sum_{i=1}^{3} m_i + \omega_\rho n_\rho + \omega_\lambda n_\lambda. \tag{3}$$

We use the usual definitions for $n_{\rho(\lambda)} = 2k_{\rho(\lambda)} + l_{\rho(\lambda)}$, $k_{\rho(\lambda)} = 0, 1, \ldots$, and $l_{\rho(\lambda)} = 0, 1, \ldots$; where, $l_{\rho(\lambda)}$ is the orbital angular momentum of the $\rho(\lambda)$ oscillator, and $k_{\rho(\lambda)}$ is the number of nodes (radial excitations) in the $\rho(\lambda)$ oscillators.

In the three-quark model, the eigenvalues of the Hamiltonian 1, proposed in Ref. [98], are given by the following mass formula,

$$\begin{aligned} E^{3q} = {} & \sum_{i=1}^{3} m_i + \omega_\rho n_\rho + \omega_\lambda n_\lambda + a_{\text{S}}[S_{\text{tot}}(S_{\text{tot}}+1)] \\ & + a_{\text{SL}} \frac{1}{2}[J(J+1) - L_{\text{tot}}(L_{\text{tot}}+1) \\ & - S_{\text{tot}}(S_{\text{tot}}+1)] + a_{\text{I}}[I(I+1)] \\ & + a_{\text{F}} \frac{1}{3}[p(p+3) + q(q+3) + pq]. \end{aligned} \tag{4}$$

We observe that the model is completely analytical, i.e., it is an algebraic model, or in other words, the Hamiltonian of Eq. (1) in combination with Eq. (2) is completely diagonal in the harmonic oscillator, spin, flavor, and color basis. The eigenvalues are given in Eq. (4) and the eigenstates are those given in Appendix A 1. Even though the confinement potential is expected to have a linear behavior, we opted for a harmonic oscillator confinement in order to achieve a fully analytical model. However, in Ref. [26], Capstick and Isgur emphasized that the effective parameters of the quark model can compensate for model limitations.

It is worth mentioning that the model of Ref. [98] has successfully described both the singly charm and singly bottom sectors. In the charm sector, it was applied to the Ξ_c states and the authors provided an accurate description of the LHCb data concerning $\Xi_c(2923)^0$, $\Xi_c(2939)^0$, and $\Xi_c(2965)^0$ for both masses and widths [100], as reported in Ref. [101]. In the bottom sector, its predictions for the masses and widths of Ω_b states were subsequently confirmed by the LHCb experiment [19], which cited Ref. [98].

In Eq. (4), the spin-dependent term splits the states with different $\mathbf{S}_{\text{tot}}$. The contribution of this term is smaller than in the charm baryons sector, in agreement with the heavy quark spin symmetry (see Sec. II F). The spin-orbit interaction, which is small in light baryons [25,37], turns out to be fundamental to describe the heavy-light baryon mass patterns [98]. The effect of the spin-orbit term is to split the states with different $\mathbf{J}$. Finally, the flavor-dependent term splits the baryons belonging to the flavor sextet, $\mathbf{6}_{\text{F}}$ with $(p, q) = (2, 0)$, from the baryons of the antitriplet, $\bar{\mathbf{3}}_{\text{F}}$ with $(p, q) = (0, 1)$.

B. Applications of the equal-spacing mass formulas

The mass formula presented in Eq. (4), which was introduced in [98], can be used to calculate the mass splitting between states of the same multiplet

$$\begin{aligned} m(A) - m(A') = {} & m_1 + m_2 - m_1' - m_2' + \omega_\rho n_\rho + \omega_\lambda n_\lambda - (\omega_\rho' n_\rho' + \omega_\lambda' n_\lambda') + a_{\text{S}}[S_{\text{tot}}(S_{\text{tot}}+1) - S'_{\text{tot}}(S'_{\text{tot}}+1)] \\ & + a_{\text{SL}} \frac{1}{2}[J(J+1) - L_{\text{tot}}(L_{\text{tot}}+1) - S_{\text{tot}}(S_{\text{tot}}+1) - J'(J'+1) + L'_{\text{tot}}(L'_{\text{tot}}+1) + S'_{\text{tot}}(S'_{\text{tot}}+1)] \\ & + a_{\text{I}}[I(I+1) - I'(I'+1)]. \end{aligned} \tag{5}$$

For example, in the charm sector, the experimental mass splitting, as from LHCb [101]

$$\begin{aligned} &m(\Omega_c(3050)) - m(\Xi_c'(2923)) \\ &\simeq m(\Omega_c(3065)) - m(\Xi_c'(2939)) \\ &\simeq m(\Omega_c(3090)) - m(\Xi_c'(2965)) \\ &\simeq 125 \text{ MeV} \end{aligned}$$

can be immediately explained by using Eq. (5) and the parameters from Ref. [102]

$$m(^{2S+1}(\Omega_c)_J) - m(^{2S+1}(\Xi_c')_J) = 115 \pm 30 \text{ MeV},$$

which is in agreement with the experimental data [101].

It is natural to expect a similar pattern in the bottom sector; therefore, the equal-spacing rules can guide future experimental searches in the bottom sector. For example, the D_λ-wave excited states obey the following spacing rules:

$$m(^{2S+1}(\Omega_b)_J) - m(^{2S+1}(\Xi_b')_J) = m_s - m_n + 2(\omega_\lambda^{\Omega_b} - \omega_\lambda^{\Xi_b}) - \frac{3}{4}a_{\rm I} \simeq 95 \pm 36 \text{ MeV} \tag{6}$$

$$m(^{2S+1}(\Xi_b')_J) - m(^{2S+1}(\Sigma_b)_J) = m_s - m_n + 2(\omega_\lambda^{\Xi_b} - \omega_\lambda^{\Sigma_b}) - \frac{5}{4}a_{\rm I} \simeq 58 \pm 41 \text{ MeV} \tag{7}$$

$$m(^{2S+1}(\Xi_b)_J) - m(^{2S+1}(\Lambda_b)_J) = m_s - m_n + 2(\omega_\lambda^{\Xi_b} - \omega_\lambda^{\Sigma_b}) + \frac{3}{4}a_{\rm I} \simeq 129 \pm 26 \text{ MeV}. \tag{8}$$

For the D_ρ-wave excited states we have

$$m(^{2S+1}(\Omega_b)_J) - m(^{2S+1}(\Xi_b')_J) = m_s - m_n + 2(\omega_\rho^{\Omega_b} - \omega_\rho^{\Xi_b}) - \frac{3}{4}a_{\rm I} \simeq 56 \pm 48 \text{ MeV} \tag{9}$$

$$m(^{2S+1}(\Xi_b')_J) - m(^{2S+1}(\Sigma_b)_J) = m_s - m_n + 2(\omega_\rho^{\Xi_b} - \omega_\rho^{\Sigma_b}) - \frac{5}{4}a_{\rm I} \simeq 4 \pm 40 \text{ MeV} \tag{10}$$

$$m(^{2S+1}(\Xi_b)_J) - m(^{2S+1}(\Lambda_b)_J) = m_s - m_n + 2(\omega_\rho^{\Xi_b} - \omega_\rho^{\Sigma_b}) + \frac{3}{4}a_{\rm I} \simeq 75 \pm 40 \text{ MeV}. \tag{11}$$

TABLE I. Fitted parameters for the three-quark model (second column) and the quark-diquark model (third column). The symbol "..." indicates that the parameter is absent in that model.

Parameter	Three-quark value	Diquark value
m_b	4930^{+12}_{-12} MeV	4677^{+100}_{-64} MeV
m_s	464^{+6}_{-6} MeV	...
m_n	299^{+10}_{-10} MeV	...
m_{D_Ω}	...	1331^{+59}_{-92} MeV
m_{D_Ξ}	...	1185^{+61}_{-92} MeV
$m_{D_{\Sigma,\Lambda}}$	...	1045^{+55}_{-94} MeV
K_b	$0.0254^{+0.0012}_{-0.0012}$ GeV^3	$0.0245^{+0.0023}_{-0.0023}$ GeV^3
$a_{\rm S}$	10^{+2}_{-3} MeV	8^{+2}_{-3} MeV
$a_{\rm SL}$	4^{+2}_{-2} MeV	6^{+3}_{-1} MeV
$a_{\rm I}$	36^{+7}_{-7} MeV	19^{+3}_{-2} MeV
$a_{\rm F}$	60^{+6}_{-5} MeV	13^{+6}_{-3} MeV

These calculations are based on the parameters reported in Table I, and the $\omega_{\lambda,\rho}^{B_b}$ values are computed for each bottom baryon by using Eq. (3). It should be noted that $\omega^{\Xi_b} = \omega^{\Xi_b'}$ and $\omega^{\Sigma_b} = \omega^{\Lambda_b}$, due to their identical quark content. Therefore, we only use three different labels: Ω_b, Ξ_b, and Σ_b.

The values obtained from these equal-spacing rules can provide additional guidance for experimentalists searching for bottom baryons.

C. Mass spectra of the bottom baryons within the quark-diquark model

If baryons are modeled as quark-diquark systems, the $H_{\rm h.o.}$ term of Eq. (1) can be expressed by using only one relative coordinate $\boldsymbol{r} = \boldsymbol{r}_1 - \boldsymbol{r}_2$ and momentum $\mathbf{p}_r = (m_b\mathbf{p}_D - m_D\mathbf{p}_b)/(m_b + m_D)$, namely, the quark-diquark model [106]. In this picture, the two light quarks are regarded as a single diquark object interacting with a heavy quark. Thus, the $H_{\rm h.o.}$ term of Eq. (1) can be expressed by using the relative coordinate $\mathbf{r}$ and its conjugate momentum $\mathbf{p}_r$ as

$$H_{\rm h.o.}^{qD} = m_D + m_b + \frac{\mathbf{p}_r^2}{2\mu} + \frac{1}{2}\mu\omega_r^2\boldsymbol{r}^2, \tag{12}$$

where m_D and m_b are the diquark and bottom quark masses, respectively, $\mu = m_b m_D/(m_b + m_D)$ is the reduced mass of the system. The $H_{\rm h.o.}^{qD}$ Hamiltonian described in Eq. (12) has the eigenstates given in Appendix A 2, see Eq. (A13), and its eigenvalues are

$$E_{\rm h.o.}^{qD} = m_D + m_b + \omega_r n_r; \quad \text{with} \quad \omega_r = \sqrt{\frac{3K_b}{\mu}}, \tag{13}$$

$n_r = 2k_r + l_r$ where $k_r = 0, 1, \ldots$ is the number of nodes, $l_r = 0, 1, \ldots$ is the orbital angular momentum of the r oscillator, and K_b is the harmonic oscillator constant.

In the quark-diquark scheme, the eigenvalues of the Hamiltonian 1, proposed in Ref. [98], are given by the following mass formula,

$$E^{qD} = m_D + m_b + \omega_r n_r + a_S[S_{tot}(S_{tot}+1)] + a_{SL}\frac{1}{2}[J(J+1) - L_{tot}(L_{tot}+1) - S_{tot}(S_{tot}+1)] + a_I[I(I+1)] + a_F\frac{1}{3}[p(p+3)+q(q+3)+pq]. \quad (14)$$

D. Singly bottom baryon states within three-quark model

We first construct the singly bottom baryon states in both the three-quark and the quark-diquark models.

In the three-quark model, the bottom baryons are described as three quark states made up of one b quark and two light quarks (u, d, or s). In this model, the spatial degrees of freedom of the bottom states are expressed by the $\boldsymbol{\rho}$ coordinate, which describes the excitations within the light quark pair, and the $\boldsymbol{\lambda}$ coordinate, which describes the excitations between the light quark pair and the bottom quark b (see Fig. 1).

The total angular momentum, $\mathbf{J} = \mathbf{L}_{tot} + \mathbf{S}_{tot}$, is the sum of the orbital angular momentum, $\mathbf{L}_{tot} = \mathbf{l}_\rho + \mathbf{l}_\lambda$, and the internal spin, $\mathbf{S}_{tot} = \mathbf{S}_{12} + \mathbf{1/2}$, which is the sum of the light quark spin, $\mathbf{S}_{12} = \mathbf{S}_1 + \mathbf{S}_2$, and the b quark spin, $\mathbf{1/2}$.

It is important to note that the color part of a baryon wave function is fully antisymmetric, representing an $SU_c(3)$ singlet of the three colors. In our model the light quarks are considered to be identical particles; hence, their wave function should be antisymmetric in order to satisfy the Pauli principle. Since the two light quarks are in the antisymmetric $\bar{\mathbf{3}}_c$ color state, the product of their spin-, flavor-, and orbital-wave functions has to be symmetric. Let us apply this principle to construct the singly bottom baryon ground and excited states up to the second energy band, $N = n_\rho + n_\lambda$ ($N = n_r$ in the case of the quark-diquark system), of the harmonic oscillator.

In the energy band $N = 0$, in which $\mathbf{l}_\rho = \mathbf{l}_\lambda = \mathbf{0}$, the spatial wave function of the two light quarks is symmetric implying that their spin-flavor wave function is symmetric. Therefore, we can only combine the antisymmetric $\bar{\mathbf{3}}_F$-plet with antisymmetric-spin configuration $\mathbf{S}_{12} = \mathbf{0}$ and the symmetric $\mathbf{6}_F$-plet with spin symmetric configuration $\mathbf{S}_{12} = \mathbf{1}$. This means that the ground state baryons made up of a light quark pair with antisymmetric-spin configuration $\mathbf{S}_{12} = \mathbf{0}$ fill an antisymmetric $\bar{\mathbf{3}}_F$-plet with total spin $\mathbf{J} = \mathbf{S}_{tot} = \frac{\mathbf{1}}{\mathbf{2}}$ (displayed on the left-hand side of Fig. 2), while the ones made up of a light quark pair with spin symmetric configuration $\mathbf{S}_{12} = \mathbf{1}$, fill one $\mathbf{6}_F$-plet with total spin $\mathbf{J} = \mathbf{S}_{tot} = \frac{\mathbf{1}}{\mathbf{2}}$, and one $\mathbf{6}_F$-plet with total spin $\mathbf{J} = \mathbf{S}_{tot} = \frac{\mathbf{3}}{\mathbf{2}}$ (displayed on the center and on the right-hand side of Fig. 2).

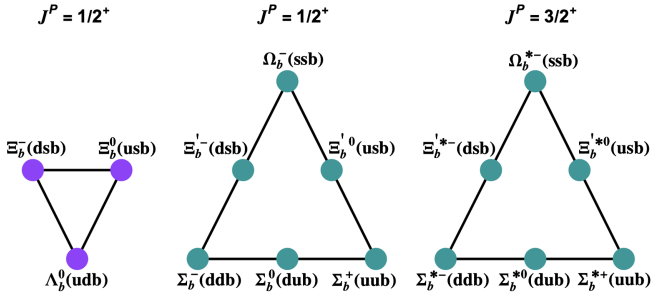

FIG. 2. The $SU_f(3)$ flavor multiplets of the ground-state singly bottom baryons: the flavor antitriplet $\bar{\mathbf{3}}_F$ with spin-parity $\mathbf{J}^P = \frac{\mathbf{1}}{\mathbf{2}}^+$ (left side), the flavor sextet $\mathbf{6}_F$ with $\mathbf{J}^P = \frac{\mathbf{1}}{\mathbf{2}}^+$ (center), and the flavor sextet $\mathbf{6}_F$ with $\mathbf{J}^P = \frac{\mathbf{3}}{\mathbf{2}}^+$ (right side).

The $\bar{\mathbf{3}}_F$-plet and the $\mathbf{6}_F$-plet with spin-parity $\mathbf{J}^P = \frac{\mathbf{1}}{\mathbf{2}}^+$ lie on the first floor of the $SU_f(4)$ $\mathbf{20}_F$-plet with the light octet baryons at the ground level, while the $\mathbf{6}_F$-plet with spin-parity $\mathbf{J}^P = \frac{\mathbf{3}}{\mathbf{2}}^+$ lies on the first floor of the $SU_f(4)$ $\mathbf{20}_F$-plet with the light decuplet baryons at the ground level. The $\bar{\mathbf{3}}_F$-plet with spin-parity $\mathbf{J}^P = \frac{\mathbf{1}}{\mathbf{2}}^+$ contains one isosinglet state, Λ_b, and two isospin $\frac{1}{2}$ states, Ξ_b^- and Ξ_b^0.

The $\mathbf{6}_F$-plet with spin-parity $\mathbf{J}^P = \frac{\mathbf{1}}{\mathbf{2}}^+$ contains one isosinglet, Ω_b^-, two isospin $\frac{1}{2}$ states, $\Xi_b^{\prime -}$ and $\Xi_b^{\prime 0}$, and three states with total isospin $\mathbf{I} = \mathbf{1}$, Σ_b^+, Σ_b^0 and Σ_b^-. The $\mathbf{6}_F$-plet with spin-parity $\mathbf{J}^P = \frac{\mathbf{3}}{\mathbf{2}}^+$ contains the one isosinglet, Ω_b^{*-}, two isospin $\frac{1}{2}$ states, $\Xi_b^{\prime *-}$ and $\Xi_b^{\prime *0}$, and three states with total isospin $\mathbf{I} = \mathbf{1}$, $\Sigma_b^{*+}, \Sigma_b^{*0}$ and Σ_b^{*-}, where the upper symbol $*$ denotes that the total spin of these states is $\frac{3}{2}$. The total spin and the $SU_f(3)$ flavor multiplets of ground state singly bottom baryons are reported in Fig. 2.

For the energy band $N = 1$, there are two different possibilities. If $\mathbf{l}_\rho = \mathbf{0}$ and $\mathbf{l}_\lambda = \mathbf{1}$, the spatial wave function is symmetric under the interchange of light quarks, implying that their spin-flavor wave function is also symmetric. Thus, in the case of the $\bar{\mathbf{3}}_F$-plet baryons, the angular momentum $\mathbf{L}_{tot} = \mathbf{1}$ is coupled with one only spin configuration, $\mathbf{S}_{tot} = \frac{\mathbf{1}}{\mathbf{2}}$ that comes from the light quark spin configuration $\mathbf{S}_{12} = \mathbf{0}$, yielding two P_λ-wave excitations, while, in the case of the $\mathbf{6}_F$-plet baryons, $\mathbf{L}_{tot} = \mathbf{1}$ is coupled with two possible spin configurations, $\mathbf{S}_{tot} = \frac{\mathbf{1}}{\mathbf{2}}, \frac{\mathbf{3}}{\mathbf{2}}$ that come from the light quark spin configuration $\mathbf{S}_{12} = \mathbf{1}$, yielding five P_λ-wave excitations.

When $\mathbf{l}_\rho = \mathbf{1}$ and $\mathbf{l}_\lambda = \mathbf{0}$, the spatial wave function is antisymmetric under the interchange of light quarks, implying that the two light quark spin-flavor wave function are also antisymmetric, hence the situation is reversed: in the case of the $\bar{\mathbf{3}}_F$-plet baryons, $\mathbf{L}_{tot} = \mathbf{1}$ is coupled with $\mathbf{S}_{tot} = \frac{\mathbf{1}}{\mathbf{2}}, \frac{\mathbf{3}}{\mathbf{2}}$ yielding to five P_ρ-wave states, while, in the case of the $\mathbf{6}_F$-plet baryons, $\mathbf{L}_{tot} = \mathbf{1}$ is coupled with $\mathbf{S}_{tot} = \frac{\mathbf{1}}{\mathbf{2}}$, yielding to two P_ρ-wave states.

In the energy band $N = 2$, there are three possibilities: the pure λ-excitations, $\mathbf{l}_\rho = \mathbf{0}, \mathbf{l}_\lambda = \mathbf{2}$, the pure ρ-excitations, $\mathbf{l}_\rho = \mathbf{2}, \mathbf{l}_\lambda = \mathbf{0}$, and the mixed case $\mathbf{l}_\rho = \mathbf{1}, \mathbf{l}_\lambda = \mathbf{1}$. In both the $\mathbf{l}_\rho = \mathbf{0}, \mathbf{l}_\lambda = \mathbf{2}$ and $\mathbf{l}_\rho = \mathbf{2}, \mathbf{l}_\lambda = \mathbf{0}$ cases the total spatial wave function is symmetric under the interchange of light quarks implying that their spin-flavor wave function is also symmetric.

If $\mathbf{l}_\rho = \mathbf{0}$ and $\mathbf{l}_\lambda = \mathbf{2}$, in the case of the $\bar{\mathbf{3}}_\mathrm{F}$-plet baryons, $\mathbf{L}_\mathrm{tot} = \mathbf{2}$ is coupled with $\mathbf{S}_\mathrm{tot} = \frac{\mathbf{1}}{\mathbf{2}}$, giving two D_λ-wave excitations, while, in the case of the $\mathbf{6}_\mathrm{F}$-plet baryons, $\mathbf{L}_\mathrm{tot} = \mathbf{2}$ is coupled with two possible spin configurations, $\mathbf{S}_\mathrm{tot} = \frac{\mathbf{1}}{\mathbf{2}}, \frac{\mathbf{3}}{\mathbf{2}}$, giving six D_λ-wave excitations. If $\mathbf{l}_\rho = \mathbf{2}$ and $\mathbf{l}_\lambda = \mathbf{0}$, in a similar way we have two D_ρ-wave excitations for the $\bar{\mathbf{3}}_\mathrm{F}$-plet and six D_ρ-wave excitations for the $\mathbf{6}_\mathrm{F}$-plet.

When $\mathbf{l}_\rho = \mathbf{1}$ and $\mathbf{l}_\lambda = \mathbf{1}$ there are three possible values of the angular momentum $\mathbf{L}_\mathrm{tot} = \mathbf{0}, \mathbf{1}, \mathbf{2}$. In the case of the $\bar{\mathbf{3}}_\mathrm{F}$-plet baryons, they are combined with $\mathbf{S}_\mathrm{tot} = \frac{\mathbf{1}}{\mathbf{2}}, \frac{\mathbf{3}}{\mathbf{2}}$, which come from the light quark spin configuration $\mathbf{S}_{12} = \mathbf{1}$, producing thirteen mixed excited states: six D-wave states, five P-wave states, and two S- wave states. In the case of the $\mathbf{6}_\mathrm{F}$-plet baryons, they are combined with $\mathbf{S}_\mathrm{tot} = \frac{\mathbf{1}}{\mathbf{2}}$, which come from the light quark spin configuration $\mathbf{S}_{12} = \mathbf{0}$, thus producing five possible states: two D-wave states, two P-wave states, and one S-wave state.

Additionally, there are two possible radial excitation modes in this energy band, $k_\rho = 0$, $k_\lambda = 1$, and $k_\rho = 1$, $k_\lambda = 0$, both corresponding to a symmetric light quark wave function since $\mathbf{L}_\mathrm{tot} = \mathbf{l}_\rho + \mathbf{l}_\lambda = \mathbf{0}$. If $k_\rho = 0$ and $k_\lambda = 1$, in the case of the $\bar{\mathbf{3}}_\mathrm{F}$-plet baryons, $\mathbf{L}_\mathrm{tot} = \mathbf{0}$ is combined with $\mathbf{S}_\mathrm{tot} = \frac{\mathbf{1}}{\mathbf{2}}$, producing one λ-radial excitation, while in the case of the $\mathbf{6}_\mathrm{F}$-plet baryons, $\mathbf{L}_\mathrm{tot} = \mathbf{0}$ is combined with $\mathbf{J} = \mathbf{S}_\mathrm{tot} = \frac{\mathbf{1}}{\mathbf{2}}, \frac{\mathbf{3}}{\mathbf{2}}$, producing two λ-radial excitations. In a similar way, if $k_\rho = 1$ and $k_\lambda = 1$, in the case of the $\bar{\mathbf{3}}_\mathrm{F}$-plet baryons, we have one ρ-radial excitation, while in the case of the $\mathbf{6}_\mathrm{F}$-plet baryons, we have two ρ-radial excitations.

E. Singly bottom baryon states within the quark-diquark model

Finally, when the bottom baryons are seen as quark-diquark systems, the two constituent light quarks of the diquark are considered to be correlated, with no internal spatial excitations ($\mathbf{l}_\rho = \mathbf{0}$); i.e., it is hypothesized that we are within the limit where the diquark internal spatial excitations are higher in energy than the scale of the resonances studied. As a result, the quark-diquark states are a subset of the previously discussed three-quark states and can be obtained by freezing the ρ coordinate. The validity of this scheme for singly bottom systems will ultimately be determined by experimental data. Further investigations and analysis are necessary in order to confirm its applicability. With the completion of the construction of states in both the three-quark and quark-diquark models, we have established a framework for understanding the properties of singly bottom baryons.

We make one last remark on the notation used throughout the paper. The three-quark quantum state is written as $|l_\lambda, l_\rho, k_\lambda, k_\rho\rangle$, with total angular momentum $\mathbf{J} = \mathbf{L}_\mathrm{tot} + \mathbf{S}_\mathrm{tot}$, where $\mathbf{L}_\mathrm{tot} = \mathbf{l}_\rho + \mathbf{l}_\lambda$ and $\mathbf{S}_\mathrm{tot} = \mathbf{S}_{12} + \frac{\mathbf{1}}{\mathbf{2}}$, $\mathbf{S}_{12}$ is the coupled spin of the light quarks. The number of nodes is $k_{\lambda,\rho}$. The quark-diquark quantum state is written as $|l_r, k_r\rangle$ where $\mathbf{L}_\mathrm{tot} = \mathbf{l}_r$ and $\mathbf{S}_\mathrm{tot} = \mathbf{S}_{12} + \frac{\mathbf{1}}{\mathbf{2}}$, and the number of nodes is k_r. For each state, we also report the information on the total spin, orbital angular momentum, and total angular momentum using the compact spectroscopic notation ${}^{2S+1}L_J \equiv {}^{2S}\mathrm{tot} + 1L_{\mathrm{tot}\,J}$.

F. Parameter determination and uncertainties

We perform a fit to describe the observed masses of singly bottom baryons, namely Λ_b, Σ_b, Ξ_b, Σ_b, and Ω_b, with the masses predicted by Eqs. (4) and (14). This fitting procedure enables us to determine the masses of the constituent quarks and diquarks (m_b, m_s, $m_{u,d}$, m_{D_Ω}, m_{D_Ξ}, and $m_{D_{\Sigma,\Lambda}}$), and the model parameters ($a_\mathrm{S}, a_\mathrm{SL}, a_\mathrm{I}, a_\mathrm{F}$, and K_b). The goal is to confirm that the parameters minimize the sum of the squared differences between the theory-predicted baryon masses and their corresponding experimental values (least-squares method).

Experimental measurements of baryon masses are associated with both statistical and systematic uncertainties. Moreover, the models presented in Eqs. (4) and (14) provide approximate descriptions of bottom baryons. To account for possible deviations between these models and experimental data, we assign a model uncertainty to each model. The calculation of the model uncertainty, denoted as σ_mod, follows the procedure outlined in Ref. [1], ensuring that the χ^2/NDF value approaches 1. The computation of χ^2 involves the equation

$$\chi^2 = \sum_i \frac{(M_{\mathrm{mod},i} - M_{\mathrm{exp},i})^2}{\sigma_\mathrm{mod}^2 + \sigma_{\mathrm{exp},i}^2}, \tag{15}$$

where $M_{\mathrm{mod},i}$ represents the predicted masses of the singly bottom baryons, $M_{\mathrm{exp},i}$ denotes the experimental masses of the singly bottom baryons included in the fitting process, along with their uncertainties $\sigma_{\mathrm{exp},i}$, and NDF refers to the number of degrees of freedom. For the three-quark model, we obtain a value of $\sigma_\mathrm{mod} = 12$ MeV, while for the quark-diquark model $\sigma_\mathrm{mod} = 20$ MeV. To obtain the model parameters, we conducted a fit using only 13 of the 22 experimentally observed states. The fitted parameters for the bottom baryon masses are shown in Table I. Our predictions align well with the observed states, showing a root-mean-square deviation of 9.6 MeV.

If we compare the parameters $a_\mathrm{S}, a_\mathrm{SL}, a_\mathrm{I}$, and a_S of Table I with the results of Ref. [102] in the charm sector, we

TABLE II. Predicted $\Lambda_b(nnb)$ masses and strong decay widths (in MeV). The flavor multiplet is indicated by the symbol $\mathcal{F}$. The first column contains the h.o. three-quark model states, $|l_\lambda, l_\rho, k_\lambda, k_\rho\rangle$, where l_λ and l_ρ are the orbital angular momenta and k_λ, k_ρ the number of nodes of the λ and ρ oscillators, with $N = n_\rho + n_\lambda$. The second column displays the spectroscopic notation $^{2S+1}L_J$ for each state. The third column contains the total angular momentum and parity $\mathbf{J}^P$. In the fourth and eighth columns, the three-quark predicted masses [Eq. (4)] and their total strong decay widths are shown, respectively. The fifth column contains the h.o. quark-diquark model state, $|l_r, k_r\rangle$, where l_r is the orbital angular momentum and k_r denotes the number of nodes, and $N = n_r$. The sixth column contains the quark-diquark predicted masses [Eq. (14)]. Our theoretical results are compared with the experimental masses and the decay widths from PDG [1] in the seventh and ninth columns, respectively. The "†" indicates that no experimental mass or decay width for that state has yet been reported. The symbol "..." indicates that there is no quark-diquark prediction for that state.

$\mathcal{F} = \bar{\mathbf{3}}_\mathrm{F}$	Three-quark			Quark-diquark			Three-quark	
$\Lambda_b(nnb)$ $\lvert l_\lambda, l_\rho, k_\lambda, k_\rho\rangle$	$^{2S+1}L_J$	$\mathbf{J}^P$	Predicted mass (MeV)	$\lvert l_r, k_r\rangle$	Predicted mass (MeV)	Experimental mass (MeV)	Predicted Γ_Strong (MeV)	Experimental Γ (MeV)
$N=0$								
$\lvert 0,0,0,0\rangle$	$^2S_{1/2}$	$\frac{1}{2}^+$	5613^{+9}_{-9}	$\lvert 0,0\rangle$	5611^{+15}_{-16}	5619.60 ± 0.17[a]	0	≈ 0
$N=1$								
$\lvert 1,0,0,0\rangle$	$^2P_{1/2}$	$\frac{1}{2}^-$	5918^{+8}_{-8}	$\lvert 1,0\rangle$	5916^{+11}_{-12}	5912.19 ± 0.17[a]	0	<0.25
$\lvert 1,0,0,0\rangle$	$^2P_{3/2}$	$\frac{3}{2}^-$	5924^{+8}_{-8}	$\lvert 1,0\rangle$	5925^{+12}_{-12}	5920.09 ± 0.17[a]	0	<0.19
$\lvert 0,1,0,0\rangle$	$^2P_{1/2}$	$\frac{1}{2}^-$	6114^{+10}_{-10}	...	...	6072.3 ± 2.9	67^{+16}_{-16}	72 ± 11
$\lvert 0,1,0,0\rangle$	$^4P_{1/2}$	$\frac{1}{2}^-$	6137^{+14}_{-14}	...	...	†	36^{+8}_{-8}	†
$\lvert 0,1,0,0\rangle$	$^2P_{3/2}$	$\frac{3}{2}^-$	6121^{+10}_{-10}	...	...	†	85^{+21}_{-21}	†
$\lvert 0,1,0,0\rangle$	$^4P_{3/2}$	$\frac{3}{2}^-$	6143^{+12}_{-12}	...	...	†	128^{+31}_{-31}	†
$\lvert 0,1,0,0\rangle$	$^4P_{5/2}$	$\frac{5}{2}^-$	6153^{+14}_{-14}	...	...	†	74^{+19}_{-19}	†
$N=2$								
$\lvert 2,0,0,0\rangle$	$^2D_{3/2}$	$\frac{3}{2}^+$	6225^{+13}_{-13}	$\lvert 2,0\rangle$	6224^{+20}_{-20}	6146.2 ± 0.4	13^{+5}_{-5}	2.9 ± 1.3
$\lvert 2,0,0,0\rangle$	$^2D_{5/2}$	$\frac{5}{2}^+$	6235^{+13}_{-13}	$\lvert 2,0\rangle$	6239^{+20}_{-20}	6152.5 ± 0.4	18^{+12}_{-13}	2.1 ± 0.9
$\lvert 0,0,1,0\rangle$	$^2S_{1/2}$	$\frac{1}{2}^+$	6231^{+12}_{-12}	$\lvert 0,1\rangle$	6233^{+20}_{-20}	†	29^{+14}_{-14}	†
$\lvert 0,0,0,1\rangle$	$^2S_{1/2}$	$\frac{1}{2}^+$	6624^{+21}_{-21}	...	...	†	130^{+32}_{-32}	†
$\lvert 1,1,0,0\rangle$	$^2D_{3/2}$	$\frac{3}{2}^+$	6421^{+16}_{-16}	...	...	†	67^{+17}_{-17}	†
$\lvert 1,1,0,0\rangle$	$^2D_{5/2}$	$\frac{5}{2}^+$	6431^{+17}_{-17}	...	...	†	108^{+28}_{-28}	†
$\lvert 1,1,0,0\rangle$	$^4D_{1/2}$	$\frac{1}{2}^+$	6438^{+22}_{-22}	...	...	†	34^{+9}_{-9}	†
$\lvert 1,1,0,0\rangle$	$^4D_{3/2}$	$\frac{3}{2}^+$	6444^{+19}_{-19}	...	...	†	95^{+25}_{-25}	†
$\lvert 1,1,0,0\rangle$	$^4D_{5/2}$	$\frac{5}{2}^+$	6454^{+17}_{-17}	...	...	†	128^{+34}_{-33}	†
$\lvert 1,1,0,0\rangle$	$^4D_{7/2}$	$\frac{7}{2}^+$	6468^{+23}_{-22}	...	...	†	122^{+34}_{-34}	†
$\lvert 1,1,0,0\rangle$	$^2P_{1/2}$	$\frac{1}{2}^-$	6423^{+16}_{-16}	...	...	†	$0.5^{+0.1}_{-0.1}$	†
$\lvert 1,1,0,0\rangle$	$^2P_{3/2}$	$\frac{3}{2}^-$	6429^{+17}_{-17}	...	...	†	$1.7^{+0.5}_{-0.5}$	†
$\lvert 1,1,0,0\rangle$	$^4P_{1/2}$	$\frac{1}{2}^-$	6446^{+19}_{-18}	...	...	†	$0.3^{+0.1}_{-0.1}$	†
$\lvert 1,1,0,0\rangle$	$^4P_{3/2}$	$\frac{3}{2}^-$	6452^{+17}_{-17}	...	...	†	$1.2^{+0.3}_{-0.3}$	†
$\lvert 1,1,0,0\rangle$	$^4P_{5/2}$	$\frac{5}{2}^-$	6462^{+19}_{-19}	...	...	†	2^{+1}_{-1}	†
$\lvert 1,1,0,0\rangle$	$^4S_{3/2}$	$\frac{3}{2}^+$	6456^{+17}_{-18}	...	...	†	32^{+8}_{-8}	†
$\lvert 1,1,0,0\rangle$	$^2S_{1/2}$	$\frac{1}{2}^+$	6427^{+16}_{-16}	...	...	†	29^{+7}_{-7}	†
$\lvert 0,2,0,0\rangle$	$^2D_{3/2}$	$\frac{3}{2}^+$	6618^{+20}_{-20}	...	...	†	131^{+33}_{-32}	†
$\lvert 0,2,0,0\rangle$	$^2D_{5/2}$	$\frac{5}{2}^+$	6628^{+21}_{-22}	...	...	†	185^{+49}_{-49}	†

[a]It indicates the experimental mass and decay width values included in the fits.

can see that a_I and a_F are quite similar, while a_S and a_SL are significantly smaller in the bottom sector than in the charm sector. In the case of the spin-spin interaction, $a_\mathrm{S} S(S+1)$, we get from the fit a value of $a_\mathrm{S} = 10^{+2}_{-3}$ MeV for the bottom sector, which is smaller than the value obtained for the charm sector, $a_\mathrm{S} = 23 \pm 3$ MeV in Ref. [102]. The decrease of a_S from the charm to the bottom sector is an effective way to take into account that the spin-spin interaction is inversely proportional to the masses of the interacting quarks, in agreement with the heavy quark spin symmetry. In the case of the spin-orbit interaction, $a_\mathrm{SL}\, \mathbf{S}_\mathrm{tot} \cdot \mathbf{L}_\mathrm{tot}$, we get from the fit a value of $a_{\mathrm{S\,L}} = 4^{+2}_{-2}$ MeV, about four times smaller than the value obtained for the charm sector, $a_\mathrm{SL} = 18 \pm 5$ MeV [102].

TABLE III. Same as Table II, but for $\Xi_b(snb)$ states. The recently discovered $\Xi_b(6087)$ [24], which is not yet on the PDG has been associated with the $1P\ 1/2^-$ state; it is reported in the table with the mass and width, as from Ref. [24]. The recently discovered $\Xi_b(6095)^0$ [24] has been considered by us as the neutral partner of $\Xi_b(6100)^-$ reported by the PDG, and in this table we reported its width as from LHCb [24]. The "†" indicates that no experimental mass or decay width for that state has yet been reported. The symbol "..." indicates that there is no quark-diquark prediction for that state.

$\mathcal{F}=\bar{\mathbf{3}}_{\mathrm{F}}$	Three-quark			Quark-diquark			Three-quark	
$\Xi_b(snb)$ $\lvert l_\lambda, l_\rho, k_\lambda, k_\rho\rangle$	$^{2S+1}L_J$	$\mathbf{J}^P$	Predicted mass (MeV)	$\lvert l_r, k_r\rangle$	Predicted mass (MeV)	Experimental mass (MeV)	Predicted Γ_{Strong} (MeV)	Experimental Γ (MeV)
$N=0$								
$\lvert 0,0,0,0\rangle$	$^2S_{1/2}$	$\frac{1}{2}^+$	5806^{+9}_{-9}	$\lvert 0,0\rangle$	5801^{+16}_{-16}	5794.5 ± 0.6[a]	0	≈ 0
$N=1$								
$\lvert 1,0,0,0\rangle$	$^2P_{1/2}$	$\frac{1}{2}^-$	6079^{+9}_{-9}	$\lvert 1,0\rangle$	6082^{+15}_{-16}	6087.2 ± 0.8	$0.2^{+0.1}_{-0.2}$	2.4 ± 0.6
$\lvert 1,0,0,0\rangle$	$^2P_{3/2}$	$\frac{3}{2}^-$	6085^{+9}_{-9}	$\lvert 1,0\rangle$	6092^{+15}_{-15}	6100.3 ± 0.6[a]	$1.1^{+0.6}_{-0.6}$	0.9 ± 0.4
$\lvert 0,1,0,0\rangle$	$^2P_{1/2}$	$\frac{1}{2}^-$	6248^{+11}_{-11}	...	...	†	9^{+2}_{-2}	†
$\lvert 0,1,0,0\rangle$	$^4P_{1/2}$	$\frac{1}{2}^-$	6271^{+15}_{-15}	...	...	†	6^{+1}_{-2}	†
$\lvert 0,1,0,0\rangle$	$^2P_{3/2}$	$\frac{3}{2}^-$	6255^{+11}_{-11}	...	...	†	66^{+16}_{-16}	†
$\lvert 0,1,0,0\rangle$	$^4P_{3/2}$	$\frac{3}{2}^-$	6277^{+14}_{-14}	...	...	†	26^{+7}_{-7}	†
$\lvert 0,1,0,0\rangle$	$^4P_{5/2}$	$\frac{5}{2}^-$	6287^{+15}_{-15}	...	...	†	68^{+16}_{-16}	†
$N=2$								
$\lvert 2,0,0,0\rangle$	$^2D_{3/2}$	$\frac{3}{2}^+$	6354^{+13}_{-13}	$\lvert 2,0\rangle$	6368^{+24}_{-21}	6327.3 ± 2.5	$1.9^{+0.8}_{-0.8}$	<2.2
$\lvert 2,0,0,0\rangle$	$^2D_{5/2}$	$\frac{5}{2}^+$	6364^{+13}_{-13}	$\lvert 2,0\rangle$	6383^{+23}_{-21}	6332.7 ± 2.5	$1.5^{+0.5}_{-0.5}$	<1.6
$\lvert 0,0,1,0\rangle$	$^2S_{1/2}$	$\frac{1}{2}^+$	6360^{+12}_{-13}	$\lvert 0,1\rangle$	6377^{+23}_{-21}	†	5^{+2}_{-2}	†
$\lvert 0,0,0,1\rangle$	$^2S_{1/2}$	$\frac{1}{2}^+$	6699^{+19}_{-19}	...	...	†	179^{+28}_{-28}	†
$\lvert 1,1,0,0\rangle$	$^2D_{3/2}$	$\frac{3}{2}^+$	6524^{+16}_{-16}	...	...	†	46^{+12}_{-12}	†
$\lvert 1,1,0,0\rangle$	$^2D_{5/2}$	$\frac{5}{2}^+$	6534^{+17}_{-17}	...	...	†	108^{+27}_{-27}	†
$\lvert 1,1,0,0\rangle$	$^4D_{1/2}$	$\frac{1}{2}^+$	6540^{+22}_{-22}	...	...	†	20^{+5}_{-5}	†
$\lvert 1,1,0,0\rangle$	$^4D_{3/2}$	$\frac{3}{2}^+$	6546^{+19}_{-19}	...	...	†	67^{+18}_{-18}	†
$\lvert 1,1,0,0\rangle$	$^4D_{5/2}$	$\frac{5}{2}^+$	6556^{+17}_{-18}	...	...	†	100^{+26}_{-26}	†
$\lvert 1,1,0,0\rangle$	$^4D_{7/2}$	$\frac{7}{2}^+$	6570^{+22}_{-22}	...	...	†	114^{+30}_{-30}	†
$\lvert 1,1,0,0\rangle$	$^2P_{1/2}$	$\frac{1}{2}^-$	6526^{+16}_{-16}	...	...	†	$0.3^{+0.1}_{-0.1}$	†
$\lvert 1,1,0,0\rangle$	$^2P_{3/2}$	$\frac{3}{2}^-$	6532^{+16}_{-16}	...	...	†	2^{+1}_{-1}	†
$\lvert 1,1,0,0\rangle$	$^4P_{1/2}$	$\frac{1}{2}^-$	6548^{+19}_{-19}	...	...	†	$0.2^{+0.1}_{-0.1}$	†
$\lvert 1,1,0,0\rangle$	$^4P_{3/2}$	$\frac{3}{2}^-$	6554^{+18}_{-17}	...	...	†	$0.9^{+0.3}_{-0.3}$	†
$\lvert 1,1,0,0\rangle$	$^4P_{5/2}$	$\frac{5}{2}^-$	6564^{+19}_{-19}	...	...	†	3^{+1}_{-1}	†
$\lvert 1,1,0,0\rangle$	$^4S_{3/2}$	$\frac{3}{2}^+$	6558^{+18}_{-18}	...	...	†	33^{+8}_{-8}	†
$\lvert 1,1,0,0\rangle$	$^2S_{1/2}$	$\frac{1}{2}^+$	6530^{+16}_{-16}	...	...	†	31^{+7}_{-8}	†
$\lvert 0,2,0,0\rangle$	$^2D_{3/2}$	$\frac{3}{2}^+$	6693^{+20}_{-19}	...	...	†	127^{+31}_{-31}	†
$\lvert 0,2,0,0\rangle$	$^2D_{5/2}$	$\frac{5}{2}^+$	6703^{+20}_{-20}	...	...	†	98^{+25}_{-25}	†

[a]It indicates the experimental mass and decay width values included in the fits.

Since the spin-orbit interaction, $a_{\mathrm{SL}}\,\mathbf{S}_{\mathrm{tot}} \cdot \mathbf{L}_{\mathrm{tot}}$, is a relativistic interaction, the decrease of a_{SL} from the charm to the bottom sector agrees with the fact that the b quark is heavier than the charm quark.

To incorporate both experimental and model uncertainties into the fitting process, we perform a statistical simulation using error propagation. This involves a random sampling of the experimental singly bottom baryon masses from Gaussian distributions with means equal to the central mass values and widths equal to the squared sum of the uncertainties. The fitting procedure was repeated 10^4 times, and in each iteration we used a sampled mass corresponding to an experimentally observed state included in the fit. The model parameters obtained from these 10^4 fits follow Gaussian distributions, where the parameter values are the means of these distributions and the parameter uncertainties are defined as the difference from the distribution quantiles at the 68% confidence level to obtain its confidence interval (CI). This methodology is known as Monte Carlo bootstrap uncertainty propagation [105,107]. The fitting and error

TABLE IV. Same as Table II, but for $\Sigma_b(nnb)$ states. The "†" indicates that no experimental mass or decay width for that state has yet been reported. The symbol "..." indicates that there is no quark-diquark prediction for that state.

$\mathcal{F}=\mathbf{6}_{\mathrm{F}}$	Three-quark			Quark-diquark			Three-quark	
$\Sigma_b(nnb)$ $\lvert l_\lambda, l_\rho, k_\lambda, k_\rho\rangle$	$^{2S+1}L_J$	$\mathbf{J}^P$	Predicted mass (MeV)	$\lvert l_r, k_r\rangle$	Predicted mass (MeV)	Experimental mass (MeV)	Predicted Γ_{Strong} (MeV)	Experimental Γ (MeV)
$N=0$								
$\lvert 0,0,0,0\rangle$	$^2S_{1/2}$	$\frac{1}{2}^+$	5804^{+8}_{-8}	$\lvert 0,0\rangle$	5811^{+13}_{-14}	5813.1 ± 0.3[a]	4^{+2}_{-2}	5.0 ± 0.5
$\lvert 0,0,0,0\rangle$	$^4S_{3/2}$	$\frac{3}{2}^+$	5832^{+8}_{-8}	$\lvert 0,0\rangle$	5835^{+14}_{-13}	5832.5 ± 0.5[a]	10^{+3}_{-3}	9.9 ± 0.9[a]
$N=1$								
$\lvert 1,0,0,0\rangle$	$^2P_{1/2}$	$\frac{1}{2}^-$	6108^{+10}_{-10}	$\lvert 1,0\rangle$	6098^{+14}_{-13}	6096.9 ± 1.8[a]	24^{+6}_{-6}	30 ± 7
$\lvert 1,0,0,0\rangle$	$^4P_{1/2}$	$\frac{1}{2}^-$	6131^{+12}_{-13}	$\lvert 1,0\rangle$	6113^{+15}_{-14}	†	13^{+3}_{-3}	†
$\lvert 1,0,0,0\rangle$	$^2P_{3/2}$	$\frac{3}{2}^-$	6114^{+10}_{-10}	$\lvert 1,0\rangle$	6107^{+14}_{-14}	†	84^{+20}_{-20}	†
$\lvert 1,0,0,0\rangle$	$^4P_{3/2}$	$\frac{3}{2}^-$	6137^{+10}_{-10}	$\lvert 1,0\rangle$	6122^{+14}_{-13}	†	57^{+14}_{-14}	†
$\lvert 1,0,0,0\rangle$	$^4P_{5/2}$	$\frac{5}{2}^-$	6147^{+12}_{-12}	$\lvert 1,0\rangle$	6137^{+15}_{-14}	†	96^{+23}_{-23}	†
$\lvert 0,1,0,0\rangle$	$^2P_{1/2}$	$\frac{1}{2}^-$	6304^{+13}_{-13}	...	...	†	134^{+31}_{-32}	†
$\lvert 0,1,0,0\rangle$	$^2P_{3/2}$	$\frac{3}{2}^-$	6311^{+13}_{-13}	...	...	†	129^{+32}_{-32}	†
$N=2$								
$\lvert 2,0,0,0\rangle$	$^2D_{3/2}$	$\frac{3}{2}^+$	6415^{+15}_{-15}	$\lvert 2,0\rangle$	6388^{+22}_{-22}	†	58^{+15}_{-15}	†
$\lvert 2,0,0,0\rangle$	$^2D_{5/2}$	$\frac{5}{2}^+$	6425^{+16}_{-16}	$\lvert 2,0\rangle$	6404^{+22}_{-22}	†	130^{+33}_{-33}	†
$\lvert 2,0,0,0\rangle$	$^4D_{1/2}$	$\frac{1}{2}^+$	6431^{+21}_{-21}	$\lvert 2,0\rangle$	6393^{+22}_{-22}	†	78^{+19}_{-20}	†
$\lvert 2,0,0,0\rangle$	$^4D_{3/2}$	$\frac{3}{2}^+$	6437^{+17}_{-17}	$\lvert 2,0\rangle$	6403^{+21}_{-21}	†	106^{+27}_{-27}	†
$\lvert 2,0,0,0\rangle$	$^4D_{5/2}$	$\frac{5}{2}^+$	6448^{+15}_{-15}	$\lvert 2,0\rangle$	6418^{+20}_{-21}	†	133^{+33}_{-33}	†
$\lvert 2,0,0,0\rangle$	$^4D_{7/2}$	$\frac{7}{2}^+$	6462^{+20}_{-20}	$\lvert 2,0\rangle$	6440^{+23}_{-22}	†	145^{+38}_{-39}	†
$\lvert 0,0,1,0\rangle$	$^2S_{1/2}$	$\frac{1}{2}^+$	6421^{+15}_{-15}	$\lvert 0,1\rangle$	6397^{+22}_{-21}	†	119^{+29}_{-29}	†
$\lvert 0,0,1,0\rangle$	$^4S_{3/2}$	$\frac{3}{2}^+$	6450^{+15}_{-15}	$\lvert 0,1\rangle$	6421^{+20}_{-21}	†	121^{+30}_{-30}	†
$\lvert 0,0,0,1\rangle$	$^2S_{1/2}$	$\frac{1}{2}^+$	6813^{+24}_{-24}	...	...	†	710^{+156}_{-184}	†
$\lvert 0,0,0,1\rangle$	$^4S_{3/2}$	$\frac{3}{2}^+$	6842^{+24}_{-23}	...	...	†	973^{+243}_{-243}	†
$\lvert 1,1,0,0\rangle$	$^2D_{3/2}$	$\frac{3}{2}^+$	6611^{+19}_{-19}	...	...	†	376^{+93}_{-95}	†
$\lvert 1,1,0,0\rangle$	$^2D_{5/2}$	$\frac{5}{2}^+$	6621^{+20}_{-20}	...	...	†	252^{+67}_{-66}	†
$\lvert 1,1,0,0\rangle$	$^2P_{1/2}$	$\frac{1}{2}^-$	6613^{+19}_{-19}	...	...	†	4^{+1}_{-1}	†
$\lvert 1,1,0,0\rangle$	$^2P_{3/2}$	$\frac{3}{2}^-$	6619^{+20}_{-20}	...	...	†	5^{+1}_{-1}	†
$\lvert 1,1,0,0\rangle$	$^2S_{1/2}$	$\frac{1}{2}^+$	6617^{+19}_{-19}	...	...	†	58^{+15}_{-16}	†
$\lvert 0,2,0,0\rangle$	$^2D_{3/2}$	$\frac{3}{2}^+$	6807^{+23}_{-23}	...	...	†	549^{+130}_{-130}	†
$\lvert 0,2,0,0\rangle$	$^2D_{5/2}$	$\frac{5}{2}^+$	6817^{+24}_{-25}	...	...	†	616^{+172}_{-170}	†
$\lvert 0,2,0,0\rangle$	$^4D_{1/2}$	$\frac{1}{2}^+$	6824^{+27}_{-27}	...	...	†	1349^{+320}_{-321}	†
$\lvert 0,2,0,0\rangle$	$^4D_{3/2}$	$\frac{3}{2}^+$	6830^{+24}_{-24}	...	...	†	741^{+176}_{-175}	†
$\lvert 0,2,0,0\rangle$	$^4D_{5/2}$	$\frac{5}{2}^+$	6840^{+23}_{-23}	...	...	†	376^{+90}_{-89}	†
$\lvert 0,2,0,0\rangle$	$^4D_{7/2}$	$\frac{7}{2}^+$	6854^{+28}_{-28}	...	...	†	1178^{+331}_{-334}	†

[a]It indicates the experimental mass and decay width values included in the fits.

propagation procedures are conducted by means of MINUIT [108] and NumPy [109].

The thirteen masses and their uncertainties used in the fit are from PDG [1] and they are marked with "a" in Tables II–VI.

G. Bottom baryon mass spectrum results

In this section, we present our results for the masses of bottom baryons. We study the Λ_b, Ξ_b, Σ_b, Ξ_b', and Ω_b states simultaneously.

Our predictions for the Λ_b, Ξ_b, Σ_b, Ξ_b', and Ω_b states are reported in Tables II–VI, respectively. In the fourth column of Tables II–VI, we provide the theoretical masses calculated using the three-quark model Hamiltonian given by Eq. (4), along with their errors calculated by means of the Monte Carlo bootstrap method. In the sixth column, we present our theoretical results for the quark-diquark model description calculated by using the Hamiltonian given by Eq. (14). In the seventh column, we report the experimental masses, as from PDG [1].

TABLE V. Same as Table II, but for $\Xi_b'(snb)$ states. The "†" indicates that no experimental mass or decay width for that state has yet been reported. The symbol "..." indicates that there is no quark-diquark prediction for that state.

$\mathcal{F}=\mathbf{6}_{\mathrm{F}}$	Three-quark			Quark-diquark			Three-quark	
$\Xi_b'(snb)$ $\lvert l_\lambda, l_\rho, k_\lambda, k_\rho\rangle$	$^{2S+1}L_J$	$\mathbf{J}^P$	Predicted Mass (MeV)	$\lvert l_r, k_r\rangle$	Predicted Mass (MeV)	Experimental Mass (MeV)	Predicted Γ_{Strong} (MeV)	Experimental Γ (MeV)
$N=0$								
$\lvert 0,0,0,0\rangle$	$^2S_{1/2}$	$\frac{1}{2}^+$	5925^{+6}_{-6}	$\lvert 0,0\rangle$	5927^{+13}_{-13}	5935.02 ± 0.05[a]	0	<0.08
$\lvert 0,0,0,0\rangle$	$^4S_{3/2}$	$\frac{3}{2}^+$	5953^{+7}_{-7}	$\lvert 0,0\rangle$	5951^{+13}_{-14}	5953.8 ± 0.6[a]	$0.2^{+0.1}_{-0.1}$	0.90 ± 0.18
$N=1$								
$\lvert 1,0,0,0\rangle$	$^2P_{1/2}$	$\frac{1}{2}^-$	6198^{+7}_{-7}	$\lvert 1,0\rangle$	6199^{+14}_{-15}	†	3^{+1}_{-1}	†
$\lvert 1,0,0,0\rangle$	$^4P_{1/2}$	$\frac{1}{2}^-$	6220^{+10}_{-10}	$\lvert 1,0\rangle$	6213^{+14}_{-14}	†	4^{+1}_{-1}	†
$\lvert 1,0,0,0\rangle$	$^2P_{3/2}$	$\frac{3}{2}^-$	6204^{+7}_{-7}	$\lvert 1,0\rangle$	6208^{+14}_{-14}	†	29^{+7}_{-7}	†
$\lvert 1,0,0,0\rangle$	$^4P_{3/2}$	$\frac{3}{2}^-$	6226^{+7}_{-7}	$\lvert 1,0\rangle$	6223^{+14}_{-13}	†	8^{+2}_{-2}	†
$\lvert 1,0,0,0\rangle$	$^4P_{5/2}$	$\frac{5}{2}^-$	6237^{+10}_{-10}	$\lvert 1,0\rangle$	6238^{+14}_{-14}	6227.9 ± 1.6	31^{+8}_{-8}	19.9 ± 2.6
$\lvert 0,1,0,0\rangle$	$^2P_{1/2}$	$\frac{1}{2}^-$	6367^{+9}_{-9}	...	...	†	197^{+48}_{-49}	†
$\lvert 0,1,0,0\rangle$	$^2P_{3/2}$	$\frac{3}{2}^-$	6374^{+10}_{-10}	...	...	†	97^{+24}_{-24}	†
$N=2$								
$\lvert 2,0,0,0\rangle$	$^2D_{3/2}$	$\frac{3}{2}^+$	6473^{+12}_{-12}	$\lvert 2,0\rangle$	6474^{+20}_{-22}	†	14^{+5}_{-5}	†
$\lvert 2,0,0,0\rangle$	$^2D_{5/2}$	$\frac{5}{2}^+$	6483^{+13}_{-13}	$\lvert 2,0\rangle$	6489^{+21}_{-22}	†	30^{+11}_{-11}	†
$\lvert 2,0,0,0\rangle$	$^4D_{1/2}$	$\frac{1}{2}^+$	6489^{+18}_{-18}	$\lvert 2,0\rangle$	6479^{+22}_{-22}	†	25^{+10}_{-10}	†
$\lvert 2,0,0,0\rangle$	$^4D_{3/2}$	$\frac{3}{2}^+$	6495^{+14}_{-14}	$\lvert 2,0\rangle$	6488^{+21}_{-21}	†	35^{+12}_{-12}	†
$\lvert 2,0,0,0\rangle$	$^4D_{5/2}$	$\frac{5}{2}^+$	6506^{+11}_{-11}	$\lvert 2,0\rangle$	6504^{+20}_{-21}	†	46^{+13}_{-13}	†
$\lvert 2,0,0,0\rangle$	$^4D_{7/2}$	$\frac{7}{2}^+$	6520^{+18}_{-18}	$\lvert 2,0\rangle$	6526^{+20}_{-22}	†	47^{+14}_{-14}	†
$\lvert 0,0,1,0\rangle$	$^2S_{1/2}$	$\frac{1}{2}^+$	6479^{+11}_{-12}	$\lvert 0,1\rangle$	6483^{+21}_{-22}	†	47^{+14}_{-14}	†
$\lvert 0,0,1,0\rangle$	$^4S_{3/2}$	$\frac{3}{2}^+$	6508^{+12}_{-12}	$\lvert 0,1\rangle$	6507^{+20}_{-21}	†	79^{+26}_{-26}	†
$\lvert 0,0,0,1\rangle$	$^2S_{1/2}$	$\frac{1}{2}^+$	6818^{+19}_{-19}	...	...	†	599^{+149}_{-149}	†
$\lvert 0,0,0,1\rangle$	$^4S_{3/2}$	$\frac{3}{2}^+$	6847^{+19}_{-19}	...	...	†	630^{+157}_{-157}	†
$\lvert 1,1,0,0\rangle$	$^2D_{3/2}$	$\frac{3}{2}^+$	6642^{+15}_{-15}	...	...	†	234^{+59}_{-60}	†
$\lvert 1,1,0,0\rangle$	$^2D_{5/2}$	$\frac{5}{2}^+$	6653^{+17}_{-17}	...	...	†	116^{+30}_{-29}	†
$\lvert 1,1,0,0\rangle$	$^2P_{1/2}$	$\frac{1}{2}^-$	6644^{+15}_{-15}	...	...	†	3^{+1}_{-1}	†
$\lvert 1,1,0,0\rangle$	$^2P_{3/2}$	$\frac{3}{2}^-$	6651^{+16}_{-16}	...	...	†	3^{+1}_{-1}	†
$\lvert 1,1,0,0\rangle$	$^2S_{1/2}$	$\frac{1}{2}^+$	6649^{+15}_{-15}	...	...	†	59^{+14}_{-14}	†
$\lvert 0,2,0,0\rangle$	$^2D_{3/2}$	$\frac{3}{2}^+$	6812^{+19}_{-19}	...	...	†	315^{+81}_{-85}	†
$\lvert 0,2,0,0\rangle$	$^2D_{5/2}$	$\frac{5}{2}^+$	6822^{+20}_{-20}	...	...	†	209^{+54}_{-55}	†
$\lvert 0,2,0,0\rangle$	$^4D_{1/2}$	$\frac{1}{2}^+$	6828^{+22}_{-22}	...	...	†	529^{+156}_{-151}	†
$\lvert 0,2,0,0\rangle$	$^4D_{3/2}$	$\frac{3}{2}^+$	6834^{+20}_{-20}	...	...	†	364^{+94}_{-93}	†
$\lvert 0,2,0,0\rangle$	$^4D_{5/2}$	$\frac{5}{2}^+$	6845^{+19}_{-19}	...	...	†	194^{+48}_{-47}	†
$\lvert 0,2,0,0\rangle$	$^4D_{7/2}$	$\frac{7}{2}^+$	6859^{+24}_{-24}	...	...	†	349^{+98}_{-98}	†

[a]It indicates the experimental mass and decay width values included in the fits.

Furthermore, we compare our theoretical results with the experimental data [1] in Figs. 3–7 for the three-quark model, and in Figs. 8–12 for the quark-diquark model.

As one can observe, our theoretical mass predictions are in good agreement with the available experimental data. It is noteworthy that the model of Ref. [98] has relatively few parameters, specifically, eleven. We use data from 13 well-established singly bottom baryons out of 22 states; hence, the remaining states are predictions.

In addition, in Tables VII–XI we compare our mass spectra with the previous three-quark studies such as NRQM [33,39,41], QCDSR [48,50,51], χQM [56], and LQCD [59]. However the previous articles did not give explicit internal construction, but only the flavor and total J of the states; thus, we made a tentative assignment using the values of the masses and the total spin J.

In Tables VII–XI, we do report the following results: a variational approach of the non-relativistic three-body problem in singly bottom baryons was done but only

TABLE VI. Same as Table II, but for $\Omega_b(ssb)$ states. The "†" indicates that no experimental mass or decay width for that state has yet been reported. The symbol "..." indicates that there is no quark-diquark prediction for that state.

$\mathcal{F}=\mathbf{6}_{\mathrm{F}}$	Three-quark			Quark-diquark			Three-quark	
$\Omega_b(ssb)$ $\lvert l_\lambda, l_\rho, k_\lambda, k_\rho\rangle$	$^{2S+1}L_J$	$\mathbf{J}^P$	Predicted mass (MeV)	$\lvert l_r, k_r\rangle$	Predicted mass (MeV)	Experimental mass (MeV)	Predicted Γ_{Strong} (MeV)	Experimental Γ (MeV)
$N=0$								
$\lvert 0,0,0,0\rangle$	$^2S_{1/2}$	$\frac{1}{2}^+$	6064^{+8}_{-8}	$\lvert 0,0\rangle$	6059^{+13}_{-12}	6045.2 ± 1.2[a]	0	≈0
$\lvert 0,0,0,0\rangle$	$^4S_{3/2}$	$\frac{3}{2}^+$	6093^{+9}_{-8}	$\lvert 0,0\rangle$	6083^{+13}_{-14}	†	0	†
$N=1$								
$\lvert 1,0,0,0\rangle$	$^2P_{1/2}$	$\frac{1}{2}^-$	6315^{+7}_{-7}	$\lvert 1,0\rangle$	6318^{+9}_{-10}	6315.6 ± 0.6[a]	5^{+1}_{-1}	<4.2
$\lvert 1,0,0,0\rangle$	$^4P_{1/2}$	$\frac{1}{2}^-$	6337^{+10}_{-10}	$\lvert 1,0\rangle$	6333^{+11}_{-11}	6330.3 ± 0.6[a]	11^{+3}_{-3}	<4.7
$\lvert 1,0,0,0\rangle$	$^2P_{3/2}$	$\frac{3}{2}^-$	6321^{+8}_{-8}	$\lvert 1,0\rangle$	6328^{+10}_{-10}	6339.7 ± 0.6	24^{+6}_{-6}	<1.8
$\lvert 1,0,0,0\rangle$	$^4P_{3/2}$	$\frac{3}{2}^-$	6343^{+7}_{-7}	$\lvert 1,0\rangle$	6342^{+10}_{-10}	6349.8 ± 0.6	6^{+2}_{-2}	<3.2
$\lvert 1,0,0,0\rangle$	$^4P_{5/2}$	$\frac{5}{2}^-$	6353^{+11}_{-11}	$\lvert 1,0\rangle$	6358^{+11}_{-10}	†	40^{+10}_{-10}	†
$\lvert 0,1,0,0\rangle$	$^2P_{1/2}$	$\frac{1}{2}^-$	6465^{+9}_{-8}	⋯	⋯	†	10^{+2}_{-2}	†
$\lvert 0,1,0,0\rangle$	$^2P_{3/2}$	$\frac{3}{2}^-$	6471^{+10}_{-10}	⋯	⋯	†	54^{+14}_{-14}	†
$N=2$								
$\lvert 2,0,0,0\rangle$	$^2D_{3/2}$	$\frac{3}{2}^+$	6568^{+11}_{-11}	$\lvert 2,0\rangle$	6581^{+14}_{-15}	†	4^{+1}_{-1}	†
$\lvert 2,0,0,0\rangle$	$^2D_{5/2}$	$\frac{5}{2}^+$	6578^{+12}_{-12}	$\lvert 2,0\rangle$	6596^{+15}_{-15}	†	10^{+2}_{-2}	†
$\lvert 2,0,0,0\rangle$	$^4D_{1/2}$	$\frac{1}{2}^+$	6584^{+17}_{-17}	$\lvert 2,0\rangle$	6585^{+17}_{-17}	†	$1.0^{+0.3}_{-0.3}$	†
$\lvert 2,0,0,0\rangle$	$^4D_{3/2}$	$\frac{3}{2}^+$	6590^{+13}_{-13}	$\lvert 2,0\rangle$	6595^{+16}_{-16}	†	3^{+1}_{-1}	†
$\lvert 2,0,0,0\rangle$	$^4D_{5/2}$	$\frac{5}{2}^+$	6600^{+10}_{-10}	$\lvert 2,0\rangle$	6610^{+15}_{-15}	†	8^{+2}_{-2}	†
$\lvert 2,0,0,0\rangle$	$^4D_{7/2}$	$\frac{7}{2}^+$	6614^{+18}_{-18}	$\lvert 2,0\rangle$	6632^{+17}_{-16}	†	18^{+10}_{-9}	†
$\lvert 0,0,1,0\rangle$	$^2S_{1/2}$	$\frac{1}{2}^+$	6574^{+11}_{-11}	$\lvert 0,1\rangle$	6590^{+15}_{-15}	†	20^{+6}_{-6}	†
$\lvert 0,0,1,0\rangle$	$^4S_{3/2}$	$\frac{3}{2}^+$	6602^{+11}_{-11}	$\lvert 0,1\rangle$	6614^{+15}_{-15}	†	17^{+6}_{-6}	†
$\lvert 0,0,0,1\rangle$	$^2S_{1/2}$	$\frac{1}{2}^+$	6874^{+17}_{-17}	⋯	⋯	†	398^{+119}_{-119}	†
$\lvert 0,0,0,1\rangle$	$^4S_{3/2}$	$\frac{3}{2}^+$	6902^{+17}_{-17}	⋯	⋯	†	257^{+64}_{-64}	†
$\lvert 1,1,0,0\rangle$	$^2D_{3/2}$	$\frac{3}{2}^+$	6718^{+14}_{-14}	⋯	⋯	†	116^{+39}_{-39}	†
$\lvert 1,1,0,0\rangle$	$^2D_{5/2}$	$\frac{5}{2}^+$	6728^{+15}_{-15}	⋯	⋯	†	82^{+22}_{-23}	†
$\lvert 1,1,0,0\rangle$	$^2P_{1/2}$	$\frac{1}{2}^-$	6720^{+14}_{-14}	⋯	⋯	†	$1.1^{+0.4}_{-0.4}$	†
$\lvert 1,1,0,0\rangle$	$^2P_{3/2}$	$\frac{3}{2}^-$	6726^{+15}_{-15}	⋯	⋯	†	2^{+1}_{-1}	†
$\lvert 1,1,0,0\rangle$	$^2S_{1/2}$	$\frac{1}{2}^+$	6724^{+14}_{-14}	⋯	⋯	†	72^{+21}_{-21}	†
$\lvert 0,2,0,0\rangle$	$^2D_{3/2}$	$\frac{3}{2}^+$	6868^{+17}_{-17}	⋯	⋯	†	180^{+56}_{-54}	†
$\lvert 0,2,0,0\rangle$	$^2D_{5/2}$	$\frac{5}{2}^+$	6878^{+19}_{-19}	⋯	⋯	†	157^{+39}_{-39}	†
$\lvert 0,2,0,0\rangle$	$^4D_{1/2}$	$\frac{1}{2}^+$	6884^{+21}_{-21}	⋯	⋯	†	126^{+31}_{-32}	†
$\lvert 0,2,0,0\rangle$	$^4D_{3/2}$	$\frac{3}{2}^+$	6890^{+18}_{-18}	⋯	⋯	†	195^{+47}_{-47}	†
$\lvert 0,2,0,0\rangle$	$^4D_{5/2}$	$\frac{5}{2}^+$	6900^{+17}_{-17}	⋯	⋯	†	172^{+41}_{-41}	†
$\lvert 0,2,0,0\rangle$	$^4D_{7/2}$	$\frac{7}{2}^+$	6914^{+23}_{-23}	⋯	⋯	†	230^{+62}_{-63}	†

[a]It indicates the experimental mass and decay width values included in the fits.

for ground states [33]. The chiral quark model [36] was applied only for S and P wave states. The Regge phenomenology [42], was applied just for singly bottom ground states. The QCD-inspired relativistic quark-diquark picture [37,38]. We did not add the results of [40] because only ground states and few exited states for Λ_b, and Ξ_b were considered. In Ref. [47], the hypercentral constituent quark model, was applied to study only P-wave Ω_b states. The QCD sum rules [27,49] only include S- and P-wave states. Finally, we did not add the results using Schwinger-Dyson equation approach from Ref. [53], because only ground states were considered. Silvestre-Brac made the calculation of the mass spectra for Λ_b, Σ_b, Ξ_b, Ξ_b', and Ω_b using a non-relativistic quark model within the Faddeev formalism [29]. The Λ_b, Σ_b, Ξ_b, Ξ_b', and Ω_b ground and excited states (up to 1 GeV) were displayed in the figures with a large energy scale, but the numerical values for the excited states were not provided in a table; thus, we could not add his results to our tables.

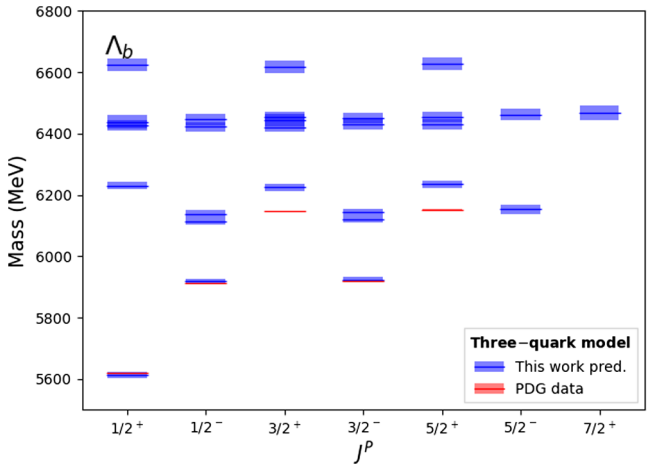

FIG. 3. Λ_b mass spectra and tentative quantum number assignments based on the three-quark model Hamiltonian of Eqs. (1) and (2). The theoretical predictions and their uncertainties (blue lines and bands) are compared with the experimental results (red lines and bands) given in the PDG [1]. The experimental errors are too small to be reported on this energy scale.

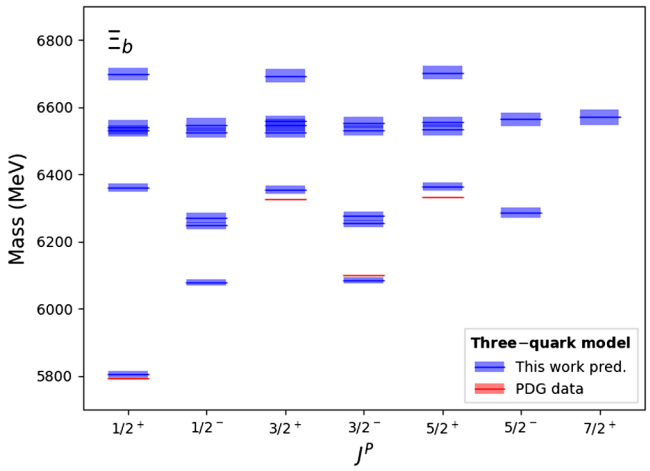

FIG. 4. Same as Fig. 3, but for Ξ_b states.

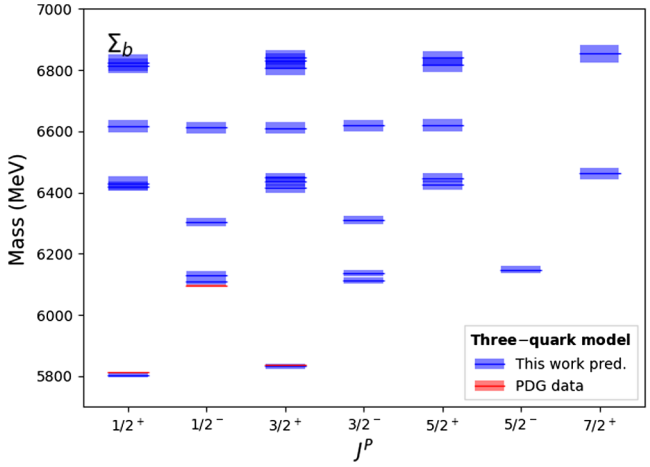

FIG. 5. Same as Fig. 3, but for Σ_b states.

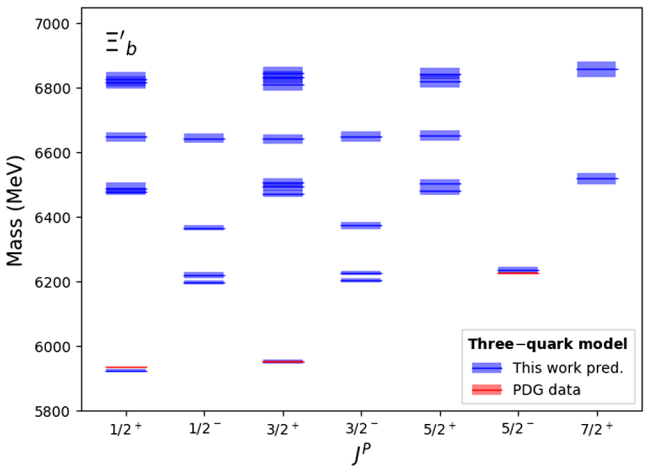

FIG. 6. Same as Fig. 3, but for Ξ'_b states.

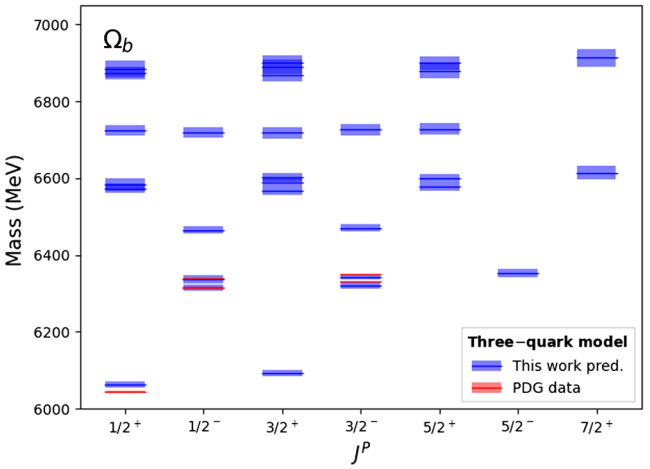

FIG. 7. Same as Fig. 3, but for Ω_b states.

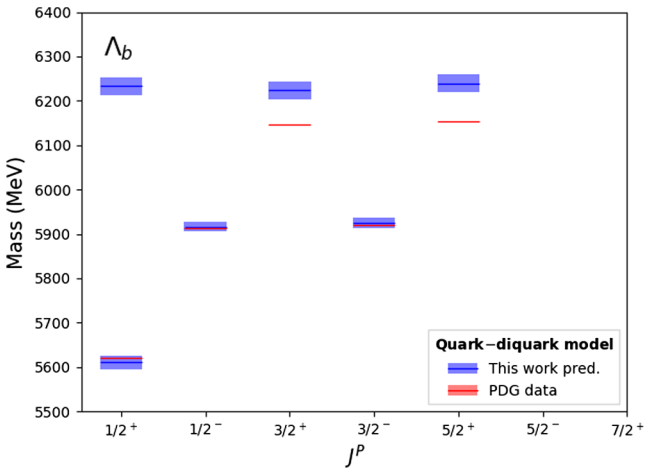

FIG. 8. Λ_b mass spectra and tentative quantum number assignments based on the quark-diquark model Hamiltonian of Eqs. (1) and (12). The theoretical predictions and their uncertainties (blue lines and bands) are compared with the experimental results (red lines and bands) given in the PDG [1]. The experimental errors are too small to be reported on this energy scale.

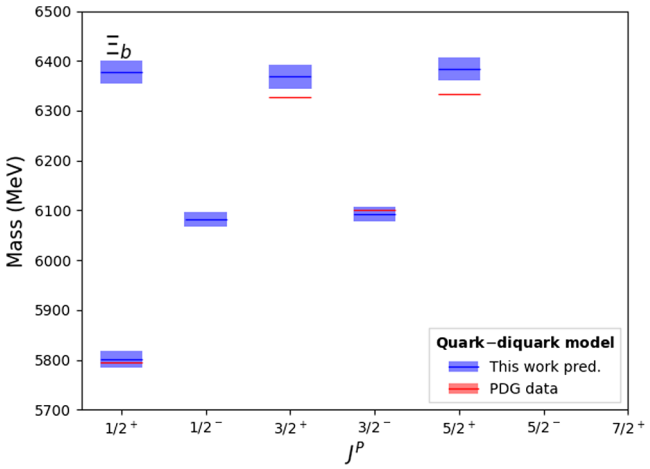

FIG. 9. Same as Fig. 8, but for Ξ_b states.

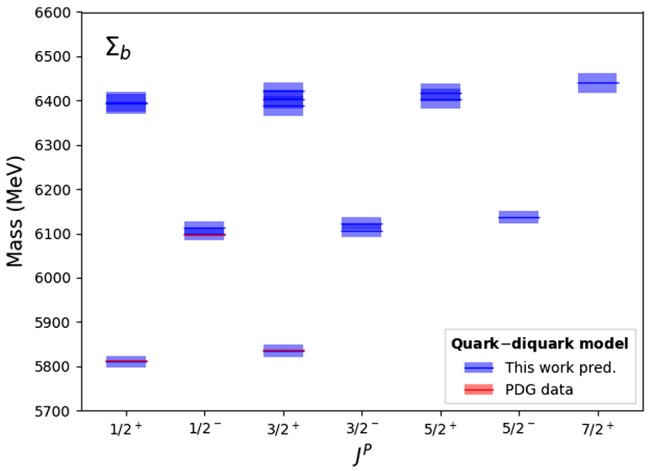

FIG. 10. Same as Fig. 8, but for Σ_b states.

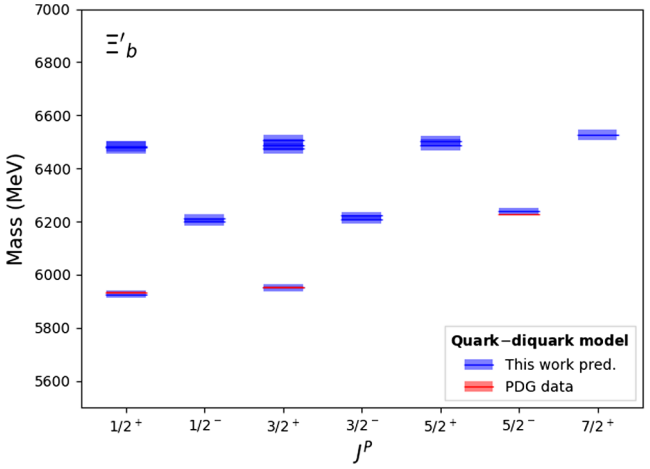

FIG. 11. Same as Fig. 8, but for Ξ'_b states.

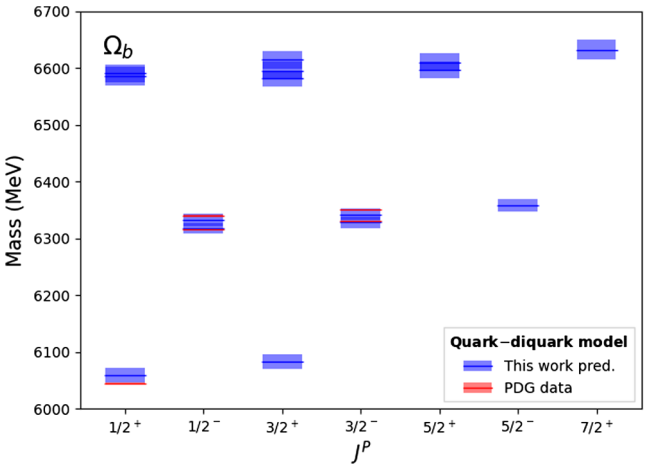

FIG. 12. Same as Fig. 8, but for Λ_b states.

Only NRQM [39,41], RQM [26] and QCD sum rules [48,50,51] made predictions for some D-wave states, see Tables VII–XI. However, they did not provide predictions for all possible mass states within the D-wave. Due to the lack of data, we cannot reach any conclusion about the differences between the predictions for each model. It is crucial to emphasize that the validation of the model of Ref. [98] requires the identification of the bottom baryon multiplets through additional data. However, the difficulty in identifying new bottom baryons within the data remains a challenge.

III. STRONG DECAY WIDTHS

We investigate the open-flavor strong decay widths of the Λ_b, Ξ_b, Σ_b, Ξ'_b, and Ω_b states. We calculate the three-quark strong-decay widths by using the $^3P_0$ model. In the $^3P_0$ model the transition operator is given by [102,110–114].

$$T^\dagger = -3\gamma_0 \int d\mathbf{p}_4 d\mathbf{p}_5 \delta(\mathbf{p}_4+\mathbf{p}_5) C_{45} F_{45} \times [\chi_{45} \times \mathcal{Y}_1(\mathbf{p}_4-\mathbf{p}_5)]_0^{(0)} b_4^\dagger(\mathbf{p}_4) d_5^\dagger(\mathbf{p}_5). \quad (16)$$

Here, γ_0 is the pair-creation strength, and $b_4^\dagger(\mathbf{p}_4)$ and $d_5^\dagger(\mathbf{p}_5)$ are the creation operators for a quark and an antiquark with momenta $\mathbf{p}_4$ and $\mathbf{p}_5$, respectively.

The $q\bar{q}$ pair is characterized by a color-singlet wave function C_{45}, a flavor-singlet wave function F_{45}, a spin-triplet wave function χ_{45} with spin $\mathbf{S}_{45}=\mathbf{1}$ and a solid spherical harmonic $\mathcal{Y}_1(\mathbf{p}_4-\mathbf{p}_5)$, since the quark and antiquark are in a relative P-wave.

According to the $^3P_0$ model, the decay of the baryon A proceeds via the creation from the vacuum of the $q\bar{q}$ pair; this pair recombines into an outgoing baryon B and a meson C, as depicted in Fig. 13. The total strong decay width Γ_{Strong} is the sum of the partial decay width of the

TABLE VII. Comparison of our predicted three-quark $\Lambda_b(nnb)$ masses with other three-quark model predictions (in MeV). The flavor multiplet is indicated by the symbol $\mathcal{F}$. The first column contains the three-quark model state, $|l_\lambda, l_\rho, k_\lambda, k_\rho\rangle$, where $l_{\lambda,\rho}$ are the orbital angular momenta and $k_{\lambda,\rho}$ the number of nodes of the λ and ρ oscillators. The second column displays the spectroscopic notation $^{2S+1}L_J$ for each state. The third column reports our predicted masses, computed within the three-quark model. Our results are compared with those of Refs. [41] (fourth column), [48,50,51] (fifth column), [39] (sixth column), [56] (seventh column), [59] (eighth column), [35] (ninth column), [33] (tenth column), and [26] (eleventh column). Our theoretical results are also compared with the experimental masses as from PDG [1] (twelfth column). The symbol "..." indicates that there is no prediction for that state. The "†" indicates that there is no reported experimental mass for that state up to now.

$\Lambda_b(snb)$ $\lvert l_\lambda, l_\rho, k_\lambda, k_\rho\rangle$	$\mathcal{F}=\bar{\mathbf{3}}_F$ $^{2S+1}L_J$	This work	NRQM [41]	QCDSR [48,50,51]	NRQM [39]	χQM [56]	LQCD [59]	CQC [35]	NRQM [33]	RQM [26]	Experimental
$N=0$											
$\lvert 0,0,0,0\rangle$	$^2S_{1/2}$	5613^{+9}_{-9}	5618	5637	5612	5620	5667	5624	5629	5585	5619.60 ± 0.17
$N=1$											
$\lvert 1,0,0,0\rangle$	$^2P_{1/2}$	5918^{+8}_{-8}	5938	6010	5939	5914	...	5947	...	5912	5912.19 ± 0.17
$\lvert 1,0,0,0\rangle$	$^2P_{3/2}$	5924^{+8}_{-8}	5939	6010	5941	5927	...	...	...	5920	5920.09 ± 0.17
$\lvert 0,1,0,0\rangle$	$^2P_{1/2}$	6114^{+10}_{-10}	6236	...	6180	6207	...	6245	...	6100	†
$\lvert 0,1,0,0\rangle$	$^4P_{1/2}$	6137^{+14}_{-14}	6273	5870	...	6233	...	...	...	6165	†
$\lvert 0,1,0,0\rangle$	$^2P_{3/2}$	6121^{+10}_{-10}	6273	...	6191	...	...	...	...	6185	†
$\lvert 0,1,0,0\rangle$	$^4P_{3/2}$	6143^{+12}_{-12}	6285	5880	...	...	...	...	...	6190	†
$\lvert 0,1,0,0\rangle$	$^4P_{5/2}$	6153^{+14}_{-14}	6289	...	6206	...	...	...	...	6205	†
$N=2$											
$\lvert 2,0,0,0\rangle$	$^2D_{3/2}$	6225^{+13}_{-13}	6211	6010	6181	6172	...	6388	...	6145	6146.2 ± 0.4
$\lvert 2,0,0,0\rangle$	$^2D_{5/2}$	6235^{+13}_{-13}	6212	6010	6183	6178	...	...	...	6165	6152.5 ± 0.4
$\lvert 0,0,1,0\rangle$	$^2S_{1/2}$	6231^{+12}_{-12}	6153	...	6107	6121	...	6106	...	6045	†
$\lvert 0,0,0,1\rangle$	$^2S_{1/2}$	6624^{+21}_{-21}	...	...	...	...	...	...	...	...	†
$\lvert 1,1,0,0\rangle$	$^2D_{3/2}$	6421^{+16}_{-16}	6488	...	6401	...	...	...	...	...	†
$\lvert 1,1,0,0\rangle$	$^2D_{5/2}$	6431^{+17}_{-17}	6530	6560	6422	...	...	...	...	...	†
$\lvert 1,1,0,0\rangle$	$^4D_{1/2}$	6438^{+22}_{-22}	6467	...	...	...	...	...	...	...	†
$\lvert 1,1,0,0\rangle$	$^4D_{3/2}$	6444^{+19}_{-19}	6511	6360	...	...	...	...	...	...	†
$\lvert 1,1,0,0\rangle$	$^4D_{5/2}$	6454^{+17}_{-17}	6539	6360	...	...	...	...	...	...	†
$\lvert 1,1,0,0\rangle$	$^4D_{7/2}$	6468^{+23}_{-22}	...	6560	6433	...	...	...	...	...	†
$\lvert 1,1,0,0\rangle$	$^2P_{1/2}$	6423^{+16}_{-16}	...	...	...	...	...	...	...	6260	†
$\lvert 1,1,0,0\rangle$	$^2P_{3/2}$	6429^{+17}_{-17}	...	...	...	...	...	...	...	6265	†
$\lvert 1,1,0,0\rangle$	$^4P_{1/2}$	6446^{+19}_{-18}	...	6220	...	...	...	...	...	6470	†
$\lvert 1,1,0,0\rangle$	$^4P_{3/2}$	6452^{+17}_{-17}	...	6230	...	...	...	...	...	6510	†
$\lvert 1,1,0,0\rangle$	$^4P_{5/2}$	6462^{+19}_{-19}	...	...	...	...	...	...	...	6360	†
$\lvert 1,1,0,0\rangle$	$^4S_{3/2}$	6456^{+17}_{-18}	...	...	...	...	...	...	...	...	†
$\lvert 1,1,0,0\rangle$	$^2S_{1/2}$	6427^{+16}_{-16}	...	...	...	...	...	...	...	...	†
$\lvert 0,2,0,0\rangle$	$^2D_{3/2}$	6618^{+20}_{-20}	...	6520	...	...	...	6637	...	...	†
$\lvert 0,2,0,0\rangle$	$^2D_{5/2}$	6628^{+21}_{-22}	...	6520	...	...	...	...	...	...	†

singly bottom baryon A decaying to the open-flavor channels BC. That is, $\Gamma_{\text{Strong}} = \sum_{BC} \Gamma_{\text{Strong}}(A \to BC)$, where the strong partial decay widths $\Gamma_{\text{Strong}}(A \to BC)$ are calculated by using

$$\Gamma_{\text{Strong}}(A \to BC) = \frac{2\pi\gamma_0^2}{2J_A+1}\Phi_{A\to BC}\sum_{M_{J_A},M_{J_B}} |\mathcal{M}^{M_{J_A},M_{J_B}}|^2, \tag{17}$$

where $\Phi_{A\to BC}$ is the relativistic phase space factor [110,114] and

$$\mathcal{M}^{M_{J_A},M_{J_B}} = \langle \Psi_B \Psi_C | T^\dagger | \Psi_A \rangle \tag{18}$$

is the $^3P_0$ transition amplitude calculated over the eigenstates of the Hamiltonian operator of Eq. (2), Ψ_A, Ψ_B, and Ψ_C, which are the harmonic oscillator wave functions. The conventions used for the h.o. wave functions are given in Ref. [102]. In Eq. (18), $T^\dagger$ is the $^3P_0$ transition operator defined in Eq. (16), and the sum runs over the third components M_{J_A} and M_{J_B} of the total angular momenta J_A and J_B of A and B, respectively. Since we fitted all the parameters of the model (see Table I) to the experimental masses reported in the PDG [1], the harmonic oscillator

TABLE VIII. Same as Table VII, but for $\Xi_b(snb)$ states. The "†" indicates that there is no reported experimental mass for that state up to now.

$\Xi_b(snb)$ $\lvert l_\lambda, l_\rho, k_\lambda, k_\rho\rangle$	$\mathcal{F}=\bar{\mathbf{3}}_{\mathrm{F}}$ $^{2S+1}L_J$	This work	NRQM [41]	QCDSR [48,50,51]	NRQM [39]	χQM [56]	LQCD [59]	CQC [35]	NRQM [33]	RQM [26]	Experimental
$N=0$											
$\lvert 0,0,0,0\rangle$	$^2S_{1/2}$	5806^{+9}_{-9}	⋯	5780	5844	5796	5901	5801	5800	⋯	5794.5 ± 0.6
$N=1$											
$\lvert 1,0,0,0\rangle$	$^2P_{1/2}$	6079^{+9}_{-9}	⋯	6270	6108	6069	⋯	6109	⋯	⋯	†
$\lvert 1,0,0,0\rangle$	$^2P_{3/2}$	6085^{+9}_{-9}	⋯	6280	6110	6080	⋯	⋯	⋯	⋯	6100.3 ± 0.6
$\lvert 0,1,0,0\rangle$	$^2P_{1/2}$	6248^{+11}_{-11}	⋯	⋯	⋯	6084	⋯	6223	⋯	⋯	†
$\lvert 0,1,0,0\rangle$	$^4P_{1/2}$	6271^{+15}_{-15}	⋯	6060	⋯	6540	⋯	⋯	⋯	⋯	†
$\lvert 0,1,0,0\rangle$	$^2P_{3/2}$	6255^{+11}_{-11}	⋯	⋯	⋯	⋯	⋯	⋯	⋯	⋯	†
$\lvert 0,1,0,0\rangle$	$^4P_{3/2}$	6277^{+14}_{-14}	⋯	6070	⋯	6554	⋯	⋯	⋯	⋯	†
$\lvert 0,1,0,0\rangle$	$^4P_{5/2}$	6287^{+15}_{-15}	⋯	⋯	6312	⋯	⋯	⋯	⋯	⋯	†
$N=2$											
$\lvert 2,0,0,0\rangle$	$^2D_{3/2}$	6354^{+13}_{-13}	⋯	6190	6294	6307	⋯	⋯	⋯	⋯	6327.3 ± 2.5
$\lvert 2,0,0,0\rangle$	$^2D_{5/2}$	6364^{+13}_{-13}	⋯	6190	6333	6313	⋯	⋯	⋯	⋯	6332.7 ± 2.5
$\lvert 0,0,1,0\rangle$	$^2S_{1/2}$	6360^{+12}_{-13}	⋯	⋯	⋯	6260	⋯	6258	⋯	⋯	†
$\lvert 0,0,0,1\rangle$	$^2S_{1/2}$	6699^{+19}_{-19}	⋯	⋯	⋯	⋯	⋯	⋯	⋯	⋯	†
$\lvert 1,1,0,0\rangle$	$^2D_{3/2}$	6524^{+16}_{-16}	⋯	⋯	⋯	⋯	⋯	⋯	⋯	⋯	†
$\lvert 1,1,0,0\rangle$	$^2D_{5/2}$	6534^{+17}_{-17}	⋯	6860	⋯	⋯	⋯	⋯	⋯	⋯	†
$\lvert 1,1,0,0\rangle$	$^4D_{1/2}$	6540^{+22}_{-22}	⋯	⋯	⋯	⋯	⋯	⋯	⋯	⋯	†
$\lvert 1,1,0,0\rangle$	$^4D_{3/2}$	6546^{+19}_{-19}	⋯	6840	⋯	⋯	⋯	⋯	⋯	⋯	†
$\lvert 1,1,0,0\rangle$	$^4D_{5/2}$	6556^{+17}_{-18}	⋯	6840	⋯	⋯	⋯	⋯	⋯	⋯	†
$\lvert 1,1,0,0\rangle$	$^4D_{7/2}$	6570^{+22}_{-22}	⋯	6860	6524	⋯	⋯	⋯	⋯	⋯	†
$\lvert 1,1,0,0\rangle$	$^2P_{1/2}$	6526^{+16}_{-16}	⋯	⋯	⋯	⋯	⋯	⋯	⋯	⋯	†
$\lvert 1,1,0,0\rangle$	$^2P_{3/2}$	6532^{+16}_{-16}	⋯	⋯	⋯	⋯	⋯	⋯	⋯	⋯	†
$\lvert 1,1,0,0\rangle$	$^4P_{1/2}$	6548^{+19}_{-19}	⋯	6820	⋯	⋯	⋯	⋯	⋯	⋯	†
$\lvert 1,1,0,0\rangle$	$^4P_{3/2}$	6554^{+18}_{-17}	⋯	6820	⋯	⋯	⋯	⋯	⋯	⋯	†
$\lvert 1,1,0,0\rangle$	$^4P_{5/2}$	6564^{+19}_{-19}	⋯	⋯	⋯	⋯	⋯	⋯	⋯	⋯	†
$\lvert 1,1,0,0\rangle$	$^4S_{3/2}$	6558^{+18}_{-18}	⋯	⋯	⋯	⋯	⋯	⋯	⋯	⋯	†
$\lvert 1,1,0,0\rangle$	$^2S_{1/2}$	6530^{+16}_{-16}	⋯	⋯	⋯	⋯	⋯	⋯	⋯	⋯	†
$\lvert 0,2,0,0\rangle$	$^2D_{3/2}$	6693^{+20}_{-19}	⋯	6570	⋯	⋯	⋯	⋯	⋯	⋯	†
$\lvert 0,2,0,0\rangle$	$^2D_{5/2}$	6703^{+20}_{-20}	⋯	6570	⋯	⋯	⋯	⋯	⋯	⋯	†

wave functions do not depend on any free parameters. The $\alpha^2_{\rho(\lambda)}$ are related to the harmonic oscillator frequencies, $\omega_{\rho(\lambda)}$, through m_ρ and m_λ: $\alpha^2_{\rho(\lambda)} = \omega_{\rho(\lambda)} m_{\rho(\lambda)}$. Thus, $\alpha_{\rho(\lambda)}$ depends on the harmonic oscillator constant K_b and the quark masses, which are fitted to reproduce the bottom baryon mass spectra (see Table I). In the Λ_b and Σ_b sectors, $\alpha_\rho = 381$ MeV and $\alpha_\lambda = 487$ MeV; in the Ξ_b and Ξ_b' sectors $\alpha_\rho = 403$ MeV and $\alpha_\lambda = 512$ MeV; and in the Ω_b sector, $\alpha_\rho = 425$ MeV and $\alpha_\lambda = 536$ MeV. The only free parameter is the pair-creation strength of the strong decays, $\gamma_0 = 21 \pm 3$, which is fitted to reproduce the $\Sigma_b^* \to \Lambda_b \pi$ experimental strong decay width [1], this means that the other decay widths reported in the present manuscript are predictions. The uncertainty in γ_0 is computed as the sum in quadrature of the model uncertainty $\sigma_{\mathrm{mod}} = 2.4$ and the experimental uncertainty $\sigma_{\mathrm{exp}} = 1.0$. Moreover, when we calculate the strong decay widths, we take into account the uncertainties associated with the mass model parameters, the decay product masses, and the pair-creation strength γ_0. The procedure of error propagation for the strong decay widths of the three-quark system was carried out by means of the bootstrap method (see Sec. II F).

The decay widths are calculated for the 1S, 1P, 1D, 2P, and 2S singly bottom baryons; the available open-flavor channels include the multiplets of the light pseudoscalar and vector mesons and the heavy bottom mesons. In the calculation of the strong-decay width, there is an extra parameter R related to the meson size: we use $R = 2.1$ GeV^{-1} [102,115,116].

TABLE IX. Same as Table VII, but for $\Sigma_b(nnb)$ states. The "†" indicates that there is no reported experimental mass for that state up to now.

$\Sigma_b(nnb)$ $\lvert l_\lambda, l_\rho, k_\lambda, k_\rho\rangle$	$\mathcal{F}=\mathbf{6}_F$ $^{2S+1}L_J$	This work	NRQM [41]	QCDSR [48,50,51]	NRQM [39]	χQM [56]	LQCD [59]	CQC [35]	NRQM [33]	RQM [26]	Experimental
$N=0$											
$\lvert 0,0,0,0\rangle$	$^2S_{1/2}$	5804^{+8}_{-8}	5823	5809	5833	5810	5820	5807	5844	5795	5813.1 ± 0.3
$\lvert 0,0,0,0\rangle$	$^4S_{3/2}$	5832^{+8}_{-8}	5845	5835	5858	5829	5836	5829	5874	5805	5832.5 ± 0.5
$N=1$											
$\lvert 1,0,0,0\rangle$	$^2P_{1/2}$	6108^{+10}_{-10}	6127	⋯	6099	6043	⋯	6103	⋯	6070	6096.9 ± 1.8
$\lvert 1,0,0,0\rangle$	$^4P_{1/2}$	6131^{+12}_{-13}	6135	6020	6106	6065	⋯	⋯	⋯	6070	†
$\lvert 1,0,0,0\rangle$	$^2P_{3/2}$	6114^{+10}_{-10}	6132	⋯	6101	6079	⋯	⋯	⋯	6070	†
$\lvert 1,0,0,0\rangle$	$^4P_{3/2}$	6137^{+10}_{-10}	6141	5960	6105	6117	⋯	⋯	⋯	6085	†
$\lvert 1,0,0,0\rangle$	$^4P_{5/2}$	6147^{+12}_{-12}	6144	5980	6172	6129	⋯	⋯	⋯	6090	†
$\lvert 0,1,0,0\rangle$	$^2P_{1/2}$	6304^{+13}_{-13}	6246	5910	⋯	⋯	⋯	6241	⋯	6170	†
$\lvert 0,1,0,0\rangle$	$^2P_{3/2}$	6311^{+13}_{-13}	6246	5920	⋯	⋯	⋯	⋯	⋯	6180	†
$N=2$											
$\lvert 2,0,0,0\rangle$	$^2D_{3/2}$	6415^{+15}_{-15}	6356	⋯	6308	6316	⋯	6260	⋯	6250	†
$\lvert 2,0,0,0\rangle$	$^2D_{5/2}$	6425^{+16}_{-16}	6397	⋯	6325	6341	⋯	⋯	⋯	6325	†
$\lvert 2,0,0,0\rangle$	$^4D_{1/2}$	6431^{+21}_{-21}	6343	⋯	⋯	6304	⋯	⋯	⋯	6300	†
$\lvert 2,0,0,0\rangle$	$^4D_{3/2}$	6437^{+17}_{-17}	6393	⋯	⋯	6330	⋯	⋯	⋯	6320	†
$\lvert 2,0,0,0\rangle$	$^4D_{5/2}$	6448^{+15}_{-15}	6402	⋯	6328	6365	⋯	⋯	⋯	6335	†
$\lvert 2,0,0,0\rangle$	$^4D_{7/2}$	6462^{+20}_{-20}	⋯	⋯	6333	6373	⋯	⋯	⋯	6340	†
$\lvert 0,0,1,0\rangle$	$^2S_{1/2}$	6421^{+15}_{-15}	6395	⋯	6294	6274	⋯	6247	⋯	6290	†
$\lvert 0,0,1,0\rangle$	$^4S_{3/2}$	6450^{+15}_{-15}	⋯	⋯	⋯	6286	⋯	⋯	⋯	⋯	†
$\lvert 0,0,0,1\rangle$	$^2S_{1/2}$	6813^{+24}_{-24}	⋯	⋯	⋯	⋯	⋯	⋯	⋯	6400	†
$\lvert 0,0,0,1\rangle$	$^4S_{3/2}$	6842^{+24}_{-23}	⋯	⋯	⋯	⋯	⋯	⋯	⋯	⋯	†
$\lvert 1,1,0,0\rangle$	$^2D_{3/2}$	6611^{+19}_{-19}	⋯	⋯	⋯	⋯	⋯	⋯	⋯	⋯	†
$\lvert 1,1,0,0\rangle$	$^2D_{5/2}$	6621^{+20}_{-20}	6505	⋯	⋯	⋯	⋯	⋯	⋯	⋯	†
$\lvert 1,1,0,0\rangle$	$^2P_{1/2}$	6613^{+19}_{-19}	⋯	⋯	⋯	⋯	⋯	⋯	⋯	6440	†
$\lvert 1,1,0,0\rangle$	$^2P_{3/2}$	6619^{+20}_{-20}	⋯	⋯	⋯	⋯	⋯	⋯	⋯	6445	†
$\lvert 1,1,0,0\rangle$	$^2S_{1/2}$	6617^{+19}_{-19}	⋯	⋯	⋯	⋯	⋯	⋯	⋯	⋯	†
$\lvert 0,2,0,0\rangle$	$^2D_{3/2}$	6807^{+23}_{-23}	⋯	⋯	⋯	⋯	⋯	⋯	⋯	⋯	†
$\lvert 0,2,0,0\rangle$	$^2D_{5/2}$	6817^{+24}_{-25}	⋯	⋯	⋯	⋯	⋯	⋯	⋯	⋯	†
$\lvert 0,2,0,0\rangle$	$^4D_{1/2}$	6824^{+27}_{-27}	⋯	⋯	⋯	⋯	⋯	⋯	⋯	⋯	†
$\lvert 0,2,0,0\rangle$	$^4D_{3/2}$	6830^{+24}_{-24}	⋯	⋯	⋯	⋯	⋯	⋯	⋯	⋯	†
$\lvert 0,2,0,0\rangle$	$^4D_{5/2}$	6840^{+23}_{-23}	⋯	⋯	⋯	⋯	⋯	⋯	⋯	⋯	†
$\lvert 0,2,0,0\rangle$	$^4D_{7/2}$	6854^{+28}_{-28}	⋯	⋯	6554	⋯	⋯	⋯	⋯	6535	†

The baryon and meson flavor wave functions are given in Appendixes B and C, respectively. The possible flavor couplings, $\mathcal{F}_{A\to BC}=\langle\phi_B\phi_C|\phi_0\phi_A\rangle$, which have been calculated for the first time in this study, are given in Appendix D. The masses of the decay products are listed in Table XXVII in Appendix F.

A. Bottom baryon strong decay width results

Our theoretical strong-decay widths, calculated by using the $^3P_0$ model, by means of Eq. (17), are presented in the eighth column of Tables II–VI. The results exhibit good agreement with the experimental widths [1], which are reported in the ninth column of Tables II–VI. This agreement is remarkable since the $^3P_0$ model has only one free parameter, the pair-creation strength, which is fitted to reproduce the $\Sigma_b^*\to\Lambda_b\pi$ experimental strong decay width [1].

In addition, we compare our strong decay widths with those of the previous studies such as NRQM [66], χQM [67,68], and the $^3P_0$ model [71–73,75,76,98,100], as shown in Tables XII–XVI. We observe that in Refs. [71–73,75,76] instead of using the eigenfunctions from their particular quark model, the authors use harmonic oscillator wave functions and fit the root mean square radii (which depend on the $\alpha_{\rho(\lambda)}$) to the reproduction of the strong decay widths, since it is well known that the results do not depend on the wave functions [83], they depend on the root

TABLE X. Same as Table VII, but for $\Xi_b'(snb)$ states. The "†" indicates that there is no reported experimental mass for that state up to now.

$\Xi_b'(snb)$ $\lvert l_\lambda, l_\rho, k_\lambda, k_\rho\rangle$	$\mathcal{F}=\mathbf{6}_{\mathrm{F}}$ $^{2S+1}L_J$	This work	NRQM [41]	QCDSR [48,50,51]	NRQM [39]	χQM [56]	LQCD [59]	CQC [35]	NRQM [33]	RQM [26]	Experimental
$N=0$											
$\lvert 0,0,0,0\rangle$	$^2S_{1/2}$	5925^{+6}_{-6}	⋯	5903	5958	5934	5946	5939	5939	⋯	5935.02 ± 0.05
$\lvert 0,0,0,0\rangle$	$^4S_{3/2}$	5954^{+7}_{-7}	⋯	⋯	⋯	5952	⋯	5961	5970	⋯	5953.8 ± 0.6
$N=1$											
$\lvert 1,0,0,0\rangle$	$^2P_{1/2}$	6198^{+7}_{-7}	⋯	⋯	6192	6164	⋯	⋯	⋯	⋯	†
$\lvert 1,0,0,0\rangle$	$^4P_{1/2}$	6220^{+10}_{-10}	⋯	6240	⋯	6183	⋯	⋯	⋯	⋯	†
$\lvert 1,0,0,0\rangle$	$^2P_{3/2}$	6204^{+7}_{-7}	⋯	⋯	6194	6195	⋯	⋯	⋯	⋯	†
$\lvert 1,0,0,0\rangle$	$^4P_{3/2}$	6227^{+7}_{-7}	⋯	6170	⋯	6227	⋯	⋯	⋯	⋯	†
$\lvert 1,0,0,0\rangle$	$^4P_{5/2}$	6237^{+10}_{-10}	⋯	6180	6204	6238	⋯	⋯	⋯	⋯	6227.9 ± 1.6
$\lvert 0,1,0,0\rangle$	$^2P_{1/2}$	6367^{+9}_{-9}	⋯	6110	⋯	⋯	⋯	⋯	⋯	⋯	†
$\lvert 0,1,0,0\rangle$	$^2P_{3/2}$	6373^{+10}_{-10}	⋯	6110	⋯	⋯	⋯	⋯	⋯	⋯	†
$N=2$											
$\lvert 2,0,0,0\rangle$	$^2D_{3/2}$	6473^{+12}_{-12}	⋯	⋯	5982	6423	⋯	⋯	⋯	⋯	†
$\lvert 2,0,0,0\rangle$	$^2D_{5/2}$	6483^{+13}_{-13}	⋯	⋯	6402	6444	⋯	⋯	⋯	⋯	†
$\lvert 2,0,0,0\rangle$	$^4D_{1/2}$	6489^{+18}_{-18}	⋯	⋯	⋯	6411	⋯	⋯	⋯	⋯	†
$\lvert 2,0,0,0\rangle$	$^4D_{3/2}$	6495^{+14}_{-14}	⋯	⋯	⋯	6434	⋯	⋯	⋯	⋯	†
$\lvert 2,0,0,0\rangle$	$^4D_{5/2}$	6506^{+11}_{-11}	⋯	⋯	⋯	6465	⋯	⋯	⋯	⋯	†
$\lvert 2,0,0,0\rangle$	$^4D_{7/2}$	6520^{+18}_{-18}	⋯	⋯	6405	6472	⋯	⋯	⋯	⋯	†
$\lvert 0,0,1,0\rangle$	$^2S_{1/2}$	6479^{+11}_{-12}	⋯	⋯	⋯	6381	⋯	6360	⋯	⋯	†
$\lvert 0,0,1,0\rangle$	$^4S_{3/2}$	6508^{+12}_{-11}	⋯	⋯	⋯	6392	⋯	⋯	⋯	⋯	†
$\lvert 0,0,0,1\rangle$	$^2S_{1/2}$	6818^{+19}_{-19}	⋯	⋯	⋯	⋯	⋯	⋯	⋯	⋯	†
$\lvert 0,0,0,1\rangle$	$^4S_{3/2}$	6847^{+19}_{-19}	⋯	⋯	⋯	⋯	⋯	⋯	⋯	⋯	†
$\lvert 1,1,0,0\rangle$	$^2D_{3/2}$	6642^{+15}_{-15}	⋯	⋯	⋯	⋯	⋯	⋯	⋯	⋯	†
$\lvert 1,1,0,0\rangle$	$^2D_{5/2}$	6653^{+16}_{-16}	⋯	⋯	⋯	⋯	⋯	⋯	⋯	⋯	†
$\lvert 1,1,0,0\rangle$	$^2P_{1/2}$	6644^{+15}_{-15}	⋯	⋯	⋯	⋯	⋯	⋯	⋯	⋯	†
$\lvert 1,1,0,0\rangle$	$^2P_{3/2}$	6650^{+16}_{-16}	⋯	⋯	⋯	⋯	⋯	⋯	⋯	⋯	†
$\lvert 1,1,0,0\rangle$	$^2S_{1/2}$	6648^{+15}_{-15}	⋯	⋯	⋯	⋯	⋯	⋯	⋯	⋯	†
$\lvert 0,2,0,0\rangle$	$^2D_{3/2}$	6812^{+19}_{-19}	⋯	⋯	⋯	⋯	⋯	⋯	⋯	⋯	†
$\lvert 0,2,0,0\rangle$	$^2D_{5/2}$	6822^{+20}_{-20}	⋯	⋯	⋯	⋯	⋯	⋯	⋯	⋯	†
$\lvert 0,2,0,0\rangle$	$^4D_{1/2}$	6828^{+22}_{-22}	⋯	⋯	⋯	⋯	⋯	⋯	⋯	⋯	†
$\lvert 0,2,0,0\rangle$	$^4D_{3/2}$	6834^{+20}_{-20}	⋯	⋯	⋯	⋯	⋯	⋯	⋯	⋯	†
$\lvert 0,2,0,0\rangle$	$^4D_{5/2}$	6845^{+19}_{-19}	⋯	⋯	⋯	⋯	⋯	⋯	⋯	⋯	†
$\lvert 0,2,0,0\rangle$	$^4D_{7/2}$	6859^{+24}_{-25}	⋯	⋯	⋯	⋯	⋯	⋯	⋯	⋯	†

mean square radii, on the quantum numbers, and on the considered channels [83]. We also use harmonic oscillator wave functions. In our case, however, we observed that these functions were the eigenstates of the model of Ref. [98]. Thus we did not have $\alpha_{\rho(\lambda)}$ as a free parameters ($\alpha_{\rho(\lambda)}$ was fixed by the fit to the spectra).

From Tables XII–XVI one can see that these studies included only a subset of the possible mesons in their calculations.

It is worth noting that the experimental widths encompass contributions from strong, electromagnetic, and weak interactions. However, the dominant contribution is typically from the strong decay process. It is important to note that this contribution is relatively small compared with the uncertainties associated with the strong decay width.

Additionally, the partial decay widths of each open-flavor channel are given in Tables XVII–XXI. The partial decay widths obtained in this study will provide valuable information for experimentalists in their efforts to identify bottom baryons. The knowledge of potential decay channels can greatly assist in the identification process by guiding the analysis of experimental data.

Nevertheless, in the singly bottom baryon sector, there are a few cases in which the strong decay is suppressed due to the absence of phase space, leading to the dominance of electromagnetic or even weak interactions. Specifically, the ground states, Λ_b, Ξ_b, and Ω_b, can only decay via weak

TABLE XI. Same as Table VII, but for $\Omega_b(ssb)$ states. The "†" indicates that there is no reported experimental mass for that state up to now.

$\Omega_b(ssb)$ $\lvert l_\lambda, l_\rho, k_\lambda, k_\rho\rangle$	$\mathcal{F}=\mathbf{6}_{\rm F}$ $^{2S+1}L_J$	This work	NRQM [41]	QCDSR [48,50,51]	NRQM [39]	χQM [56]	LQCD [59]	CQC [35]	NRQM [33]	RQM [26]	Experimental
$N=0$											
$\lvert 0,0,0,0\rangle$	$^2S_{1/2}$	6064^{+8}_{-8}	6076	6036	6081	6047	6014	6056	6030	⋯	6045.2 ± 1.2
$\lvert 0,0,0,0\rangle$	$^4S_{3/2}$	6093^{+9}_{-8}	6094	6063	6102	6064	6019	6079	6061	⋯	†
$N=1$											
$\lvert 1,0,0,0\rangle$	$^2P_{1/2}$	6315^{+7}_{-7}	6333	⋯	6301	6273	⋯	6340	⋯	⋯	6315.6 ± 0.6
$\lvert 1,0,0,0\rangle$	$^4P_{1/2}$	6337^{+10}_{-10}	6340	6500	6312	6290	⋯	⋯	⋯	⋯	6330.3 ± 0.6
$\lvert 1,0,0,0\rangle$	$^2P_{3/2}$	6321^{+8}_{-8}	6336	⋯	6304	6301	⋯	⋯	⋯	⋯	6339.7 ± 0.6
$\lvert 1,0,0,0\rangle$	$^4P_{3/2}$	6343^{+7}_{-7}	6344	6430	6311	6329	⋯	⋯	⋯	⋯	6349.8 ± 0.6
$\lvert 1,0,0,0\rangle$	$^4P_{5/2}$	6353^{+11}_{-11}	6345	6430	6311	6339	⋯	⋯	⋯	⋯	†
$\lvert 0,1,0,0\rangle$	$^2P_{1/2}$	6465^{+9}_{-8}	6437	6340	⋯	⋯	⋯	6458	⋯	⋯	†
$\lvert 0,1,0,0\rangle$	$^2P_{3/2}$	6471^{+10}_{-10}	6438	6340	⋯	⋯	⋯	⋯	⋯	⋯	†
$N=2$											
$\lvert 2,0,0,0\rangle$	$^2D_{3/2}$	6568^{+11}_{-11}	6528	⋯	6478	6522	⋯	6493	⋯	⋯	†
$\lvert 2,0,0,0\rangle$	$^2D_{5/2}$	6578^{+12}_{-12}	6561	⋯	6492	6541	⋯	⋯	⋯	⋯	†
$\lvert 2,0,0,0\rangle$	$^4D_{1/2}$	6584^{+17}_{-17}	6517	⋯	⋯	6511	⋯	⋯	⋯	⋯	†
$\lvert 2,0,0,0\rangle$	$^4D_{3/2}$	6590^{+13}_{-13}	6559	⋯	⋯	6532	⋯	⋯	⋯	⋯	†
$\lvert 2,0,0,0\rangle$	$^4D_{5/2}$	6600^{+10}_{-10}	6566	⋯	6494	6559	⋯	⋯	⋯	⋯	†
$\lvert 2,0,0,0\rangle$	$^4D_{7/2}$	6614^{+18}_{-18}	⋯	⋯	6497	6567	⋯	⋯	⋯	⋯	†
$\lvert 0,0,1,0\rangle$	$^2S_{1/2}$	6574^{+11}_{-11}	6561	⋯	6472	6480	⋯	6479	⋯	⋯	†
$\lvert 0,0,1,0\rangle$	$^4S_{3/2}$	6602^{+11}_{-11}	⋯	⋯	⋯	6491	⋯	⋯	⋯	⋯	†
$\lvert 0,0,0,1\rangle$	$^2S_{1/2}$	6874^{+17}_{-17}	⋯	⋯	⋯	⋯	⋯	⋯	⋯	⋯	†
$\lvert 0,0,0,1\rangle$	$^4S_{3/2}$	6902^{+17}_{-17}	⋯	⋯	⋯	⋯	⋯	⋯	⋯	⋯	†
$\lvert 1,1,0,0\rangle$	$^2D_{3/2}$	6718^{+14}_{-14}	⋯	⋯	⋯	⋯	⋯	⋯	⋯	⋯	†
$\lvert 1,1,0,0\rangle$	$^2D_{5/2}$	6728^{+15}_{-15}	6657	⋯	⋯	⋯	⋯	⋯	⋯	⋯	†
$\lvert 1,1,0,0\rangle$	$^2P_{1/2}$	6720^{+14}_{-14}	⋯	⋯	⋯	⋯	⋯	⋯	⋯	⋯	†
$\lvert 1,1,0,0\rangle$	$^2P_{3/2}$	6726^{+15}_{-15}	⋯	⋯	⋯	⋯	⋯	⋯	⋯	⋯	†
$\lvert 1,1,0,0\rangle$	$^2S_{1/2}$	6724^{+14}_{-14}	⋯	⋯	⋯	⋯	⋯	⋯	⋯	⋯	†
$\lvert 0,2,0,0\rangle$	$^2D_{3/2}$	6868^{+17}_{-17}	⋯	⋯	⋯	⋯	⋯	⋯	⋯	⋯	†
$\lvert 0,2,0,0\rangle$	$^2D_{5/2}$	6878^{+19}_{-19}	⋯	⋯	⋯	⋯	⋯	⋯	⋯	⋯	†
$\lvert 0,2,0,0\rangle$	$^4D_{1/2}$	6884^{+21}_{-21}	⋯	⋯	⋯	⋯	⋯	⋯	⋯	⋯	†
$\lvert 0,2,0,0\rangle$	$^4D_{3/2}$	6890^{+18}_{-18}	⋯	⋯	⋯	⋯	⋯	⋯	⋯	⋯	†
$\lvert 0,2,0,0\rangle$	$^4D_{5/2}$	6900^{+17}_{-17}	⋯	⋯	⋯	⋯	⋯	⋯	⋯	⋯	†
$\lvert 0,2,0,0\rangle$	$^4D_{7/2}$	6914^{+23}_{-23}	⋯	⋯	6667	⋯	⋯	⋯	⋯	⋯	†

interaction. In the case of Ξ_b', and Ω_b^*, all the strong decay channels are closed due to the lack of phase space. In such cases, the decay width is primarily dominated by electromagnetic interaction.

IV. ELECTROMAGNETIC DECAY WIDTHS

In this subsection, we compute the electromagnetic decays of Λ_b, Ξ_b, Σ_b, Ξ_b', and Ω_b baryons from P-wave excited states transitioning to ground states, as well as for ground state to ground state transitions.

The calculation of the radiative-decay widths of bottom baryons is done within the constituent quark model. The transition operator describing the emission of a left-handed photon from a singly bottom baryon A to another singly bottom baryon A', i.e., $A \to A'\gamma$, in the nonrelativistic approximation, is given by:

$$\mathcal{H}_{\rm em} = 2\sqrt{\frac{\pi}{\mathrm{k}_0}}\sum_{j=1}^{3}\mu_j \times \left[\mathrm{k}\mathbf{s}_{j,-}e^{-i\mathbf{k}\cdot\mathbf{r}_j} - \frac{1}{2}(\mathbf{p}_{j,-}e^{-i\mathbf{k}\cdot\mathbf{r}_j} + e^{-i\mathbf{k}\cdot\mathbf{r}_j}\mathbf{p}_{j,-})\right], \quad (19)$$

where $\mathbf{r}_j$, $\mathbf{p}_j$, $\mathbf{s}_j$, and μ_j stand for the coordinate, momentum, spin and magnetic moment of the jth quark, respectively, k_0 is the photon energy and $\mathbf{k} = \mathrm{k}\hat{\mathbf{z}}$ corresponds to the momentum of a photon emitted in the $\hat{z}$ direction. Hence, the partial decay widths of the electromagnetic transitions are given by

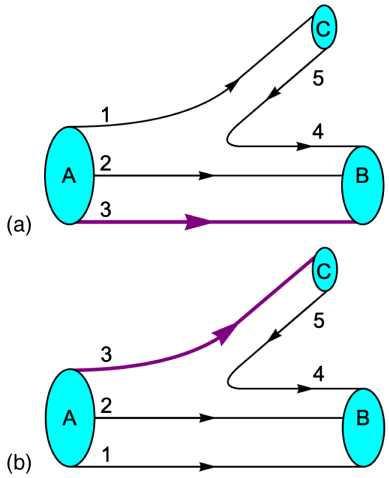

FIG. 13. The $^3P_0$ pair-creation model. The violet line 3 denotes a bottom quark, while the remaining black lines denote light quarks. In diagram (a) the bottom baryon A decays to a bottom baryon B and a light meson C. In diagram (b) the bottom baryon A decays to a light baryon B and a bottom meson C.

$$\Gamma_{\rm em}(A \to A'\gamma) = \Phi_{A\to A'\gamma}\frac{1}{(2\pi)^2}\frac{2}{2J_A+1}\sum_{M_{J_A}>0}|A_{M_{J_A}}|^2, \quad (20)$$

where J_A is the initial state total angular momentum, $A_{M_{J_A}}$ is the transition amplitude for a given helicity M_{J_A},

$$A_{M_{J_A}} = \langle J_{A'}, M_{J_A}-1|\mathcal{H}_{\rm em}|J_A, M_{J_A}\rangle, \quad (21)$$

and $\Phi_{A\to A'\gamma}$ is the phase space factor, which in the rest frame of the initial baryon is given by

$$\Phi_{A\to A'\gamma} = 4\pi\frac{E_{A'}}{m_A}\mathrm{k}^2, \quad (22)$$

where $E_{A'} = \sqrt{m_{A'}^2+\mathrm{k}^2}$ is the energy of the final state, m_A and $m_{A'}$ are the masses of the initial and final baryon, respectively, and

$$\mathrm{k} = \frac{m_A^2 - m_{A'}^2}{2m_A} \quad (23)$$

is the final state of photon energy.

The Hamiltonian in Eq. (19). consists of two parts. The first part is proportional to the spin-flip operator

$$\mathrm{k}\mathbf{s}_{j,-}\exp\left[-i\mathbf{k}\cdot\mathbf{r}_j\right] \equiv \mathrm{k}\mathbf{s}_{j,-}\hat{U}_j. \quad (24)$$

This part can be evaluated straightforwardly by observing that the $\hat{U}_j$ operators can be written as

$$\hat{U}_1 = \exp[-i\mathbf{k}\cdot\mathbf{r}_1] = \exp\left[-i\frac{1}{\sqrt{2}}\mathbf{k}\cdot\boldsymbol{\rho} - i\frac{\sqrt{\frac{3}{2}}m_b}{2m_\rho+m_b}\mathbf{k}\cdot\boldsymbol{\lambda}\right], \quad (25)$$

$$\hat{U}_2 = \exp[-i\mathbf{k}\cdot\mathbf{r}_2] = \exp\left[i\frac{1}{\sqrt{2}}\mathbf{k}\cdot\boldsymbol{\rho} - i\frac{\sqrt{\frac{3}{2}}m_b}{2m_\rho+m_b}\mathbf{k}\cdot\boldsymbol{\lambda}\right], \quad (26)$$

$$\hat{U}_3 = \exp[-i\mathbf{k}\cdot\mathbf{r}_3] = \exp\left[i\frac{\sqrt{6}m}{2m_\rho+m_b}\mathbf{k}\cdot\boldsymbol{\lambda}\right]. \quad (27)$$

The second part of the Hamiltonian in Eq. (19) is proportional to the orbit-flip operator

$$\mathbf{p}_{j,-}\hat{U}_j + \hat{U}_j\mathbf{p}_{j,-} \equiv \hat{T}_{j,-}. \quad (28)$$

Here $\mathbf{p}_{j,-}$ denotes the momentum ladder operator,

$$\mathbf{p}_{j,-} = \mathbf{p}_{j,x} - i\mathbf{p}_{j,y}, \quad (29)$$

whose components are given by

$$\begin{aligned}\mathbf{p}_{1,-} &= \frac{1}{\sqrt{2}}\mathbf{p}_{\rho,-} + \frac{1}{\sqrt{6}}\mathbf{p}_{\lambda,-},\\ \mathbf{p}_{2,-} &= -\frac{1}{\sqrt{2}}\mathbf{p}_{\rho,-} + \frac{1}{\sqrt{6}}\mathbf{p}_{\lambda,-},\\ \mathbf{p}_{3,-} &= -\sqrt{\frac{2}{3}}\mathbf{p}_{\lambda,-},\end{aligned} \quad (30)$$

for $j=1$, 2 and 3, respectively. Using the previous equations, we express the orbit flip operators $\hat{T}_{j,-} = \mathbf{p}_{j,-}\hat{U}_j + \hat{U}_j\mathbf{p}_{j,-}$ as follows

$$\begin{aligned}\hat{T}_{1,-} = &\left(\frac{1}{\sqrt{2}}\mathbf{p}_{\rho,-} + \frac{1}{\sqrt{6}}\mathbf{p}_{\lambda,-}\right)\hat{U}_1\\ &+ \hat{U}_1\left(\frac{1}{\sqrt{2}}\mathbf{p}_{\rho,-} + \frac{1}{\sqrt{6}}\mathbf{p}_{\lambda,-}\right),\end{aligned} \quad (31)$$

$$\begin{aligned}\hat{T}_{2,-} = &\left(-\frac{1}{\sqrt{2}}\mathbf{p}_{\rho,-} + \frac{1}{\sqrt{6}}\mathbf{p}_{\lambda,-}\right)\hat{U}_2\\ &+ \hat{U}_2\left(-\frac{1}{\sqrt{2}}\mathbf{p}_{\rho,-} + \frac{1}{\sqrt{6}}\mathbf{p}_{\lambda,-}\right),\end{aligned} \quad (32)$$

$$\hat{T}_{3,-} = -\sqrt{\frac{2}{3}}\mathbf{p}_{\lambda,-}\hat{U}_3 - \hat{U}_3\sqrt{\frac{2}{3}}\mathbf{p}_{\lambda,-}. \quad (33)$$

Thus the Hamiltonian of Eq. (19) can be rewritten in terms of the $\hat{U}_j$ and $\hat{T}_{j,-}$ operators in the following compact form:

$$\mathcal{H}_{\rm em} = 2\sqrt{\frac{\pi}{\mathrm{k}}}\sum_{j=1}^{3}\mu_j\left[\mathrm{k}\mathbf{s}_{j,-}\hat{U}_j - \frac{1}{2}\hat{T}_{j,-}\right]. \quad (34)$$

TABLE XII. Comparison of our predicted $\Lambda_b(nnb)$ strong decay widths with those of other theoretical studies (in MeV). The flavor multiplet is indicated by the symbol $\mathcal{F}$. The first column contains the three-quark model state, $|l_\lambda, l_\rho, k_\lambda, k_\rho\rangle$, where $l_{\lambda,\rho}$ are the orbital angular momenta and $k_{\lambda,\rho}$ the number of nodes of the λ and ρ oscillators. The second column displays each state's spectroscopic notation $^{2S+1}L_J$. In the third column, our predicted strong decay widths, computed within the $^3P_0$ model and the baryon-meson channels included in the calculation, are shown. Our results are compared with those of Refs. [72] (fourth column), [68] (fifth column), and [76] (sixth column). Our theoretical results are also compared with the experimental decay widths from PDG [1] (seventh column). The symbol "..." indicates that there is no prediction for that state. The "†" indicates that there is no reported experimental decay width for that state up to now.

$\Lambda_b(nnb)$ $\lvert l_\lambda, l_\rho, k_\lambda, k_\rho\rangle$	$\mathcal{F}=\bar{\mathbf{3}}_F$ $^{2S+1}L_J$	This work Γ (MeV)	[72] Γ (MeV)	[68] Γ (MeV)	[76] Γ (MeV)	Experimental Γ (MeV)
Channels		$\Sigma_b\pi, \Sigma_b^*\pi, \Lambda_b\eta, \Sigma_b\rho$ $\Sigma_b^*\rho, \Lambda_b\eta, \Lambda_b\omega, \Xi_bK$ $\Xi_b'K, \Xi_b^*K, \Xi_bK^*$ $\Xi_b'K^*, \Xi_b^*K^*, NB$	$\Sigma_b\pi, \Sigma_b^*\pi$	$\Sigma_b\pi, \Sigma_b^*\pi$	$\Sigma_b\pi, \Sigma_b^*\pi$	
$N=0$						
$\lvert 0,0,0,0\rangle$	$^2S_{1/2}$	0	...	...	...	≈0
$N=1$						
$\lvert 1,0,0,0\rangle$	$^2P_{1/2}$	0	...	...	...	<0.25
$\lvert 1,0,0,0\rangle$	$^2P_{3/2}$	0	...	...	...	<0.19
$\lvert 0,1,0,0\rangle$	$^2P_{1/2}$	67	...	...	...	†
$\lvert 0,1,0,0\rangle$	$^4P_{1/2}$	36	523	...	...	†
$\lvert 0,1,0,0\rangle$	$^2P_{3/2}$	85	460	...	...	†
$\lvert 0,1,0,0\rangle$	$^4P_{3/2}$	128	4	...	...	†
$\lvert 0,1,0,0\rangle$	$^4P_{5/2}$	74	3	...	...	†
$N=2$						
$\lvert 2,0,0,0\rangle$	$^2D_{3/2}$	13	...	9	...	2.9 ± 1.3
$\lvert 2,0,0,0\rangle$	$^2D_{5/2}$	18	...	9	...	2.1 ± 0.9
$\lvert 0,0,1,0\rangle$	$^2S_{1/2}$	29	9	...	36	†
$\lvert 0,0,0,1\rangle$	$^2S_{1/2}$	130	...	...	...	†
$\lvert 1,1,0,0\rangle$	$^2D_{3/2}$	67	...	...	...	†
$\lvert 1,1,0,0\rangle$	$^2D_{5/2}$	108	...	...	...	†
$\lvert 1,1,0,0\rangle$	$^4D_{1/2}$	34	...	...	...	†
$\lvert 1,1,0,0\rangle$	$^4D_{3/2}$	95	...	...	...	†
$\lvert 1,1,0,0\rangle$	$^4D_{5/2}$	128	...	...	...	†
$\lvert 1,1,0,0\rangle$	$^4D_{7/2}$	122	...	...	...	†
$\lvert 1,1,0,0\rangle$	$^2P_{1/2}$	0	...	...	...	†
$\lvert 1,1,0,0\rangle$	$^2P_{3/2}$	2	...	...	...	†
$\lvert 1,1,0,0\rangle$	$^4P_{1/2}$	0	...	...	...	†
$\lvert 1,1,0,0\rangle$	$^4P_{3/2}$	1	...	...	...	†
$\lvert 1,1,0,0\rangle$	$^4P_{5/2}$	2	...	...	...	†
$\lvert 1,1,0,0\rangle$	$^4S_{3/2}$	32	...	...	...	†
$\lvert 1,1,0,0\rangle$	$^2S_{1/2}$	29	...	...	...	†
$\lvert 0,2,0,0\rangle$	$^2D_{3/2}$	131	...	...	...	†
$\lvert 0,2,0,0\rangle$	$^2D_{5/2}$	185	...	...	...	†

In Appendix G we show the procedure of evaluating the matrix elements for the $\hat{T}_{j,-}$ operators in the electromagnetic transitions from P-wave states to ground states. This is accomplished by expressing the matrix elements of the $\hat{T}_{j,-}$ operators as a sum of matrix elements involving the $\hat{U}_j$ operators. We achieve this by evaluating the action of the ladder operators $\mathbf{p}_{\lambda/\rho,-}$ on the wave functions (see Appendix G) and we get the analytical formulas.

In the following, we use the notation $\psi_{k_\rho,l_\rho,m_{l_\rho},k_\lambda,l_\lambda,m_{l_\lambda}}(\vec{\rho},\vec{\lambda}) = \langle\vec{\rho},\vec{\lambda}|k_\rho,l_\rho,m_{l_\rho},k_\lambda,l_\lambda,m_{l_\lambda}\rangle$ for the singly bottom baryon wave functions. These wave

TABLE XIII. Comparison of our predicted $\Xi_b(snb)$ strong decay widths with those of other theoretical studies (in MeV). The flavor multiplet is indicated by the symbol $\mathcal{F}$. The first column contains the three-quark model state, $|l_\lambda, l_\rho, k_\lambda, k_\rho\rangle$, where $l_{\lambda,\rho}$ are the orbital angular momenta and $k_{\lambda,\rho}$ the number of nodes of the λ and ρ oscillators. The second column displays each state's spectroscopic notation $^{2S+1}L_J$. In the third column, our predicted strong decay widths, computed within the $^3P_0$ model and the baryon-meson channels included in the calculation, are shown. Our results are compared with those of Refs. [66] (fourth column), [68] (fifth column), [67] (sixth column), [73] (seventh column), [75] (eighth column), and [100] (ninth column). The experimental widths, as from PDG [1], are reported in the tenth column. The symbol "..." indicates that there is no prediction for that state. The "†" indicates that there is no reported experimental decay width for that state up to now.

$\Xi_b(snb)$ $\lvert l_\lambda, l_\rho, k_\lambda, k_\rho\rangle$	$\mathcal{F}=\bar{\mathbf{3}}_{\mathrm{F}}$ $^{2S+1}L_J$	This work Γ (MeV)	[66] Γ (MeV)	[68] Γ (MeV)	[67] Γ (MeV)	[73] Γ (MeV)	[75] Γ (MeV)	[100] Γ (MeV)	Experimental Γ (MeV)
Channels		$\Lambda_b K, \Xi_b\pi, \Xi_b'\pi$ $\Xi_b^*\pi, \Sigma_b K, \Sigma_b^* K$ $\Xi_b\eta, \Lambda_b K^*, \Xi_b\rho$ $\Xi_b'\rho, \Xi_b^*\rho, \Sigma_b K^*$ $\Sigma_b^* K^*, \Xi_b'\eta, \Xi_b^*\eta$ $\Xi_b\eta', \Xi_b'\eta', \Xi_b^*\eta'$ $\Xi_b\omega, \Xi_b'\omega, \Xi_b^*\omega$ $\Xi_b\phi, \Xi_b'\phi, \Xi_b^*\phi$ $\Lambda_8 B, \Lambda_8 B^*, \Sigma_8 B$ $\Lambda_8^* B$	$\Xi_b\pi, \Xi_b'\pi$	$\Xi_b'\pi, \Xi_b^*\pi$ $\Sigma_b K, \Sigma_b^* K$	$\Xi_b'\pi, \Xi_b^*\pi$	$\Xi_b'\pi, \Xi_b^*\pi$ $\Sigma_b K, \Sigma_b^* K$	$\Xi_b\pi, \Xi_b'\pi$ $\Xi_b^*\pi$	$\Sigma_b\bar{K}, \Xi_b'\pi$ $\Sigma_b^*\bar{K}, \Xi_b^*\pi$ $\Lambda_b\bar{K}, \Xi_b\pi$ $\Xi_b\eta$	
$N=0$									
$\lvert 0,0,0,0\rangle$	$^2S_{1/2}$	0	⋯	⋯	⋯	⋯	⋯	0	≈0
$N=1$									
$\lvert 1,0,0,0\rangle$	$^2P_{1/2}$	0	11	⋯	3	18	4	0	†
$\lvert 1,0,0,0\rangle$	$^2P_{3/2}$	1	≈0	⋯	3	16	3	0	<1.9
$\lvert 0,1,0,0\rangle$	$^2P_{1/2}$	9	223	⋯	⋯	⋯	⋯	0.55	†
$\lvert 0,1,0,0\rangle$	$^4P_{1/2}$	6	10	⋯	⋯	⋯	⋯	0.36	†
$\lvert 0,1,0,0\rangle$	$^2P_{3/2}$	66	⋯	⋯	⋯	⋯	⋯	1.90	†
$\lvert 0,1,0,0\rangle$	$^4P_{3/2}$	26	⋯	⋯	⋯	⋯	⋯	1.90	†
$\lvert 0,1,0,0\rangle$	$^4P_{5/2}$	68	⋯	⋯	⋯	⋯	⋯	2.16	†
$N=2$									
$\lvert 2,0,0,0\rangle$	$^2D_{3/2}$	2	⋯	7	⋯	7	⋯	0.19	<2.2
$\lvert 2,0,0,0\rangle$	$^2D_{5/2}$	2	⋯	7	⋯	6	⋯	0.10	<1.6
$\lvert 0,0,1,0\rangle$	$^2S_{1/2}$	5	⋯	⋯	⋯	7	16	⋯	†
$\lvert 0,0,0,1\rangle$	$^2S_{1/2}$	179	⋯	⋯	⋯	⋯	⋯	⋯	†
$\lvert 1,1,0,0\rangle$	$^2D_{3/2}$	46	⋯	⋯	⋯	⋯	⋯	⋯	†
$\lvert 1,1,0,0\rangle$	$^2D_{5/2}$	108	⋯	⋯	⋯	⋯	⋯	⋯	†
$\lvert 1,1,0,0\rangle$	$^4D_{1/2}$	20	⋯	⋯	⋯	⋯	⋯	⋯	†
$\lvert 1,1,0,0\rangle$	$^4D_{3/2}$	67	⋯	⋯	⋯	⋯	⋯	⋯	†
$\lvert 1,1,0,0\rangle$	$^4D_{5/2}$	100	⋯	⋯	⋯	⋯	⋯	⋯	†
$\lvert 1,1,0,0\rangle$	$^4D_{7/2}$	114	⋯	⋯	⋯	⋯	⋯	⋯	†
$\lvert 1,1,0,0\rangle$	$^2P_{1/2}$	0	⋯	⋯	⋯	⋯	⋯	⋯	†
$\lvert 1,1,0,0\rangle$	$^2P_{3/2}$	2	⋯	⋯	⋯	⋯	⋯	⋯	†
$\lvert 1,1,0,0\rangle$	$^4P_{1/2}$	0	⋯	⋯	⋯	⋯	⋯	⋯	†
$\lvert 1,1,0,0\rangle$	$^4P_{3/2}$	1	⋯	⋯	⋯	⋯	⋯	⋯	†
$\lvert 1,1,0,0\rangle$	$^4P_{5/2}$	2	⋯	⋯	⋯	⋯	⋯	⋯	†
$\lvert 1,1,0,0\rangle$	$^4S_{3/2}$	33	⋯	⋯	⋯	⋯	⋯	⋯	†
$\lvert 1,1,0,0\rangle$	$^2S_{1/2}$	31	⋯	⋯	⋯	⋯	⋯	⋯	†
$\lvert 0,2,0,0\rangle$	$^2D_{3/2}$	127	⋯	⋯	⋯	⋯	⋯	⋯	†
$\lvert 0,2,0,0\rangle$	$^2D_{5/2}$	98	⋯	⋯	⋯	⋯	⋯	⋯	†

TABLE XIV. Comparison of our predicted $\Sigma_b(nnb)$ strong decay widths with those of other theoretical studies (in MeV). The flavor multiplet is indicated by the symbol $\mathcal{F}$. The first column contains the three-quark model state, $|l_\lambda, l_\rho, k_\lambda, k_\rho\rangle$, where $l_{\lambda,\rho}$ are the orbital angular momenta and $k_{\lambda,\rho}$ the number of nodes of the λ and ρ oscillators. The second column displays each state's spectroscopic notation $^{2S+1}L_J$. In the third column, our predicted strong decay widths, computed within the $^3P_0$ model and the baryon-meson channels included in the calculation, are shown. Our results are compared with those of Refs. [72] (fourth column), [68] (fifth column), [67] (sixth column), [75] (seventh column), and [76] (eighth column). The experimental widths, as from PDG [1], are reported in the ninth column. The symbol "..." indicates that there is no prediction for that state. N_1^*, N_2^*, N_3^*, and N_4^* represent $N(1520)$, $N(1535)$, $N(1680)$, and $N(1720)$, respectively. The "†" indicates that there is no reported experimental decay width for that state up to now.

$\Sigma_b(nnb)$ $\lvert l_\lambda, l_\rho, k_\lambda, k_\rho\rangle$	$\mathcal{F}=\mathbf{6}_{\mathrm{F}}$ $^{2S+1}L_J$	This work Γ (MeV)	[72] Γ (MeV)	[68] Γ (MeV)	[67] Γ (MeV)	[75] Γ (MeV)	[76] Γ (MeV)	Experimental Γ (MeV)
Channels		$\Sigma_b\pi, \Sigma_b^*\pi, \Lambda_b\pi$ $\Sigma_b\eta, \Xi_b K, \Sigma_b\rho$ $\Sigma_b^*\rho, \Lambda_b\rho, \Sigma_b^*\eta$ $\Sigma_b\eta', \Sigma_b^*\eta', \Xi_b' K$ $\Xi_b^* K, \Xi_b K^*, \Xi_b' K^*$ $\Xi_b^* K^*, \Sigma_b\omega, \Sigma_b^*\omega$ $NB, \Sigma_8 B_s, NB^*$ $\Delta B, N_1^* B, N_2^* B$ $N_3^* B, N_4^* B$	$\Sigma_b\pi, \Sigma_b^*\pi$ $\Lambda_b\pi$	$\Sigma_b\pi, \Sigma_b^*\pi$	$\Sigma_b\pi, \Sigma_b^*\pi$ $\Lambda_b\pi$	$\Lambda_b\pi$	$\Sigma_b\pi, \Sigma_b^*\pi$ $\Lambda_b\pi, NB$ NB^*	
$N=0$								
$\lvert 0,0,0,0\rangle$	$^2S_{1/2}$	4	⋯	⋯	⋯	5	⋯	5.0 ± 0.5
$\lvert 0,0,0,0\rangle$	$^4S_{3/2}$	10	⋯	⋯	⋯	9	⋯	9.9 ± 0.9
$N=1$								
$\lvert 1,0,0,0\rangle$	$^2P_{1/2}$	24	264	⋯	23	⋯	27	30 ± 7
$\lvert 1,0,0,0\rangle$	$^4P_{1/2}$	13	209	⋯	14	⋯	109	†
$\lvert 1,0,0,0\rangle$	$^2P_{3/2}$	84	181	⋯	39	⋯	114	†
$\lvert 1,0,0,0\rangle$	$^4P_{3/2}$	57	9	⋯	26	⋯	42	†
$\lvert 1,0,0,0\rangle$	$^4P_{5/2}$	96	9	⋯	38	⋯	43	†
$\lvert 0,1,0,0\rangle$	$^2P_{1/2}$	134	261	⋯	⋯	⋯	⋯	†
$\lvert 0,1,0,0\rangle$	$^2P_{3/2}$	129	268	⋯	⋯	⋯	⋯	†
$N=2$								
$\lvert 2,0,0,0\rangle$	$^2D_{3/2}$	58	⋯	121	⋯	⋯	⋯	†
$\lvert 2,0,0,0\rangle$	$^2D_{5/2}$	130	⋯	48	⋯	⋯	⋯	†
$\lvert 2,0,0,0\rangle$	$^4D_{1/2}$	78	⋯	148	⋯	⋯	⋯	†
$\lvert 2,0,0,0\rangle$	$^4D_{3/2}$	106	⋯	85	⋯	⋯	⋯	†
$\lvert 2,0,0,0\rangle$	$^4D_{5/2}$	133	⋯	48	⋯	⋯	⋯	†
$\lvert 2,0,0,0\rangle$	$^4D_{7/2}$	145	⋯	53	⋯	⋯	⋯	†
$\lvert 0,0,1,0\rangle$	$^2S_{1/2}$	119	⋯	⋯	⋯	⋯	116	†
$\lvert 0,0,1,0\rangle$	$^4S_{3/2}$	121	⋯	⋯	⋯	⋯	122	†
$\lvert 0,0,0,1\rangle$	$^2S_{1/2}$	710	⋯	⋯	⋯	⋯	⋯	†
$\lvert 0,0,0,1\rangle$	$^4S_{3/2}$	973	⋯	⋯	⋯	⋯	⋯	†
$\lvert 1,1,0,0\rangle$	$^2D_{3/2}$	376	⋯	⋯	⋯	⋯	⋯	†
$\lvert 1,1,0,0\rangle$	$^2D_{5/2}$	252	⋯	⋯	⋯	⋯	⋯	†
$\lvert 1,1,0,0\rangle$	$^2P_{1/2}$	4	⋯	⋯	⋯	⋯	⋯	†
$\lvert 1,1,0,0\rangle$	$^2P_{3/2}$	5	⋯	⋯	⋯	⋯	⋯	†
$\lvert 1,1,0,0\rangle$	$^2S_{1/2}$	58	⋯	⋯	⋯	⋯	⋯	†
$\lvert 0,2,0,0\rangle$	$^2D_{3/2}$	549	⋯	⋯	⋯	⋯	⋯	†
$\lvert 0,2,0,0\rangle$	$^2D_{5/2}$	616	⋯	⋯	⋯	⋯	⋯	†
$\lvert 0,2,0,0\rangle$	$^4D_{1/2}$	1349	⋯	⋯	⋯	⋯	⋯	†
$\lvert 0,2,0,0\rangle$	$^4D_{3/2}$	741	⋯	⋯	⋯	⋯	⋯	†
$\lvert 0,2,0,0\rangle$	$^4D_{5/2}$	376	⋯	⋯	⋯	⋯	⋯	†
$\lvert 0,2,0,0\rangle$	$^4D_{7/2}$	1178	⋯	⋯	⋯	⋯	⋯	†

TABLE XV. Comparison of our predicted $\Xi_b'(snb)$ strong decay widths with those of other theoretical studies (in MeV). The flavor multiplet is indicated by the symbol $\mathcal{F}$. The first column contains the three-quark model state, $|l_\lambda, l_\rho, k_\lambda, k_\rho\rangle$, where $l_{\lambda,\rho}$ are the orbital angular momenta and $k_{\lambda,\rho}$ the number of nodes of the λ and ρ oscillators. The second column displays each state's spectroscopic notation $^{2S+1}L_J$. In the third column, our predicted strong decay widths, computed within the $^3P_0$ model and the baryon-meson channels included in the calculation, are shown. Our results are compared with those of Refs. [66] (fourth column), [68] (fifth column), [67] (sixth column), [73] (seventh column), [75] (eighth column), and [100] (ninth column). The experimental widths, as from PDG [1], are reported in the tenth column. The symbol "..." indicates that there is no prediction for that state. The "†" indicates that there is no reported experimental decay width for that state up to now.

$\Xi_b'(snb)$ $\lvert l_\lambda, l_\rho, k_\lambda, k_\rho\rangle$	$\mathcal{F}=\mathbf{6}_{\rm f}$ $^{2S+1}L_J$	This work Γ (MeV)	[66] Γ (MeV)	[68] Γ (MeV)	[67] Γ (MeV)	[73] Γ (MeV)	[75] Γ (MeV)	[100] Γ (MeV)	Experimental Γ (MeV)
Channels		$\Lambda_b K, \Xi_b\pi, \Xi_b'\pi$ $\Xi_b^*\pi, \Sigma_b K, \Sigma_b^* K$ $\Xi_b\eta, \Lambda_b K^*, \Xi_b\rho$ $\Xi_b'\rho, \Xi_b^*\rho, \Sigma_b K^*$ $\Sigma_b^* K^*, \Xi_b'\eta, \Xi_b^*\eta$ $\Xi_b\eta', \Xi_b'\eta', \Xi_b^*\eta'$ $\Xi_b\omega, \Xi_b'\omega, \Xi_b^*\omega$ $\Xi_b\phi, \Xi_b'\phi, \Xi_b^*\phi$ $\Sigma_8 B, \Xi_8 B_s$ $\Sigma_8 B^*, \Sigma_{10} B$	$\Xi_b\pi$	$\Lambda_b K, \Xi_b\pi$ $\Xi_b'\pi, \Xi_b^*\pi$ $\Sigma_b K, \Sigma_b^* K$	$\Lambda_b K, \Xi_b\pi$ $\Xi_b'\pi$	$\Lambda_b K, \Xi_b\pi$ $\Xi_b'\pi, \Xi_b^*\pi$ $\Sigma_b K, \Sigma_b^* K$	$\Lambda_b K, \Xi_b\pi$ $\Xi_b'\pi, \Xi_b^*\pi$	$\Sigma_b\bar{K}, \Xi_b'\pi$ $\Sigma_b^*\bar{K}, \Xi_b^*\pi$ $\Lambda_b\bar{K}, \Xi_b\pi$ $\Xi_b\eta$	
$N=0$									
$\lvert 0,0,0,0\rangle$	$^2S_{1/2}$	0	≈0	⋯	⋯	⋯	≈0	0	<0.08
$\lvert 0,0,0,0\rangle$	$^4S_{3/2}$	0.2	2	⋯	⋯	⋯	1	0.02	0.90 ± 0.18
$N=1$									
$\lvert 1,0,0,0\rangle$	$^2P_{1/2}$	3	⋯	⋯	27	371	10	0.86	†
$\lvert 1,0,0,0\rangle$	$^4P_{1/2}$	4	⋯	⋯	32	91	17	0.65	†
$\lvert 1,0,0,0\rangle$	$^2P_{3/2}$	29	⋯	⋯	24	86	25	2.92	†
$\lvert 1,0,0,0\rangle$	$^4P_{3/2}$	8	⋯	⋯	16	7	24	1.83	†
$\lvert 1,0,0,0\rangle$	$^4P_{5/2}$	31	⋯	⋯	24	7	25	3.36	19.9 ± 2.6
$\lvert 0,1,0,0\rangle$	$^2P_{1/2}$	197	⋯	⋯	⋯	⋯	⋯	5.88	†
$\lvert 0,1,0,0\rangle$	$^2P_{3/2}$	97	⋯	⋯	⋯	⋯	⋯	3.08	†
$N=2$									
$\lvert 2,0,0,0\rangle$	$^2D_{3/2}$	14	⋯	101	⋯	40	⋯	⋯	†
$\lvert 2,0,0,0\rangle$	$^2D_{5/2}$	30	⋯	25	⋯	19	⋯	⋯	†
$\lvert 2,0,0,0\rangle$	$^4D_{1/2}$	25	⋯	109	⋯	39	⋯	⋯	†
$\lvert 2,0,0,0\rangle$	$^4D_{3/2}$	35	⋯	58	⋯	22	⋯	⋯	†
$\lvert 2,0,0,0\rangle$	$^4D_{5/2}$	46	⋯	28	⋯	2	⋯	⋯	†
$\lvert 2,0,0,0\rangle$	$^4D_{7/2}$	47	⋯	41	⋯	2	⋯	⋯	†
$\lvert 0,0,1,0\rangle$	$^2S_{1/2}$	47	⋯	⋯	⋯	34	56	⋯	†
$\lvert 0,0,1,0\rangle$	$^4S_{3/2}$	79	⋯	⋯	⋯	36	58	⋯	†
$\lvert 0,0,0,1\rangle$	$^2S_{1/2}$	599	⋯	⋯	⋯	⋯	⋯	⋯	†
$\lvert 0,0,0,1\rangle$	$^4S_{3/2}$	630	⋯	⋯	⋯	⋯	⋯	⋯	†
$\lvert 1,1,0,0\rangle$	$^2D_{3/2}$	234	⋯	⋯	⋯	⋯	⋯	⋯	†
$\lvert 1,1,0,0\rangle$	$^2D_{5/2}$	116	⋯	⋯	⋯	⋯	⋯	⋯	†
$\lvert 1,1,0,0\rangle$	$^2P_{1/2}$	3	⋯	⋯	⋯	⋯	⋯	⋯	†
$\lvert 1,1,0,0\rangle$	$^2P_{3/2}$	3	⋯	⋯	⋯	⋯	⋯	⋯	†
$\lvert 1,1,0,0\rangle$	$^2S_{1/2}$	59	⋯	⋯	⋯	⋯	⋯	⋯	†
$\lvert 0,2,0,0\rangle$	$^2D_{3/2}$	315	⋯	⋯	⋯	⋯	⋯	⋯	†
$\lvert 0,2,0,0\rangle$	$^2D_{5/2}$	209	⋯	⋯	⋯	⋯	⋯	⋯	†
$\lvert 0,2,0,0\rangle$	$^4D_{1/2}$	529	⋯	⋯	⋯	⋯	⋯	⋯	†
$\lvert 0,2,0,0\rangle$	$^4D_{3/2}$	364	⋯	⋯	⋯	⋯	⋯	⋯	†
$\lvert 0,2,0,0\rangle$	$^4D_{5/2}$	194	⋯	⋯	⋯	⋯	⋯	⋯	†
$\lvert 0,2,0,0\rangle$	$^4D_{7/2}$	349	⋯	⋯	⋯	⋯	⋯	⋯	†

TABLE XVI. Comparison of our predicted $\Omega_b(ssb)$ strong decay widths with those of other theoretical studies (in MeV). The flavor multiplet is indicated by the symbol $\mathcal{F}$. The first column contains the three-quark model state, $|l_\lambda, l_\rho, k_\lambda, k_\rho\rangle$, where $l_{\lambda,\rho}$ are the orbital angular momenta and $k_{\lambda,\rho}$ the number of nodes of the λ and ρ oscillators. The second column displays each state's spectroscopic notation $^{2S+1}L_J$. In the third column, our predicted strong decay widths, computed within the $^3P_0$ model and the baryon-meson channels included in the calculation, are shown. Our results are compared with those of Refs. [68] (fourth column), [67] (fifth column), [71] (sixth column), [76] (seventh column), and [98] (eighth column). The experimental widths, as from PDG [1], are reported in the ninth column. The symbol "..." indicates that there is no prediction for that state. The "†" indicates that there is no reported experimental decay width for that state up to now.

$\Omega_b(ssb)$ $\lvert l_\lambda, l_\rho, k_\lambda, k_\rho\rangle$	$\mathcal{F}=\mathbf{6}_{\rm f}$ $^{2S+1}L_J$	This work Γ (MeV)	[68] Γ (MeV)	[67] Γ (MeV)	[71] Γ (MeV)	[76] Γ (MeV)	[98] Γ (MeV)	Experimental Γ (MeV)
Channels		$\Xi_b K, \Xi_b' K, \Xi_b^* K$ $\Xi_b K^*, \Xi_b' K^*, \Xi_b^* K^*$ $\Omega_b \eta, \Omega_b^* \eta, \Omega_b \phi$ $\Omega_b^* \phi, \Omega_b \eta', \Omega_b^* \eta'$ $\Xi_8 B, \Xi_{10} B$	$\Xi_b K, \Xi_b' K$ $\Xi_b^* K$	$\Xi_b K$	$\Xi_b K, \Xi_b' K$ $\Xi_b^* K$	$\Xi_b K, \Xi_b' K$ $\Xi_b^* K$	$\Xi_b^0 K^-$	
$N=0$								
$\lvert 0,0,0,0\rangle$	$^2S_{1/2}$	0	...	...	...	...	0	≈0
$\lvert 0,0,0,0\rangle$	$^4S_{3/2}$	0	...	...	...	...	0	†
$N=1$								
$\lvert 1,0,0,0\rangle$	$^2P_{1/2}$	5	...	49	...	33	0.5	<4.2
$\lvert 1,0,0,0\rangle$	$^4P_{1/2}$	11	...	95	...	...	2.79	<4.7
$\lvert 1,0,0,0\rangle$	$^2P_{3/2}$	24	...	2	...	...	1.14	<1.8
$\lvert 1,0,0,0\rangle$	$^4P_{3/2}$	6	...	≈0	...	2	0.62	<3.2
$\lvert 1,0,0,0\rangle$	$^4P_{5/2}$	40	...	2	...	3	4.28	†
$\lvert 0,1,0,0\rangle$	$^2P_{1/2}$	10	...	...	...	...	0	†
$\lvert 0,1,0,0\rangle$	$^2P_{3/2}$	54	...	...	...	...	0	†
$N=2$								
$\lvert 2,0,0,0\rangle$	$^2D_{3/2}$	4	20	...	108	...	...	†
$\lvert 2,0,0,0\rangle$	$^2D_{5/2}$	10	8	...	21	...	...	†
$\lvert 2,0,0,0\rangle$	$^4D_{1/2}$	1	29	...	106	...	...	†
$\lvert 2,0,0,0\rangle$	$^4D_{3/2}$	3	20	...	27	...	...	†
$\lvert 2,0,0,0\rangle$	$^4D_{5/2}$	8	7	...	3	...	...	†
$\lvert 2,0,0,0\rangle$	$^4D_{7/2}$	18	9	...	3	...	...	†
$\lvert 0,0,1,0\rangle$	$^2S_{1/2}$	20	...	...	50	16	...	†
$\lvert 0,0,1,0\rangle$	$^4S_{3/2}$	17	...	...	53	16	...	†
$\lvert 0,0,0,1\rangle$	$^2S_{1/2}$	398	...	...	...	...	...	†
$\lvert 0,0,0,1\rangle$	$^4S_{3/2}$	257	...	...	...	...	...	†
$\lvert 1,1,0,0\rangle$	$^2D_{3/2}$	116	...	...	...	...	...	†
$\lvert 1,1,0,0\rangle$	$^2D_{5/2}$	82	...	...	...	...	...	†
$\lvert 1,1,0,0\rangle$	$^2P_{1/2}$	1	...	...	...	...	...	†
$\lvert 1,1,0,0\rangle$	$^2P_{3/2}$	2	...	...	...	...	...	†
$\lvert 1,1,0,0\rangle$	$^2S_{1/2}$	72	...	...	...	...	...	†
$\lvert 0,2,0,0\rangle$	$^2D_{3/2}$	180	...	...	...	...	...	†
$\lvert 0,2,0,0\rangle$	$^2D_{5/2}$	157	...	...	...	...	...	†
$\lvert 0,2,0,0\rangle$	$^4D_{1/2}$	126	...	...	...	...	...	†
$\lvert 0,2,0,0\rangle$	$^4D_{3/2}$	195	...	...	...	...	...	†
$\lvert 0,2,0,0\rangle$	$^4D_{5/2}$	172	...	...	...	...	...	†
$\lvert 0,2,0,0\rangle$	$^4D_{7/2}$	230	...	...	...	...	...	†

TABLE XVII. Predicted electromagnetic decay widths (in KeV) for $\Lambda_b(nnb)$ states belonging to the flavor multiplet $\mathcal{F}=\bar{\mathbf{3}}_{\mathrm{F}}$. The first column reports the baryon name with its predicted mass, calculated by using the three-quark model Hamiltonian given by Eqs. (1) and (2). The second column displays $\mathbf{J}^{\mathrm{P}}$, the third column shows the internal configuration of the baryon $|l_\lambda, l_\rho, k_\lambda, k_\rho\rangle$ within the three-quark model, where $l_{\lambda,\rho}$ represent the orbital angular momenta and $k_{\lambda,\rho}$ denote the number of nodes of the λ and ρ oscillators. The fourth column presents the spectroscopic notation $^{2S+1}L_J$ for each state. Furthermore, $N=n_\rho+n_\lambda$ separates the $N=0$, 1 energy bands. Starting from the fifth column, the electromagnetic decay widths, computed by using Eq. (20), are presented. Each column corresponds to an electromagnetic decay channel, the decay products are indicated at the top of the column and their masses are shown in Table XXVII. The electromagnetic widths are given in KeV. The zero values are electromagnetic decay widths that are either too small to be shown on this scale or not permitted by phase space. Our results are compared with those of Refs. [67,104]. The symbol "..." indicates that there is no prediction for that state in Ref. [67].

$\mathcal{F}=\bar{\mathbf{3}}_{\mathrm{F}}$ $\Lambda_b(nnb)$	$\mathbf{J}^P$	$\lvert l_\lambda, l_\rho, k_\lambda, k_\rho\rangle$	$^{2S+1}L_J$	$\Lambda_b^0\gamma$	$\Sigma_b^0\gamma$	$\Sigma_b^*\gamma$	
$N=0$							
$\Lambda_b(5613)$	$\frac{1}{2}^+$	$\lvert 0,0,0,0\rangle$	$^2S_{1/2}$	0	0	0	
$N=1$							
$\Lambda_b(5918)$	$\frac{1}{2}^-$	$\lvert 1,0,0,0\rangle$	$^2P_{1/2}$	64^{+5}_{-4}	$0.4^{+0.1}_{-0.1}$	0	
				50.2	0.14	0.09	[67]
				40.7	0.2	0.0	[104]
$\Lambda_b(5924)$	$\frac{3}{2}^-$	$\lvert 1,0,0,0\rangle$	$^2P_{3/2}$	65^{+5}_{-5}	$0.5^{+0.2}_{-0.2}$	$0.1^{+0.03}_{-0.03}$	
				52.8	0.21	0.15	[67]
				43.4	0.3	0.0	[104]
$\Lambda_b(6114)$	$\frac{1}{2}^-$	$\lvert 0,1,0,0\rangle$	$^2P_{1/2}$	15^{+2}_{-2}	519^{+40}_{-39}	3^{+1}_{-1}	
				1.62	16.2	0.02	[67]
				10.2	93.3	2.0	[104]
$\Lambda_b(6137)$	$\frac{1}{2}^-$	$\lvert 0,1,0,0\rangle$	$^4P_{1/2}$	9^{+2}_{-1}	6^{+2}_{-2}	76^{+16}_{-17}	
				0.81	0.02	8.25	[67]
				5.6	3.5	6.2	[104]
$\Lambda_b(6121)$	$\frac{3}{2}^-$	$\lvert 0,1,0,0\rangle$	$^2P_{3/2}$	16^{+2}_{-2}	1025^{+101}_{-94}	3^{+1}_{-1}	
				1.81	15.1	0.03	[67]
				10.6	315.6	2.2	[104]
$\Lambda_b(6143)$	$\frac{3}{2}^-$	$\lvert 0,1,0,0\rangle$	$^4P_{3/2}$	25^{+4}_{-4}	17^{+6}_{-4}	382^{+30}_{-30}	
				2.54	0.07	9.90	[67]
				16.2	10.6	73.9	[104]
$\Lambda_b(6153)$	$\frac{5}{2}^-$	$\lvert 0,1,0,0\rangle$	$^4P_{5/2}$	17^{+3}_{-3}	12^{+4}_{-4}	1023^{+111}_{-108}	
				...	...	...	[67]
				11.0	7.8	216.5	[104]

functions are expressed in terms of ω_ρ and ω_λ using the relation $\alpha^2_{\rho,\lambda}=\omega_{\rho,\lambda}m_{\rho,\lambda}$, and we use the usual definitions for $n_{\rho(\lambda)}=2k_{\rho(\lambda)}+l_{\rho(\lambda)}$, $k_{\rho(\lambda)}=0,1,\ldots,$ and $l_{\rho(\lambda)}=0,1,\ldots$; where $l_{\rho(\lambda)}$ is the orbital angular momentum of the $\rho(\lambda)$ oscillator, and $k_{\rho(\lambda)}$ is the number of nodes (radial excitations) in the $\rho(\lambda)$ oscillators.

The $\hat{U}_j$ matrix elements from the ground states to ground states are given by

$$\langle 0,0,0,0,0,0|\hat{U}_1|0,0,0,0,0,0\rangle = \langle 0,0,0,0,0,0|\hat{U}_2|0,0,0,0,0,0\rangle = \exp\left[-\frac{1}{8}\mathrm{k}^2\left(\frac{1}{\alpha_\rho^2}+\frac{3{m_b}^2}{\alpha_\lambda^2(2m_\rho+m_b)^2}\right)\right], \tag{35}$$

$$\langle 0,0,0,0,0,0|\hat{U}_3|0,0,0,0,0,0\rangle = \exp\left[-\frac{3\mathrm{k}^2m_\rho^2}{2\alpha_\lambda^2(2m_\rho+m_b)^2}\right]. \tag{36}$$

TABLE XVIII. Same as Table XVII, but for $\Xi_b(snb)$ states belonging to the flavor multiplet $\mathcal{F} = \bar{\mathbf{3}}_{\mathrm{F}}$.

$\mathcal{F} = \bar{\mathbf{3}}_{\mathrm{F}}$ $\Xi_b(snb)$	$\mathbf{J}^P$	$\lvert l_\lambda, l_\rho, k_\lambda, k_\rho\rangle$	$^{2S+1}L_J$	$\Xi_b^0\gamma$	$\Xi_b^-\gamma$	$\Xi_b'^0\gamma$	$\Xi_b'^-\gamma$	$\Xi_b'^{*0}\gamma$	$\Xi_b'^{*-}\gamma$	
$N = 0$										
$\Xi_b(5806)$	$\frac{1}{2}^+$	$\lvert 0,0,0,0\rangle$	$^2S_{1/2}$	0	0	0	0	0	0	
$N = 1$										
$\Xi_b(6079)$	$\frac{1}{2}^-$	$\lvert 1,0,0,0\rangle$	$^2P_{1/2}$	122^{+16}_{-13}	126^{+10}_{-10}	$1.1^{+0.3}_{-0.3}$	0	$0.2^{+0.06}_{-0.06}$	0	
				63.6	135	1.32	0.0	2.04	0.0	[67]
				83.1	91.5	0.6	0.0	0.1	0.0	[104]
$\Xi_b(6085)$	$\frac{3}{2}^-$	$\lvert 1,0,0,0\rangle$	$^2P_{3/2}$	125^{+16}_{-13}	126^{+10}_{-10}	$1.3^{+0.4}_{-0.4}$	0	$0.2^{+0.06}_{-0.06}$	0	
				68.3	147	1.68	0.0	2.64	0.0	[67]
				88.9	96.1	0.7	0.0	0.2	0.0	[104]
$\Xi_b(6248)$	$\frac{1}{2}^-$	$\lvert 0,1,0,0\rangle$	$^2P_{1/2}$	19^{+5}_{-4}	28^{+6}_{-5}	494^{+36}_{-34}	9^{+2}_{-1}	$2^{+0.6}_{-0.6}$	0	
				1.86	7.19	94.3	0.0	0.62	0.0	[67]
				13.3	21.8	144.5	3.1.	1.7	0.0	[104]
$\Xi_b(6271)$	$\frac{1}{2}^-$	$\lvert 0,1,0,0\rangle$	$^4P_{1/2}$	11^{+4}_{-3}	17^{+4}_{-4}	5^{+2}_{-2}	$0.1^{+0.03}_{-0.03}$	75^{+14}_{-15}	$1.4^{+0.4}_{-0.4}$	
				0.93	3.59	0.16	0.0	80.0	0.0	[67]
				7.5	12.3	2.9	0.1	14.7	0.3	[104]
$\Xi_b(6255)$	$\frac{3}{2}^-$	$\lvert 0,1,0,0\rangle$	$^2P_{3/2}$	20^{+5}_{-4}	29^{+6}_{-5}	950^{+98}_{-89}	17^{+4}_{-3}	3^{+1}_{-1}	0	
				2.10	8.13	69.4	0.0	0.80	0.0	[67]
				14.0	23.0	377.2	8.0	1.9	0.0	[104]
$\Xi_b(6277)$	$\frac{3}{2}^-$	$\lvert 0,1,0,0\rangle$	$^4P_{3/2}$	33^{+9}_{-7}	48^{+11}_{-10}	14^{+5}_{-4}	$0.3^{+0.1}_{-0.1}$	363^{+28}_{-27}	7^{+1}_{-1}	
				2.94	11.4	0.8	0.0	78.0	0.0	[67]
				22.2	36.3	8.8	0.2	109.7	2.3	[104]
$\Xi_b(6287)$	$\frac{5}{2}^-$	$\lvert 0,1,0,0\rangle$	$^4P_{5/2}$	23^{+6}_{-5}	34^{+8}_{-7}	10^{+4}_{-3}	$0.2^{+0.06}_{-0.06}$	945^{+106}_{-99}	17^{+4}_{-3}	
				...	...	...	...	...	...	[67]
				15.4	25.3	6.5	0.1	245.2	5.2	[104]

The $\hat{T}_{j,-}$ matrix elements from the ground states to ground states are all 0, i.e.

$$\begin{aligned}\langle 0,0,0,0,0,0|\hat{T}_{1,-}|0,0,0,0,0,0\rangle &= \langle 0,0,0,0,0,0|\hat{T}_{2,-}|0,0,0,0,0,0\rangle \\ &= \langle 0,0,0,0,0,0|\hat{T}_{3,-}|0,0,0,0,0,0\rangle = 0\end{aligned} \tag{37}$$

The $\hat{U}_j$ matrix elements from P_ρ-wave states to ground states are

$$\begin{aligned}\langle 0,0,0,0,0,0|\hat{U}_1|0,1,m_{l\rho},0,0,0\rangle &= -\langle 0,0,0,0,0,0|\hat{U}_2|0,1,m_{l\rho},0,0,0\rangle \\ &= -\frac{i\mathrm{k}}{2\alpha_\rho}\exp\left[-\frac{1}{8}\mathrm{k}^2\left(\frac{1}{\alpha_\rho^2}+\frac{3{m_b}^2}{\alpha_\lambda^2(2m_\rho+m_b)^2}\right)\right],\end{aligned} \tag{38}$$

$$\langle 0,0,0,0,0,0|\hat{U}_3|0,1,m_{l\rho},0,0,0\rangle = 0, \tag{39}$$

and from the P_λ-wave states to ground states

$$\begin{aligned}\langle 0,0,0,0,0,0|\hat{U}_1|0,0,0,0,1,m_{l_\lambda}\rangle &= \langle 0,0,0,0,0,0|\hat{U}_2|0,0,0,0,1,m_{l_\lambda}\rangle \\ &= -\frac{i\sqrt{3}\mathrm{k}m_b}{2\alpha_\lambda(2m_\rho+m_b)}\exp\left[-\frac{1}{8}\mathrm{k}^2\left(\frac{1}{\alpha_\rho^2}+\frac{3{m_b}^2}{\alpha_\lambda^2(2m_\rho+m_b)^2}\right)\right],\end{aligned} \tag{40}$$

$$\langle 0,0,0,0,0,0|\hat{U}_3|0,0,0,0,1,m_{l_\lambda}\rangle = \frac{i\sqrt{3}\mathrm{k}m_\rho}{\alpha_\lambda(2m_\rho+m_b)}\exp\left[-\frac{3\mathrm{k}^2m_\rho^2}{2\alpha_\lambda^2(2m_\rho+m_b)^2}\right]. \tag{41}$$

TABLE XIX. Same as Table XVII, but for $\Sigma_b(nnb)$ states belonging to the flavor multiplet $\mathcal{F}=\mathbf{6}_{\mathrm{F}}$.

$\mathcal{F}=\mathbf{6}_{\mathrm{F}}$ $\Sigma_b(nnb)$	$\mathbf{J}^P$	$\lvert l_\lambda,l_\rho,k_\lambda,k_\rho\rangle$	$^{2S+1}L_J$	$\Sigma_b^+\gamma$	$\Sigma_b^0\gamma$	$\Sigma_b^-\gamma$	$\Lambda_b^0\gamma$	$\Sigma_b^{*+}\gamma$	$\Sigma_b^{*0}\gamma$	$\Sigma_b^{*-}\gamma$	
$N=0$											
$\Sigma_b(5804)$	$\frac{1}{2}^+$	$\lvert 0,0,0,0\rangle$	$^2S_{1/2}$	0	0	0	150^{+46}_{-40}	0	0	0	
$\Sigma_b(5832)$	$\frac{3}{2}^+$	$\lvert 0,0,0,0\rangle$	$^4S_{3/2}$	$0.5^{+0.2}_{-0.2}$	0	$0.1^{+0.03}_{-0.03}$	215^{+56}_{-51}	0	0	0	
$N=1$											
$\Sigma_b(6108)$	$\frac{1}{2}^-$	$\lvert 1,0,0,0\rangle$	$^2P_{1/2}$	407^{+46}_{-47}	34^{+3}_{-3}	73^{+10}_{-10}	195^{+32}_{-27}	6^{+3}_{-2}	$0.4^{+0.1}_{-0.1}$	$2^{+1}_{-0.6}$	
				1016	74.9	212	133	16.9	1.03	4.36	[67]
				267.7	21.3	50.9	156.2	5.3	0.3	1.5	[104]
$\Sigma_b(6131)$	$\frac{1}{2}^-$	$\lvert 1,0,0,0\rangle$	$^4P_{1/2}$	13^{+5}_{-4}	$0.8^{+0.2}_{-0.2}$	3^{+1}_{-1}	111^{+19}_{-17}	36^{+18}_{-17}	4^{+1}_{-1}	5^{+2}_{-2}	
				5.31	0.32	1.37	63.6	867	63.6	182	[67]
				8.9	0.5	2.5	85.3	19.2	1.9	2.7	[104]
$\Sigma_b(6114)$	$\frac{3}{2}^-$	$\lvert 1,0,0,0\rangle$	$^2P_{3/2}$	1202^{+132}_{-122}	89^{+10}_{-9}	252^{+28}_{-26}	202^{+31}_{-28}	7^{+3}_{-2}	$0.4^{+0.1}_{-0.1}$	$2^{+0.6}_{-0.6}$	
				483	37.9	94	129	15.6	0.95	4.02	[67]
				864.7	59.3	196.2	162.2	5.8	0.3	1.6	[104]
$\Sigma_b(6137)$	$\frac{3}{2}^-$	$\lvert 1,0,0,0\rangle$	$^4P_{3/2}$	40^{+12}_{-10}	$2^{+0.6}_{-0.6}$	10^{+3}_{-3}	321^{+46}_{-42}	316^{+31}_{-32}	26^{+2}_{-2}	59^{+7}_{-7}	
				13.1	0.8	3.39	170	527	39.8	107	[67]
				27.2	1.5	7.7	247.4	209.6	16.2	41.6	[104]
$\Sigma_b(6147)$	$\frac{5}{2}^-$	$\lvert 1,0,0,0\rangle$	$^4P_{5/2}$	29^{+10}_{-8}	$2^{+0.6}_{-0.6}$	7^{+2}_{-2}	218^{+34}_{-30}	1222^{+151}_{-141}	90^{+11}_{-10}	256^{+33}_{-30}	
				8.07	0.49	2.08	83.3	426	32.6	85.3	[67]
				20.0	1.1	5.7	168.2	589.4	39.5	137.0	[104]
$\Sigma_b(6304)$	$\frac{1}{2}^-$	$\lvert 0,1,0,0\rangle$	$^2P_{1/2}$	247^{+45}_{-40}	15^{+3}_{-2}	62^{+11}_{-10}	424^{+42}_{-42}	103^{+22}_{-19}	6^{+1}_{-1}	26^{+5}_{-5}	
				…	…	…	…	…	…	…	[67]
				182.1	10.3	50.2	526.5	79.3	4.5	21.9	[104]
$\Sigma_b(6311)$	$\frac{3}{2}^-$	$\lvert 0,1,0,0\rangle$	$^2P_{3/2}$	256^{+46}_{-41}	16^{+3}_{-3}	64^{+12}_{-10}	414^{+39}_{-39}	107^{+22}_{-19}	7^{+1}_{-1}	27^{+5}_{-5}	
				…	…	…	…	…	…	…	[67]
				189.2	10.7	52.1	523.1	82.8	4.7	22.8	[104]

The $\hat{T}_{j,-}$ matrix elements from P_ρ-wave states to ground states are

$$\begin{aligned}\langle 0,0,0,0,0,0|\hat{T}_{1,-}|0,1,m_{l\rho},0,0,0\rangle &= -\langle 0,0,0,0,0,0|\hat{T}_{2,-}|0,1,m_{l\rho},0,0,0\rangle \\ &= i\sqrt{2}\alpha_\rho \exp\left[-\frac{1}{8}\mathrm{k}^2\left(\frac{1}{\alpha_\rho^2}+\frac{3{m_b}^2}{\alpha_\lambda^2(2m_\rho+m_b)^2}\right)\right]\delta_{m_{l_\rho},1},\end{aligned} \tag{42}$$

$$\langle 0,0,0,0,0,0|\hat{T}_{3,-}|0,1,m_{l\rho},0,0,0\rangle = 0, \tag{43}$$

and finally from P_λ-wave states to ground states we have

$$\begin{aligned}\langle 0,0,0,0,0,0|\hat{T}_{1,-}|0,0,0,0,1,m_{l_\lambda}\rangle &= \langle 0,0,0,0,0,0|\hat{T}_{2,-}|0,0,0,0,1,m_{l_\lambda}\rangle \\ &= i\sqrt{\frac{2}{3}}\alpha_\lambda \exp\left[\frac{-\mathrm{k}^2}{8}\left(\frac{1}{\alpha_\rho^2}+\frac{3m_b^2}{\alpha_\lambda^2(2m_\rho+m_b)^2}\right)\right]\delta_{m_{l_\lambda},1},\end{aligned} \tag{44}$$

$$\langle 0,0,0,0,0,0|\hat{T}_{3,-}|0,0,0,0,1,m_{l_\lambda}\rangle = -2i\sqrt{\frac{2}{3}}\alpha_\lambda \exp\left[\frac{-3\mathrm{k}^2m_\rho^2}{2\alpha_\lambda^2(2m_\rho+m_b)^2}\right]\delta_{m_{l_\lambda},1}. \tag{45}$$

We observe that, if we replace $\mathbf{p}_\lambda$ with $im_\lambda \mathrm{k}_0\boldsymbol{\lambda}$, and $\mathbf{p}_\rho$ with $im_\rho \mathrm{k}_0\boldsymbol{\rho}$, we obtain the analytical expressions given in Eq. (48) of Ref. [104],[1] thus confirming that Ref. [104] does not contain the exact electromagnetic calculation. This explains the different results for the electromagnetic decay widths in the two articles, as can be observed in Tables XVII–XXI.

[1]In a private communication, Roelof Bijker confirmed that in Ref. [104] they calculated the electromagnetic decay by replacing $\mathbf{p}_\lambda$ with $im_\lambda \mathrm{k}_0\boldsymbol{\lambda}$ and $\mathbf{p}_\rho$ with $im_\rho \mathrm{k}_0\boldsymbol{\rho}$.

TABLE XX. Same as Table XVII, but for $\Xi_b'(snb)$ states belonging to the flavor multiplet $\mathcal{F} = \mathbf{6}_{\mathrm{F}}$.

$\mathcal{F} = \mathbf{6}_{\mathrm{F}}$ $\Xi_b'(snb)$	$\mathbf{J}^P$	$\lvert l_\lambda, l_\rho, k_\lambda, k_\rho\rangle$	$^{2S+1}L_J$	$\Xi_b^0\gamma$	$\Xi_b^-\gamma$	$\Xi_b'^0\gamma$	$\Xi_b'^-\gamma$	$\Xi_b'^{*0}\gamma$	$\Xi_b'^{*-}\gamma$	
$N = 0$										
$\Xi_b'(5925)$	$\frac{1}{2}^+$	$\lvert 0,0,0,0\rangle$	$^2S_{1/2}$	33^{+16}_{-13}	$0.6^{+0.2}_{-0.2}$	0	0	0	0	
$\Xi_b'(5953)$	$\frac{3}{2}^+$	$\lvert 0,0,0,0\rangle$	$^4S_{3/2}$	60^{+24}_{-20}	$1.1^{+0.3}_{-0.3}$	$0.1^{+0.03}_{-0.03}$	$0.1^{+0.03}_{-0.03}$	0	0	
$N = 1$										
$\Xi_b'(6198)$	$\frac{1}{2}^-$	$\lvert 1,0,0,0\rangle$	$^2P_{1/2}$	65^{+13}_{-11}	$1.2^{+0.3}_{-0.3}$	78^{+9}_{-8}	71^{+7}_{-6}	$0.4^{+0.1}_{-0.1}$	$0.6^{+0.2}_{-0.2}$	
				72.2	0.0	76.3	190	0.89	3.54	[67]
				50.7	1.1	52.9	50.8	0.3	0.5	[104]
$\Xi_b'(6220)$	$\frac{1}{2}^-$	$\lvert 1,0,0,0\rangle$	$^4P_{1/2}$	40^{+9}_{-8}	$0.7^{+0.2}_{-0.2}$	$1^{+0.3}_{-0.3}$	$1.4^{+0.4}_{-0.4}$	11^{+2}_{-2}	9^{+2}_{-2}	
				34	0.0	0.25	1.48	69.5	164	[67]
				29.3	0.6	0.6	1.0	6.9	5.6	[104]
$\Xi_b'(6204)$	$\frac{3}{2}^-$	$\lvert 1,0,0,0\rangle$	$^2P_{3/2}$	68^{+13}_{-12}	$1.3^{+0.4}_{-0.4}$	157^{+18}_{-15}	167^{+15}_{-15}	$0.4^{+0.1}_{-0.1}$	$1^{+0.3}_{-0.3}$	
				72.8	0.0	43.9	92.3	0.9	3.6	[67]
				53.9	1.1	111.5	128.1	0.3	0.6	[104]
$\Xi_b'(6226)$	$\frac{3}{2}^-$	$\lvert 1,0,0,0\rangle$	$^4P_{3/2}$	117^{+21}_{-19}	$2^{+0.6}_{-0.6}$	3^{+1}_{-1}	4^{+1}_{-1}	57^{+6}_{-5}	54^{+5}_{-4}	
				94.0	0.0	0.67	2.94	47.5	104	[67]
				87.1	1.8	1.7	3.0	38.8	38.5	[104]
$\Xi_b'(6237)$	$\frac{5}{2}^-$	$\lvert 1,0,0,0\rangle$	$^4P_{5/2}$	82^{+18}_{-15}	$2^{+0.6}_{-0.6}$	$2^{+0.6}_{-0.6}$	3^{+1}_{-1}	157^{+21}_{-18}	168^{+19}_{-17}	
				47.7	0.0	0.44	1.88	41.5	88.2	[67]
				61.6	1.3	1.3	2.2	69.4	82.7	[104]
$\Xi_b'(6367)$	$\frac{1}{2}^-$	$\lvert 0,1,0,0\rangle$	$^2P_{1/2}$	644^{+54}_{-52}	12^{+3}_{-2}	19^{+3}_{-3}	28^{+5}_{-4}	7^{+1}_{-1}	11^{+2}_{-2}	
				...	...	...	...	...	...	[67]
				708.1	15.0	13.4	21.9	5.5	9.0	[104]
$\Xi_b'(6374)$	$\frac{3}{2}^-$	$\lvert 0,1,0,0\rangle$	$^2P_{3/2}$	637^{+52}_{-50}	12^{+3}_{-2}	20^{+4}_{-3}	29^{+5}_{-5}	8^{+2}_{-1}	12^{+2}_{-2}	
				...	...	...	...	...	...	[67]
				714.7	15.2	14.1	23.0	5.9	9.6	[104]

TABLE XXI. Same as Table XVII, but for $\Omega_b(ssb)$ states belonging to the flavor multiplet $\mathcal{F} = \mathbf{6}_{\mathrm{F}}$.

$\mathcal{F} = \mathbf{6}_{\mathrm{F}}$ $\Omega_b(ssb)$	$\mathbf{J}^P$	$\lvert l_\lambda, l_\rho, k_\lambda, k_\rho\rangle$	$^{2S+1}L_J$	$\Omega_b\gamma$	$\Omega_b^*\gamma$	
$N = 0$						
$\Omega_b(6064)$	$\frac{1}{2}^+$	$\lvert 0,0,0,0\rangle$	$^2S_{1/2}$	0	0	
$\Omega_b(6093)$	$\frac{3}{2}^+$	$\lvert 0,0,0,0\rangle$	$^4S_{3/2}$	$0.1^{+0.03}_{-0.03}$	0	
$N = 1$						
$\Omega_b(6315)$	$\frac{1}{2}^-$	$\lvert 1,0,0,0\rangle$	$^2P_{1/2}$	51^{+5}_{-4}	$0.2^{+0.06}_{-0.06}$	
				154	1.49	[67]
				36.0	0.2	[104]
$\Omega_b(6337)$	$\frac{1}{2}^-$	$\lvert 1,0,0,0\rangle$	$^4P_{1/2}$	$0.5^{+0.2}_{-0.2}$	8^{+2}_{-2}	
				0.64	99.23	[67]
				0.4	5.1	[104]
$\Omega_b(6321)$	$\frac{3}{2}^-$	$\lvert 1,0,0,0\rangle$	$^2P_{3/2}$	99^{+10}_{-10}	$0.2^{+0.06}_{-0.06}$	
				83.4	1.51	[67]
				73.7	0.2	[104]
$\Omega_b(6343)$	$\frac{3}{2}^-$	$\lvert 1,0,0,0\rangle$	$^4P_{3/2}$	$2^{+0.6}_{-0.6}$	38^{+3}_{-3}	
				1.81	70.68	[67]
				1.1	26.7	[104]
$\Omega_b(6353)$	$\frac{5}{2}^-$	$\lvert 1,0,0,0\rangle$	$^4P_{5/2}$	$1^{+0.2}_{-0.3}$	99^{+12}_{-12}	
				1.21	63.26	[67]
				0.9	45.1	[104]

(Table continued)

TABLE XXI. *(Continued)*

$\mathcal{F}=\mathbf{6}_{\mathrm{F}}$ $\Omega_b(ssb)$	$\mathbf{J}^P$	$\lvert l_\lambda, l_\rho, k_\lambda, k_\rho\rangle$	$^{2S+1}L_J$	$\Omega_b\gamma$	$\Omega_b^*\gamma$	
$\Omega_b(6465)$	$\frac{1}{2}^-$	$\lvert 0,1,0,0\rangle$	$^2P_{1/2}$	12^{+2}_{-2}	4^{+1}_{-1}	
				⋯	⋯	[67]
				8.7	3.4	[104]
$\Omega_b(6471)$	$\frac{3}{2}^-$	$\lvert 0,1,0,0\rangle$	$^2P_{3/2}$	12^{+3}_{-2}	5^{+1}_{-1}	
				⋯	⋯	[67]
				9.2	3.7	[104]

Additional details regarding the relationship between the matrix elements of $\hat{T}_{j,-}$, expressed as a sum of matrix elements involving the $\hat{U}_j$ operators, are found in Appendix G 3. Our methodology outlined here enables exact analytical evaluation of the matrix elements associated with the $\hat{T}_{j,-}$ operators.

As explained in the strong decay section (Sec. III), the harmonic oscillator wave functions depend on the harmonic oscillator constant K_b and the constituent quark masses. Consequently, the electromagnetic decay width calculation does not introduce any additional parameters. Moreover, when we calculate the electromagnetic decay widths, we account for the uncertainties associated with the mass model parameters and the decay product masses. The experimental values for the decay product masses and their corresponding uncertainties are given in Appendix F. The error propagation was conducted following the Monte Carlo error propagation outlined in Sec. II F.

A. Bottom baryon electromagnetic decay width results

Our electromagnetic decay widths calculated by means of Eq. (20) are presented in Tables XVII–XXI. These results extend those obtained by several works on the subject. For example, the analysis performed in [67] employs a constituent quark model. Other studies of radiative decays in different frameworks use heavy quark symmetry [94], bound state picture [96], relativistic three-quark model [97], light cone QCD sum rules [84–90], heavy hadron chiral perturbation theory [91–93], and modified bag models [95].

The experimental widths include contributions from the strong, electromagnetic, and weak interactions, with the dominant contribution coming from the strong decays. Our electromagnetic decay widths represent a minor contribution, typically under 1.5 MeV, which is of the same order as the uncertainties on the strong decay widths.

The electromagnetic decay widths are particularly valuable in cases where the strong decays are suppressed. One notable example is the spin excitation of the Ω_b^- state, denoted as Ω_b^*, which has not yet been observed. The $\Omega_b^* \to \Omega_b^-\pi$ strong decay is prohibited due to lack of phase space and isospin conservation in strong interactions. Therefore, the $\Omega_b^* \to \Omega_b^-\gamma$ decay mode becomes a particularly important channel, as it serves as a "golden channel" for the observation of the Ω_b^* state.

In addition, we compare our electromagnetic decay widths with the previous studies such as χQM [67] and NRQM [104] as shown in Tables XVII–XXI.

V. ASSIGNMENTS AND DISCUSSION

First, we will make the assignments of the bottom baryons reported in PDG [1] using our theoretical results for Λ_b, Ξ_b, Σ_b, Ξ_b', and Ω_b. Our first criterion is to use the mass spectrum to identify resonances of bottom baryons, while the decay width serves as a secondary criterion. The classification within the quark-diquark model is the same as that of the three-quark model when it comes to describing ground states and $\boldsymbol{\lambda}$-mode excitations. However, it is important to note that in the quark-diquark model, the $\boldsymbol{\rho}$-modes which exist in the three-quark model, are absent (see Tables II–VI).

A. Λ_b baryons

We make the assignment of the six Λ_b states reported by the PDG [1], using our predictions given in Table II.

1. Λ_b^0

The Λ_b^0 is identified as the ground state with $\mathbf{J}^P = \frac{1}{2}^+$, and its theoretical mass is well reproduced in both the three-quark and quark-diquark models.

2. $\Lambda_b(5912)^0$ and $\Lambda_b(5920)^0$

The $\Lambda_b(5912)^0$ and $\Lambda_b(5920)^0$ are identified as the two P_λ waves with $\mathbf{J}^P = \frac{1}{2}^-$ and $\mathbf{J}^P = \frac{3}{2}^-$, respectively. Our theoretical predictions for their mass are in agreement with the experimental values. There are no strong decay channels, so their strong decay widths are zero.

3. $\Lambda_b(6070)^0$

LHCb observed $\Lambda_b(6070)^0$ [21] with mass and decay width

$$m[\Lambda_b(6072)^0] = 6072.3 \pm 2.9 \pm 0.6 \pm 0.2 \text{ MeV}, \quad (46)$$

$$\Gamma[\Lambda_b(6072)^0] = 72 \pm 11 \pm 2 \text{ MeV}, \tag{47}$$

and suggested the assignment to the first radial excitation of Λ_b with $\mathbf{J}^P = \frac{1}{2}^+$. However, its quantum numbers have not yet been determined experimentally.

In the model of Ref. [98], if we consider it as a Roper-like state, there is a deviation of approximately 3% in its mass, and its width is (29 ± 14) MeV.

As we are aware of the limitations of the harmonic oscillator model in reproducing the masses of Roper-like states, we also calculate the decay width of $\Lambda_b(6072)$ by using its experimental mass as input, and considering it to be a $2S$ state. The calculated width is found to be 3.1 MeV, a reduction of 90% due to the closure of some dominant open flavor channels; this is even more unfavorable when compared with the experimental decay width of 72 MeV. This suggests that $\Lambda_b(6072)$ cannot conclusively be considered a $2S$ state. Nevertheless, we can identify $\Lambda_b(6072)$ as a P_ρ state with $\mathbf{J}^P = \frac{1}{2}^-$, featuring an internal spin of $\mathbf{S}_{\text{tot}} = \frac{1}{2}$. In this scenario, its experimental width is accurately reproduced, although the mass is slightly overestimated.

4. $\Lambda_b(6146)^0$ and $\Lambda_b(6152)^0$

$\Lambda_b(6146)^0$ and $\Lambda_b(6152)^0$ are identified as the two D_λ excitations with quantum numbers $\mathbf{J}^P = \frac{3}{2}^+$ and $\mathbf{J}^P = \frac{5}{2}^+$, respectively, but their quantum numbers have not yet been measured. In this case, our theoretical predictions for the mass have a small deviation of 1%, and their theoretical widths are slightly overestimated.

B. Ξ_b and Ξ_b' baryons

We shall now make the assignments for the states Ξ_b and Ξ_b' reported in PDG [1]. In the flavor space, the Ξ_b states belong to the $\bar{\mathbf{3}}_{\text{F}}$ configuration and the Ξ_b' states belong to the $\mathbf{6}_{\text{F}}$ configuration. Invariance of the strong interaction under $SU_I(2)$ isospin transformations leads to isospin conservation and the appearance of degenerate isospin multiplets. In the case of the Ξ_b and Ξ_b' baryons, both belong to isospin doublets. In this case, the assignment is more complicated because there are several theoretically excited states in the same energy range for Ξ_b and Ξ_b'. Here we use our results reported in Tables III for Ξ_b and V for Ξ_b'.

1. Ξ_b

Both our three-quark and quark-diquark models predict that the masses of the isospin partner Ξ_b^0 and Ξ_b^- are degenerate, which is in agreement with experimental data [1]. In our model, we assign to them the quantum numbers $\mathbf{J}^P = \frac{1}{2}^+$, even though these quantum numbers have not yet been directly measured.

2. $\Xi_b'(5935)^-$

The $\Xi_b'(5935)^-$ is considered to be the ground state of the sextuplet. Its predicted mass agrees with the experimental data in the three-quark and the quark-diquark models, its assignment is $\mathbf{J}^P = \frac{1}{2}^+$, but the quantum numbers have not yet been measured, nor has its charged partner, $\Xi_b'(5935)^0$, been observed.

3. $\Xi_b'(5955)^-$ and $\Xi_b'(5945)^0$

The spin excitations of $\Xi_b'(5935)^-$ are $\Xi_b'(5955)^-$ and $\Xi_b'(5945)^0$ these are identified as $\mathbf{J}^P = \frac{3}{2}^+$, but their quantum numbers are based on the expectations of the quark model. The predicted masses of the $\Xi_b'(5955)^-$ and $\Xi_b'(5945)^0$ are degenerate and in agreement with experimental data. Their widths is also well reproduced in our model.

4. $\Xi_b'(6100)^-$

$\Xi_b'(6100)^-$ is identified as a P-wave state, $\mathbf{J}^P = \frac{1}{2}^-$, but its $\mathbf{J}^P$ remains to be confirmed. It is identified as one of the two P_λ excitations of Ξ_b belonging to the $\bar{\mathbf{3}}_{\text{F}}$, with total internal spin $\mathbf{S}_{\text{tot}} = \frac{1}{2}$. Both its mass and width have been well described.

5. $\Xi_b'(6227)^-$ and $\Xi_b'(6227)^0$

Finally, the PDG reports $\Xi_b'(6227)^-$ and $\Xi_b'(6227)^0$, which in our model are identified with the fifth P_λ excitation of Ξ_b' with $\mathbf{J}^P = \frac{5}{2}^-$ and total internal spin $\mathbf{S}_{\text{tot}} = \frac{3}{2}$. Its predicted mass is compatible with the experimental value, and its width is well reproduced. However, it could be identified as $\mathbf{J}^P = \frac{3}{2}^-$ since these states also have similar mass. With this assignment, however, the predicted width has a deviation of 6 MeV from the experimental value.

6. $\Xi_b(6327)^0$ and $\Xi_b(6333)^0$

Recently, the PDG [1] added the two $\Xi_b(6327)^0$ and $\Xi_b(6333)^0$ states observed by LHCb [23]. The observed masses of these states are $m(\Xi_b(6327)^0) = 6327.28^{+0.23}_{-0.21} \pm 0.12 \pm 0.24$ MeV and $m(\Xi_b(6333)^0) = 6332.69^{+0.17}_{-0.18} \pm 0.03 \pm 0.22$ MeV, respectively. In the model of Ref. [98], we identify them as the two D_λ excitations, with quantum numbers $\mathbf{J}^P = \frac{3}{2}^+$ and $\mathbf{J}^P = \frac{5}{2}^+$, respectively, belonging to the $\bar{\mathbf{3}}_{\text{F}}$ configuration.

7. $\Xi_b(6087)^0$ and $\Xi_b(6095)^0$

Last year, LHCb reported the discovery of $\Xi_b(6087)^0$ and $\Xi_b(6095)^0$ states [24], which are not yet listed in the PDG. We associate $\Xi_b(6087)$ [24] with the $1P$ $1/2^-$ state. Our predicted mass of (6079 ± 9) MeV is in good agreement with its experimental mass of (6087.2 ± 0.8) MeV and our predicted width is slightly underestimated.

We consider the $\Xi_b(6095)^0$ to be the $1P$ $3/2^-$ neutral partner of $\Xi_b(6100)^-$. Our predicted mass of (6085 ± 9) MeV is in good agreement with its experimental mass of (6095.4 ± 0.7) MeV and also our predicted width of (1.1 ± 0.6) MeV agrees with the experimental width of (0.5 ± 0.4) MeV.

C. Σ_b baryons

The PDG [1] reports only four Σ_b states and their quantum numbers have not yet been measured. We use our results of Σ_b shown in Table IV to identify them.

1. Σ_b

Σ_b is identified as $\mathbf{J}^P = \frac{1}{2}^+$: its mass agrees well in both the three-quark and quark-diquark models, and our theoretical width agrees perfectly with the experimental result.

2. Σ_b^*

The spin excitation Σ_b^* is identified as $\mathbf{J}^P = \frac{3}{2}^+$ and our predictions for mass and width agree well with the experimental data.

3. $\Sigma_b(6097)^-$ and $\Sigma_b(6097)^+$

The $\Sigma_b(6097)^-$ and $\Sigma_b(6097)^+$ states are two of the three charge states of $\Sigma_b(6097)$ that are degenerate in the model of Ref. [98], since we assume isospin symmetry. Our predicted mass and width for $\Sigma_b(6097)$ agree well with the experimental data. Our calculations indicate that this is the first P_λ excitation of Σ_b with $\mathbf{J}^P = \frac{1}{2}^-$ and internal spin $\mathbf{S}_{\rm tot} = \mathbf{1/2}$.

D. Ω_b baryons

The predicted mass spectra and strong decay widths for the Ω_b states are presented in Table VI. It is noteworthy that these new findings are in agreement with the earlier calculation in Ref. [98]. Furthermore, in comparison with the previous study of Ref. [98], we have extended our investigation to include the $1D$, $2P$, and $2S$-wave excitations.

1. Ω_b^-

Ω_b^- is identified as a $\mathbf{J}^P = \frac{1}{2}^+$ state. Its experimental mass is well reproduced in the quark-diquark description. In the three-quark model, the predicted mass has a slight deviation of 10 MeV. As Ω_b^- can only decay weakly, its strong decay width is zero.

2. Ω_b^{*-}

The spin excitation of Ω_b^-, the Ω_b^{*-} with $\mathbf{J}^P = \frac{3}{2}^+$, has not yet been observed. We suggest the $\Omega_b^* \to \Omega_b^-\gamma$ decay mode as a "golden channel" for the observation of this state, whose mass, according to our predictions, is expected to be in the 6070–6098 MeV energy range.

3. $\Omega_b(6316)^-$, $\Omega_b(6330)^-$, $\Omega_b(6340)^-$, and $\Omega_b(6350)^-$

The four Ω_b resonances, namely $\Omega_b(6316)^-$, $\Omega_b(6330)^-$, $\Omega_b(6340)^-$, and $\Omega_b(6350)^-$, observed and discovered in LHCb [19], have to be confirmed in other experiments, and their quantum numbers have also not been measured yet. They are identified in our model as four of the five P_λ excitations.

The mass and width of $\Omega_b(6316)^-$ are well reproduced. This state is identified as $\mathbf{J}^P = \frac{1}{2}^-$, with internal spin $\mathbf{S}_{\rm tot} = \frac{1}{2}$. The assignment for $\Omega_b(6330)^-$ is also $\mathbf{J}^P = \frac{1}{2}^-$, but with internal spin $\mathbf{S}_{\rm tot} = \frac{3}{2}$. Its mass is well reproduced in calculations with both the three-quark and quark-diquark models, and our theoretical width is compatible with the experimental data. The mass of $\Omega_b(6340)^-$ is well reproduced in both the three-quark and quark-diquark models, but the experimental width is slightly overestimated. Our preferred assignment is $\mathbf{J}^P = \frac{3}{2}^-$, with internal spin $\mathbf{S}_{\rm tot} = \frac{1}{2}$. Finally, the mass and width of $\Omega_b(6350)^-$ are well reproduced in our calculation, it is described as a $\mathbf{J}^P = \frac{3}{2}^-$ state with internal spin $\mathbf{S}_{\rm tot} = \frac{3}{2}$.

In the present study, the fifth Ω_b^- P_λ excitation is characterized by a large width, thus its observation will require a high statistical significance at the LHC. According to our predictions, this state is expected to have a mass in the range of 6345–6365 MeV, with a width of approximately 40 MeV. In our three-quark model, we predict two additional P_ρ excitations which do not appear in the quark-diquark description. They do not couple to the $\Xi_b^0 K^-$ channel, which is the channel where LHCb observed the four excited Ω_b^- states, but they exhibit a strong coupling in the $\Xi_b^{\prime 0} K^-$ channel. Therefore, the experimental search for these two P_ρ excitations is a fundamental step toward assessing whether the bottom baryons are a three-quark system or a quark-diquark system.

E. Further comments

On using the $^3P_0$ model, our theoretical strong-decay widths exhibit good agreement with the experimental widths [1]. This agreement is remarkable since the $^3P_0$ model has only one free parameter, the pair-creation strength, which is fitted to reproduce the $\Sigma_b^* \to \Lambda_b \pi$ experimental strong decay width [1]. Notably, the theoretical masses reproduce the trend observed in the available data reported in PDG [1], as shown in Fig. 14, where we present the spectra of singly bottom baryons computed by means of the three-quark model. The $\bar{\mathbf{3}}_{\rm F}$ singly bottom baryons are depicted in purple, and purple lines represent their mass predictions. The $\mathbf{6}_{\rm F}$ singly bottom baryons are shown in teal, with their mass predictions indicated by teal

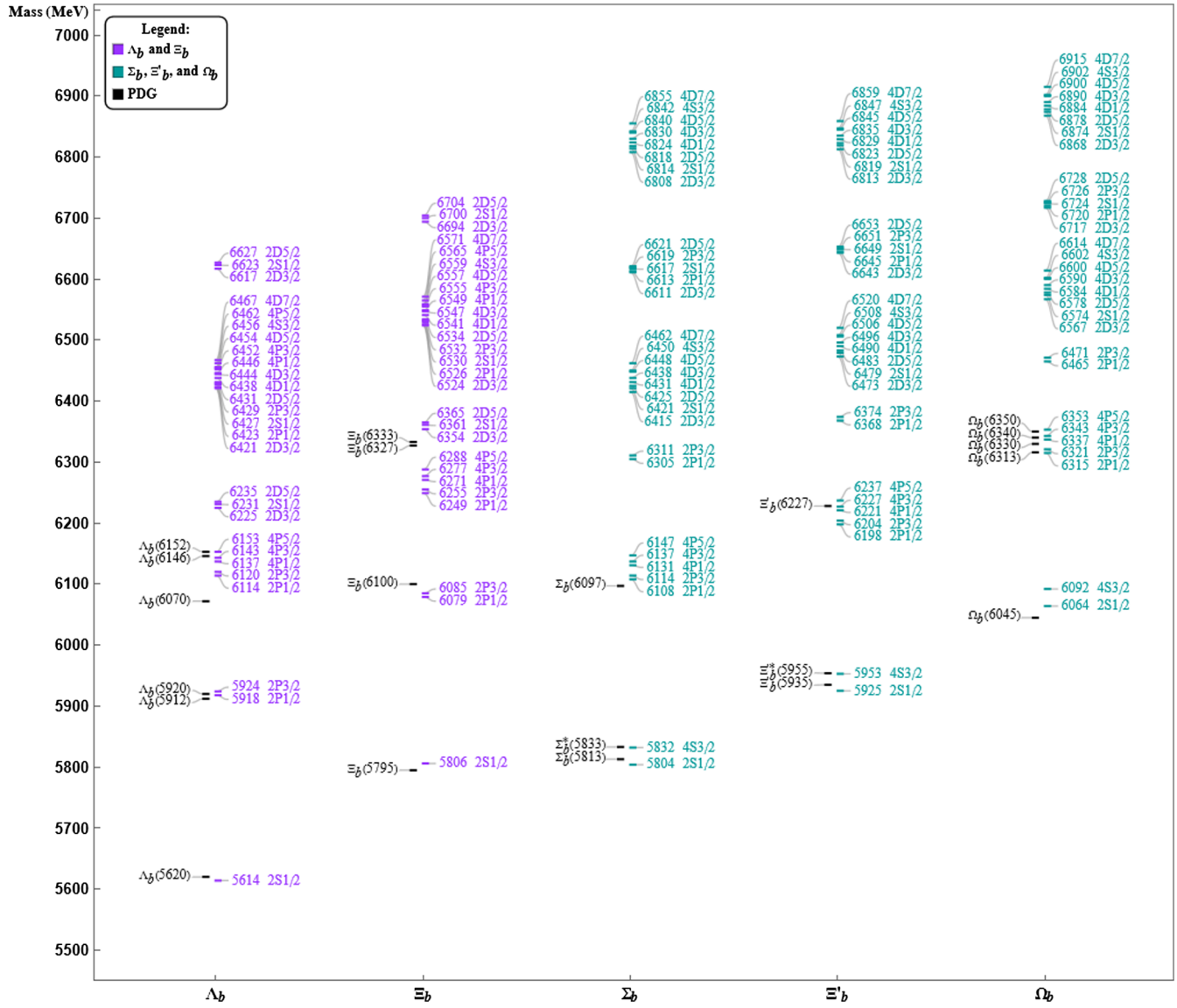

FIG. 14. Comparison between the singly bottom baryon mass predictions, computed by using the three-quark model Hamiltonian of Eqs. (1) and (2), and the experimental data from PDG [1]. The predicted masses for the $\bar{\mathbf{3}}_{\mathrm{F}}$ and $\mathbf{6}_{\mathrm{F}}$ states are displayed in purple and teal, respectively, while the experimental masses are shown in black [1].

lines. The experimentally known states and their corresponding experimental values are displayed in black [1].

Moreover, we studied many strong decay channels that had never been investigated before. Indeed, this is the first time that the $\Lambda_b\eta$, $\Sigma_b\rho$, $\Sigma_b^*\rho$, $\Lambda_b\eta'$, $\Lambda_b\omega$, Ξ_bK, $\Xi_b'K$, Ξ_b^*K, Ξ_bK^*, $\Xi_b'K^*$, and $\Xi_b^*K^*$ channels have been considered in the calculation of the strong decay widths of the excited Λ_b states; the $\Sigma_b\eta$, Ξ_bK, $\Sigma_b\rho$, $\Sigma_b^*\rho$, $\Lambda_b\rho$, $\Sigma_b^*\eta$, $\Sigma_b\eta'$, $\Sigma_b^*\eta'$, $\Xi_b'K$, Ξ_b^*K, Ξ_bK^*, $\Xi_b'K^*$, $\Xi_b^*K^*$, $\Sigma_b\omega$, $\Sigma_b^*\omega$, Σ_8B_s, ΔB, $N(1520)B$, $N(1535)B$, $N(1680)B$, and $N(1720)B$ channels in the calculation of the strong decay widths of the excited Σ_b states; the Λ_bK^*, $\Xi_b\rho$, $\Xi_b'\rho$, $\Xi_b^*\rho$, Σ_bK^*, $\Sigma_b^*K^*$, $\Xi_b\eta'$, $\Xi_b'\eta'$, $\Xi_b^*\eta'$, $\Xi_b\omega$, $\Xi_b'\omega$, $\Xi_b^*\omega$, $\Xi_b\phi$, $\Xi_b'\phi$, $\Xi_b^*\phi$, Ξ_8B_s, Σ_8B^*, and $\Sigma_{10}B$ channels in the calculation of the strong decay widths of the excited Ξ_b and Ξ_b' states; the Ξ_bK^*, $\Xi_b'K^*$, $\Xi_b^*K^*$, $\Omega_b\eta$, $\Omega_b^*\eta$, $\Omega_b\phi$, $\Omega_b^*\phi$, $\Omega_b\eta'$, $\Omega_b^*\eta'$, Ξ_8B, and $\Xi_{10}B$ channels in the calculation of the strong decay widths of the Ω_b states.

In the present article, the Coulomb plus linear confining term is not considered. We want to stress that, in the model of Ref. [98], the color factor is the same for all baryons and so the color dependence is reabsorbed in the a_{S} spin-spin parameter. From Tables VII–XI, it can be observed that our results and those that consider a coulomb plus linear confining term agree, except for radial excitations. In Ref. [26], Capstick and Isgur emphasized that the effective parameters of the quark model can compensate for model limitations.

In the study of light baryons, it is well known that the harmonic oscillator quark model does not reproduce the order of the Roper and $1P$ states, since the Roper $N(1440)$

lies below the 1P wave excitations $N(1520)$ and $N(1535)$, while it yields a good reproduction for all the other states.

The scenario concerning the Roper-like states in the heavy sector differs significantly. It is crucial to emphasize that, in the heavy sector, the Roper-like candidates (2S excitations) lie above the 1P waves. Specifically, in the charm sector, the Roper candidate $\Lambda_c(2765)$ [117] lies 150 MeV above the P wave excitations $\Lambda_c(2595)$ and $\Lambda_c(2625)$ [118].

Similarly, in the bottom sector, the Roper candidate $\Lambda_b(6070)$ lies 100 MeV above the P wave excitations $\Lambda_b(5912)$ and $\Lambda_b(5920)$.

Thus, in the heavy sector, the harmonic oscillator quark model, which is known to work well for all the other states, can also be applied to the Roper-like states, however, the reader must be aware of the potential limitations of this model in reproducing the 2S states.

More experimental data will be necessary in order to determine the quantum numbers and the decay channels of the Roper-like candidates, thereby ascertaining whether they are genuine 2S states, as we will discuss later, on the basis of our strong partial decay width calculations.

Heavy quark symmetry, which is valid within the infinite heavy quark mass limit ($m_Q \to \infty$), has implications for singly bottom baryons, as discussed in Refs. [119–121]. For example, in the infinite heavy quark mass limit ($m_Q \to \infty$), the total angular momentum j_q of the light degrees of freedom is conserved, and hadrons with $J = j_q \pm \frac{1}{2}$ form a degenerate doublet, i.e., two degenerate states [121] (unless $j_q = 0$, in which case a single state with $J = \frac{1}{2}$ is observed). In reality, the experimental mass-splitting of those doublets, as for example Σ_b and Σ_b^*, Ξ_b' and Ξ_b^*, and Ω_b and Ω_b^*, is not zero but about 30 MeV, showing that the experimental situation is in agreement with a heavy quark symmetry slightly broken by the finite mass of the heavy quark; the theoretical mass results of the present article reproduce the experimental mass splitting. In Ref. [121], the authors also estimated some strong decay amplitude ratios, in the limit of $m_Q \to \infty$, but without including the phase space and what they called the "barrier penetration" factor $(p_\pi^{2L+1} \exp[-p_\pi^2/(1\ \mathrm{GeV}^2)])^{1/2}$; as an example, the authors predicted for the $\Lambda_b(\frac{5}{2}^-) \to \Sigma_b\pi$ and $\Lambda_b(\frac{5}{2}^-) \to \Sigma_b^*\pi$ ratio a value of 0.53, in the approximation of the decays in purely D waves. In the present article, by contrast, this ratio is 0.79, including the "barrier penetration" factor, since, in reality, in the decay of a P-wave $\Lambda_b(\frac{5}{2}^-)$ to $\Sigma_b^*\pi$, there is a superposition of two partial waves, the D and the G waves. Nevertheless, one can observe a qualitative agreement, since there is a mass dependence, as expected [122].

In the three-quark model, scattering states are not considered. It is important to note that some excited states can be close to the threshold energy of a baryon-meson system, which implies a significant component of a hadronic molecule in the wave function of the state [123]. However, in the quark model description, the corrections to the observables related to the molecular component might be hidden in the model parameters [26,124].

On the other hand, in the molecular picture, singly bottom baryons can be dynamically generated from the meson-baryon interaction in coupled channels [125–131]. Specifically, the singly bottom baryons that are described as dynamically generated resonances, i.e., meson-baryon molecular states, include the $\Lambda_b(5912)$ and $\Lambda_b(5920)$ in Refs. [125,126]; the $\Omega_b(6316)$, $\Omega_b(6330)$, $\Omega_b(6340)$, and $\Omega_b(6350)$ in Ref. [127]; the $\Xi_b(6227)$ in Refs. [128,129]; seven Ω_b states within the energy range of 6405 to 6820 MeV in Ref. [130]; and the $\Lambda_b(5912)$, $\Lambda_b(5920)$, $\Xi_b(6035.4)$, and $\Xi_b(6043.3)$ in Ref. [131].

The degrees of freedom from hadron scattering schemes can be taken into account in the constituent quark model by considering an additional energy-dependent interaction [123,124,132–134]. For example, the $\Lambda_b(5912)$, and $\Lambda_b(5920)$ were studied in Ref. [135] as dressed quark-model states with $\Sigma_b^{(*)}\pi$ molecular components of the order of 30%.

VI. CONCLUSIONS

In summary, we calculate the mass spectra, strong partial decay widths, and electromagnetic decay widths of singly bottom baryons. We utilize both the three-quark and quark-diquark schemes to describe the mass spectra and predict the 1S, 1P, 1D, 2P, and 2S states, thus extending the model of Ref. [98]. We account for the propagation of parameter uncertainties by using a Monte Carlo bootstrap method. Notably, the harmonic oscillator approach allows a comprehensive description of singly bottom baryons through a global fit where the same model predicts the masses, strong partial decay widths, and electromagnetic decay widths of bottom baryons. Since we fitted all the parameters of the model Hamiltonian of Eq. (1) (see Table I) to 13 of 22 experimental masses reported in the PDG [1], the harmonic oscillator wave functions of the model do not depend on any free parameters.

Our theoretical mass spectra reproduce the general trend of experimental data, see Fig. 14. Until now, only λ-mode excited singly bottom baryons have been discovered. However, on the basis of our strong decay analysis, we tentatively assign the $2S\,\Lambda_b$ candidate, denoted as $\Lambda_b(6070)$, to a P_ρ-wave excited state with $\mathbf{J}^P = \mathbf{\frac{1}{2}^-}$. Therefore, determining its quantum numbers experimentally would be crucial in order to ascertain whether it corresponds to a radial excitation or the first P_ρ-wave excited state of the Λ_b baryon. The observation of the ρ-mode excitations could help to enhance our comprehension of the internal structure of the singly bottom baryon, and particularly in distinguishing between three-quark configurations and quark-diquark systems.

We calculate the three-quark excited $1P$, $1D$, $2P$, and $2S$ singly bottom baryon (ρ and λ modes) strong decay widths, within the $^3P_0$ model, into singly bottom baryon-(vector/pseudoscalar) meson pairs and (octet/decuplet) light baryon-(pseudoscalar/vector) bottom meson pairs. In particular, this is the first time that the $\Lambda_b\eta$, $\Sigma_b\rho$, $\Sigma_b^*\rho$, $\Lambda_b\eta'$, $\Lambda_b\omega$, Ξ_bK, $\Xi_b'K$, Ξ_b^*K, Ξ_bK^*, $\Xi_b'K^*$, $\Xi_b^*K^*$ channels have been considered in the calculation of the strong decay widths of the excited Λ_b states; the $\Sigma_b\eta$, Ξ_bK, $\Sigma_b\rho$, $\Sigma_b^*\rho$, $\Lambda_b\rho$, $\Sigma_b^*\eta$, $\Sigma_b\eta'$, $\Sigma_b^*\eta'$, $\Xi_b'K$, Ξ_b^*K, Ξ_bK^*, $\Xi_b'K^*$, $\Xi_b^*K^*$, $\Sigma_b\omega$, $\Sigma_b^*\omega$, Σ_8B_s, ΔB, $N(1520)B$, $N(1535)B$, $N(1680)B$, and $N(1720)B$ channels in the calculation of the strong decay widths of the excited Σ_b states; the Λ_bK^*, $\Xi_b\rho$, $\Xi_b'\rho$, $\Xi_b^*\rho$, Σ_bK^*, $\Sigma_b^*K^*$, $\Xi_b\eta'$, $\Xi_b'\eta'$, $\Xi_b^*\eta'$, $\Xi_b\omega$, $\Xi_b'\omega$, $\Xi_b^*\omega$, $\Xi_b\phi$, $\Xi_b'\phi$, $\Xi_b^*\phi$, Ξ_8B_s, Σ_8B^*, and $\Sigma_{10}B$ channels in the calculation of the strong decay widths of the excited Ξ_b and Ξ_b' states; and the Ξ_bK^*, $\Xi_b'K^*$, $\Xi_b^*K^*$, $\Omega_b\eta$, $\Omega_b^*\eta$, $\Omega_b\phi$, $\Omega_b^*\phi$, $\Omega_b\eta'$, $\Omega_b^*\eta'$, Ξ_8B, and $\Xi_{10}B$ channels in the calculation of the strong decay widths of the Ω_b states.

In order to provide further assistance to experimentalists in their search for bottom baryons, we report the partial decay widths for each open flavor channel in Tables XXII–XXVI.

We observe that electromagnetic decays play a dominant role for the states which cannot decay strongly. One example is the spin excitation of the Ω_b^- state, denoted as Ω_b^*, which has not yet been observed. The $\Omega_b^* \to \Omega_b^-\pi$ strong decay is prohibited due to lack of phase space and isospin conservation in strong interactions. Given that the $\Omega_b(6093)$ state has not yet been discovered, there exists a fascinating experimental opportunity to simultaneously observe a new electromagnetic decay in the bottom baryon sector and the emergence of a new state, $\Omega_b(6093)$, by exploring the $\Omega_b^-\gamma$ electromagnetic channel.

Our predictions for the masses and strong decay widths of bottom baryons exhibit good agreement with experimental data. Notably, the mass formula of Ref. [98] and the $^3P_0$ model describe the recently discovered D-wave excitations, such as $\Lambda_b(6146)^0$ and $\Lambda_b(6152)^0$, which we identify as D_λ excitations with quantum numbers $\mathbf{J}^P = \frac{3}{2}^+$ and $\mathbf{J}^P = \frac{5}{2}^+$, respectively. Additionally, the three-quark and quark-diquark models describe the new $\Xi_b^0(6327)$ and $\Xi_b^0(6333)$ states listed by the Particle Data Group (PDG) [1], which we also identify as D_λ excitations with quantum numbers $\mathbf{J}^P = \frac{3}{2}^+$ and $\mathbf{J}^P = \frac{5}{2}^+$, respectively, belonging to the $\bar{\mathbf{3}}_{\mathrm{F}}$ configuration. It is worth noting that these states were not included in our fits, making the predicted masses and widths indicative of the predictive power of the mass formula of Ref. [98] and the $^3P_0$ decay model.

Moreover, the information presented in this article, which encompasses both the mass region and the partial decay widths, enables the experimentalists (LHCb, CMS, and ATLAS) to select the most suitable decay channel in which to search for a specific resonance. Additionally, we have determined the flavor coupling coefficients for all two-body decay channels, which can be used in further theoretical investigations.

Note added. After submission of this article to ArXiv on July 2nd, 2023, a new article was submitted to ArXiv [104] a few days later on July 10th, 2023. It's important to note that both articles are independent and mainly focus on two different subjects: the present article mainly focuses on the singly bottom baryon strong decays and the predictions of the $1D$, $2P$, and $2S$ states, while Ref. [104], focuses on the $1S$- and $1P$-wave singly doubly and triply heavy baryon masses and electromagnetic decays. The authors of [104] also utilized the model introduced in [98] to investigate the masses and electromagnetic decay widths of $1S$- and $1P$-wave singly bottom baryons. However, regarding the electromagnetic decays of the $1P$-wave states, which is the small overlap of the two papers, one can observe that the matrix elements of the $\hat{T}_{j,-}$ orbit-flip operator, reported in Eq. (48) of Ref. [104], exhibit a wrong dependence on $m_{\rho(\lambda)}\mathrm{k}_0$, with k_0 being the photon energy. Indeed, in Ref. [104] the authors did not evaluate the exact expression of the orbit-flip operator since they replaced $\mathbf{p}_\lambda$ with $im_\lambda\mathrm{k}_0\boldsymbol{\lambda}$ and $\mathbf{p}_\rho$ with $im_\rho\mathrm{k}_0\boldsymbol{\rho}$ without declaring it in their article, as Roelof Bijker pointed out in private communications. By contrast, in our present article, we derived and presented the exact analytical expressions for the $\hat{T}_{j,-}$ matrix elements (see Appendix G); these depend on the photon transferred momentum k, and not on mk_0. Finally, the strong decays and the predictions of the $1D$, $2P$, and $2S$ states, which constitute some of the main results of the present manuscript, were not considered in Ref. [104]. After submission of our article, another article [78] appeared and correctly cited our paper. The authors only calculated the partial decay widths of $1D$-wave Ξ_b and Ξ_b'. Moreover, they only considered a small subset of the decay channels considered in the present article: the π, η, K, and B meson decay channels. Indeed, they did not consider the Λ_bK^*, $\Xi_b\rho$, $\Xi_b'\rho$, $\Xi_b^*\rho$, Σ_bK^*, $\Sigma_b^*K^*$, $\Xi_b\eta'$, $\Xi_b'\eta'$, $\Xi_b^*\eta'$, $\Xi_b\omega$, $\Xi_b'\omega$, $\Xi_b^*\omega$, $\Xi_b\phi$, $\Xi_b'\phi$, $\Xi_b^*\phi$, Ξ_8B_s, Σ_8B^*, $\Sigma_{10}B$ channels. In that paper [78] they used the λ mode Ξ_b and Ξ_b' masses as from the Ebert *et al.* quark-diquark model [38] and the ρ mode Ξ_b masses as from QCD sum rule [52], while the ρ mode Ξ_b' masses were estimated by adding about 100 MeV to the λ-mode excitations of Ref. [38]. Finally, they did not consider the $2S$ and $2P$ excitations, which complete the second shell.

ACKNOWLEDGMENTS

A. R.-A. acknowledges support from the Universidad de Guanajuato, the CONAHCyT and INFN. C. A. V.-A. is supported by the CONAHCyT Investigadoras e Investigadores por México project 749 and SNI 58928. A. R.-M. acknowledges the National Research Foundation of Korea Grant No. 2020R1I1A1A01066423.

A. G. acknowledges support from the CIDEGENT program with Ref. CIDEGENT/2019/015, the Spanish Ministerio de Economia y Competitividad and European Union (NextGenerationEU/PRTR) by the grant with Ref. CNS2022-13614.

APPENDIX A: BARYON WAVE FUNCTIONS

1. Three-quark baryon wave functions

In our algebraic model, the wave functions for a singly bottom baryon A, considering the color, flavor, spin, and spatial degrees of freedom, are given by

$$\Psi^{\mathrm{Tot}}_{A,J_A,M_{J_A}} = \theta_c\phi_A \sum_{M_{S_A},M_{L_A}} \langle S_A, M_{S_A}, L_A, M_{L_A}|J_A, M_{J_A}\rangle \times \chi_{S_A,M_{S_A}} \otimes \Psi_{A,L_A,M_{L_A}}(\vec{r}_1,\vec{r}_2,\vec{r}_3) \tag{A1}$$

where $\theta_c = \frac{1}{\sqrt{6}}(rgb - rbg + gbr - grb + brg - bgr)$ is the $SU_c(3)$ color singlet, ϕ_A, $\chi_{S_A,M_{S_A}}$, and $\Psi_{A,L_A,M_{L_A}}(\vec{r}_1,\vec{r}_2,\vec{r}_3)$ are the flavor, spin and spatial wave functions, respectively. For singly bottom baryons, we use the following coordinate system

$$\vec{\rho} = \frac{1}{\sqrt{2}}(\vec{r}_1 - \vec{r}_2), \tag{A2}$$

$$\vec{\lambda} = \frac{1}{\sqrt{6}}(\vec{r}_1 + \vec{r}_2 - 2\vec{r}_3), \tag{A3}$$

$$\vec{R} = \frac{m(\vec{r}_1 + \vec{r}_2) + m_b\vec{r}_3}{2m + m_b}, \tag{A4}$$

where $m = (m_1 + m_2)/2$ with m_1 and m_2 being the masses of the light quarks and m_b the mass of the bottom quark. Thus, the coordinates of the quarks are given by $\vec{r}_1 = \vec{R} + \frac{1}{\sqrt{2}}\vec{\rho} + \frac{\sqrt{\frac{3}{2}}m_b}{2m+m_b}\vec{\lambda}$, $\vec{r}_2 = \vec{R} - \frac{1}{\sqrt{2}}\vec{\rho} + \frac{\sqrt{\frac{3}{2}}m_b}{2m+m_b}\vec{\lambda}$, $\vec{r}_3 = \vec{R} - \frac{\sqrt{6}m_b}{2m+m_b}\vec{\lambda}$, with the differential volume $d^3\vec{r}_1 d^3\vec{r}_2 d^3\vec{r}_3 = 3\sqrt{3}d^3\vec{\rho}d^3\vec{\lambda}d^3\vec{R}$.

The baryon spatial wave functions in the coordinate representation are given by

$$\Psi_{A,L_A,M_{L_A}}(\vec{r}_1,\vec{r}_2,\vec{r}_3) = \frac{1}{(2\pi)^{3/2}}e^{i\vec{R}\cdot\vec{P}} \times \frac{1}{3^{3/4}} \sum_{m_{l_\rho},m_{l_\lambda}} \langle l_\rho, m_{l_\rho}, l_\lambda, m_{l_\lambda}|L_A, M_{L_A}\rangle \times \psi_{k_\rho,l_\rho,m_{l_\rho},k_\lambda,l_\lambda,m_{l_\lambda}}(\vec{\rho},\vec{\lambda}). \tag{A5}$$

Here, $\psi_{k_\rho,l_\rho,m_{l_\rho},k_\lambda,l_\lambda,m_{l_\lambda}}(\vec{\rho},\vec{\lambda})$ represents the harmonic oscillator wave functions, which can be expressed as a product of the wave functions of each harmonic oscillator:

$$\psi_{k_\rho,l_\rho,m_{l_\rho},k_\lambda,l_\lambda,m_{l_\lambda}}(\vec{\rho},\vec{\lambda}) = \psi_{k_\rho,l_\rho,m_{l_\rho}}(\vec{\rho}) \otimes \psi_{k_\lambda,l_\lambda,m_{l_\lambda}}(\vec{\lambda}). \tag{A6}$$

The wave functions of each harmonic oscillator can be expressed in terms of their radial and angular parts as

$$\psi_{k_{\rho(\lambda)},l_{\rho(\lambda)},m_{l_{\rho(\lambda)}}}(\vec{\rho}(\vec{\lambda})) = R_{k_{\rho(\lambda)}l_{\rho(\lambda)}}(\rho(\lambda))Y^{m_{l_{\rho(\lambda)}}}_{l_{\rho(\lambda)}}(\hat{\rho}(\hat{\lambda})), \tag{A7}$$

where the ρ radial part is

$$R_{k_\rho l_\rho}(\vec{\rho}) = \sqrt{\frac{\alpha_\rho^3 k_\rho! 2^{l_\rho+k_\rho+2}}{\sqrt{\pi}(2l_\rho+2k_\rho+1)!!}} \times e^{-\frac{1}{2}\alpha_\rho^2\rho^2}(\alpha_\rho\rho)^{l_\rho}L^{l_\rho+\frac{1}{2}}_{k_\rho}(\rho^2\alpha_\rho^2), \tag{A8}$$

and the λ radial part is

$$R_{k_\lambda l_\lambda}(\vec{\lambda}) = \sqrt{\frac{\alpha_\lambda^3 k_\lambda! 2^{l_\lambda+k_\lambda+2}}{\sqrt{\pi}(2l_\lambda+2k_\lambda+1)!!}}e^{-\frac{1}{2}\alpha_\lambda^2\lambda^2}(\alpha_\lambda\lambda)^{l_\lambda}L^{l_\lambda+\frac{1}{2}}_{k_\lambda}(\lambda^2\alpha_\lambda^2), \tag{A9}$$

where $L^a_k(x)$ are the generalized Laguerre polynomials. We observe that $\alpha^2_{\rho(\lambda)}$ are related to the harmonic oscillator frequencies, $\omega_{\rho(\lambda)}$, through m_ρ and m_λ: $\alpha^2_{\rho(\lambda)} = \omega_{\rho(\lambda)}m_{\rho(\lambda)}$. Thus, $\alpha_{\rho(\lambda)}$ depends on the harmonic oscillator constant K_b and the quark masses, which are fitted to reproduce the bottom baryon mass spectra (see Table I). As a result, our harmonic oscillator wave functions do not contain any free parameters.

2. Quark-diquark baryon wave functions

In the quark-diquark scheme, the wave functions for a generic baryon A, considering the color, flavor, spin, and spatial degrees of freedom, are given by

$$\Psi^{\mathrm{Tot}}_{A,J_A,M_{J_A}} = \theta_c\phi_A \sum_{M_{S_A},M_{L_A}} \langle S_A, M_{S_A}, L_A, M_{L_A}|J_A, M_{J_A}\rangle \times \chi_{S_A,M_{S_A}} \otimes \Psi_{A,L_A,M_{L_A}}(\vec{r}_1,\vec{r}_2) \tag{A10}$$

where $\theta_c = \frac{1}{\sqrt{6}}(rgb - rbg + gbr - grb + brg - bgr)$ is the color singlet wave function of $SU_c(3)$, ϕ_A, $\chi_{S_A,M_{S_A}}$, and $\Psi_{A,L_A,M_{L_A}}(\vec{r}_1,\vec{r}_2)$ are the flavor, spin and spatial wave functions, respectively.

For bottom baryons in the quark-diquark scheme, we use the following coordinate system

$$\vec{r} = \vec{r}_1 - \vec{r}_2, \tag{A11}$$

$$\vec{R} = \frac{m_D\vec{r}_1 + m_b\vec{r}_2}{m_D + m_b}, \tag{A12}$$

where $\vec{R}$ is the center of mass coordinate, $\vec{r}_1$ and $\vec{r}_2$ are the diquark and bottom quark coordinates; m_D and m_b are the diquark and bottom quark masses.

The baryon spatial wave functions in the coordinate representation are

$$\Psi_{A,L_A,M_{L_A}}(\vec{r}) = \frac{1}{(2\pi)^{3/2}} e^{i\vec{R}\cdot\vec{P}} \psi_{k_r,l_r,m_{l_r}}(\vec{r}), \tag{A13}$$

where $\psi_{k_r,l_r,m_{l_r}}(\vec{r})$ are the harmonic oscillator wave functions, which can be written in terms of their radial and angular parts as

$$\psi_{k_r,l_r,m_{l_r}}(\vec{r}) = R_{k_r,l_r}(r) Y_{l_r}^{m_{l_r}}(\hat{r}), \tag{A14}$$

with the radial part given by

$$R_{k_r,l_r}(\vec{r}) = \sqrt{\frac{\alpha_r^3 k_r! 2^{l_r+k_r+2}}{\sqrt{\pi}(2l_r+2k_r+1)!!}} e^{-\frac{1}{2}\alpha_r^2 r^2} (\alpha_r r)^{l_r} L_{k_r}^{l_r+\frac{1}{2}}(r^2\alpha_r^2), \tag{A15}$$

where $L_k^a(x)$ are the generalized Laguerre polynomials.

We observe that α_r^2 are related to the harmonic oscillator frequencies, ω_r, through m_r: $\alpha_r^2 = \omega_r m_r$. Thus, α_r depends on the harmonic oscillator constant K_b and the diquark and bottom masses, which are fitted to reproduce the bottom baryon mass spectra (see Table I).

APPENDIX B: BOTTOM-BARYON FLAVOR AND SPIN WAVE FUNCTIONS

In the bottom sector, we consider the $\bar{\mathbf{3}}_{\mathrm{F}}$-plet and the $\mathbf{6}_{\mathrm{F}}$-plet representation of the flavor wave functions. In the following subsections, we give the flavor wave functions of the singly bottom baryon A $(\Lambda_b, \Xi_b, \Sigma_b, \Xi_b', \Omega_b)$.

1. $\bar{\mathbf{3}}_{\mathrm{F}}$-plet

$$\phi_{\Xi_b^-} = \frac{1}{\sqrt{2}}(dsb - sdb), \tag{B1}$$

$$\phi_{\Xi_b^0} = \frac{1}{\sqrt{2}}(usb - sub), \tag{B2}$$

$$\phi_{\Lambda_b^0} = \frac{1}{\sqrt{2}}(udb - dub). \tag{B3}$$

2. $\mathbf{6}_{\mathrm{F}}$-plet

$$\phi_{\Omega_b^-} = ssb, \tag{B4}$$

$$\phi_{\Xi_b^{\prime-}} = \frac{1}{\sqrt{2}}(dsb + sdb), \tag{B5}$$

$$\phi_{\Xi_b^{\prime 0}} = \frac{1}{\sqrt{2}}(usb + sub), \tag{B6}$$

$$\phi_{\Sigma_b^+} = uub, \tag{B7}$$

$$\phi_{\Sigma_b^-} = ddb, \tag{B8}$$

$$\phi_{\Sigma_b^0} = \frac{1}{\sqrt{2}}(udb + dub). \tag{B9}$$

When we calculate the strong-decay width with a final state involving a light baryon, the flavor-wave function follows the convention given in Ref. [102].

The spin wave functions corresponding to the singly bottom baryons can be constructed by coupling the spins of the three constituent quarks. They are given by

$$\chi_\rho = \frac{1}{\sqrt{2}}(\uparrow\downarrow\uparrow - \downarrow\uparrow\uparrow]), \tag{B10}$$

$$\chi_\lambda = \frac{1}{\sqrt{6}}(2\uparrow\uparrow\downarrow - \uparrow\downarrow\uparrow - \downarrow\uparrow\uparrow), \tag{B11}$$

$$\chi_s = \uparrow\uparrow\uparrow. \tag{B12}$$

We observe that the spin function χ_ρ is antisymmetric under the interchange of the first two quarks; conversely, both χ_λ and χ_s are symmetric under the interchange of the first two quarks.

APPENDIX C: MESON FLAVOR WAVE FUNCTIONS

In the following, we give the flavor wave functions of a C meson used in the calculation of the strong partial decay width.

In the case of bottom-B mesons, the flavor-wave functions are the same for the pseudoscalar and vector states. We use the following:

$$\phi_{B_s^{0*}} = \phi_{B_s^0} = s\bar{b}$$
$$\phi_{B^{0*}} = \phi_{B^0} = d\bar{b}$$
$$\phi_{B^{-*}} = \phi_{B^-} = b\bar{u}.$$

The convention used in the calculation of the strong-decay width when the final state has a light meson is found in Ref. [102].

APPENDIX D: FLAVOR COUPLINGS

In the following subsections, we give the flavor coefficients $\mathcal{F}_{A\to BC}$ used to calculate the transition amplitudes. We compute $\mathcal{F}_{A\to BC} = \langle \phi_B \phi_C | \phi_0 \phi_A \rangle$ where $\phi_{(A,B,C)}$ refers to the initial flavor wave function of a bottom baryon ϕ_A, a

final baryon ϕ_B, and a final meson ϕ_C, respectively; $\phi_0^{45} = (u\bar{u} + d\bar{d} + s\bar{s})/\sqrt{3}$ is the flavor singlet-wave function of $SU_f(3)$. In addition, we compute the flavor decay coefficients of the isospin channels, since we assume that the isospin symmetry holds even though it is slightly broken. The corresponding charge channels are obtained by multiplying our $\mathcal{F}_{A\to BC}$ by the corresponding Clebsch-Gordan coefficient in the isospin space, using the convention of the isospin quantum numbers of the baryon and meson flavor wave functions found in B and C. For the light baryons, we use the convention of Ref. [102]. Thus, the flavor charge channel for a specific projection (I, M_I) in the isospin space is obtained as follows:

$$\begin{aligned}&\mathcal{F}_{A(I_A,M_{I_A})\to B(I_B,M_{I_B})C(I_C,M_{I_C})}\\&= \langle \phi_B, I_B, M_{I_B}, \phi_C, I_C, M_{I_C} | \phi_0, 0, 0, \phi_A, I_A, M_{I_A}\rangle_F\\&= \langle I_B, M_{I_B}, I_C, M_{I_C} | I_A, M_{I_A}\rangle \mathcal{F}_{A\to BC},\end{aligned} \tag{D1}$$

where $\langle I_B, M_{I_B}, I_C, M_{I_C} | I_A, M_{I_A}\rangle$ is a Clebsch-Gordan coefficient, and the flavor functions ϕ_i of each baryon and meson have a specific isospin projection M_I.

1. Bottom-baryon and pseudoscalar meson flavor couplings

We give the squared flavor-coupling coefficients, $\mathcal{F}^2_{A\to BC}$, when the final states have a pseudoscalar light meson. Here, A and B are bottom baryons, and the subindexes $\bar{\mathbf{3}}_\mathrm{F}$ and $\mathbf{6}_\mathrm{F}$ refer to the antitriplet and the sextet baryon multiples. The C is a pseudoscalar meson and the subindexes $\mathbf{8}_\mathrm{F}$ and $\mathbf{1}_\mathrm{F}$ refer to the octet and singlet meson multiplets, respectively.

(i) $A_{\bar{\mathbf{3}}_\mathrm{F}} \to B_{\mathbf{6}_\mathrm{F}} + C_{\mathbf{8}_\mathrm{F}}$

$$\begin{pmatrix}\Lambda_b\\ \Xi_b\end{pmatrix} \to \begin{pmatrix}\Xi_b' K & \Sigma_b \pi & \\ \Sigma_b K & \Xi_b' \pi & \Xi_b' \eta\end{pmatrix} = \begin{pmatrix}\frac{1}{6} & \frac{1}{2} & \\ \frac{1}{4} & \frac{1}{8} & \frac{1}{72}\end{pmatrix} \tag{D2}$$

(ii) $A_{\bar{\mathbf{3}}_\mathrm{F}} \to B_{\mathbf{6}_\mathrm{F}} + C_{\mathbf{1}_\mathrm{F}}$

$$(\Xi_b) \to (\Xi_b' \eta') = \left(\frac{1}{9}\right) \tag{D3}$$

(iii) $A_{\bar{\mathbf{3}}_\mathrm{F}} \to B_{\bar{\mathbf{3}}_\mathrm{F}} + C_{\mathbf{8}_\mathrm{F}}$

$$\begin{pmatrix}\Lambda_b\\ \Xi_b\end{pmatrix} \to \begin{pmatrix}\Xi_b K & \Lambda_b \eta & \\ \Lambda_b K & \Xi_b \pi & \Xi_b \eta\end{pmatrix} = \begin{pmatrix}\frac{1}{6} & \frac{1}{18} & \\ \frac{1}{12} & \frac{1}{8} & \frac{1}{72}\end{pmatrix} \tag{D4}$$

(iv) $A_{\bar{\mathbf{3}}_\mathrm{F}} \to B_{\bar{\mathbf{3}}_\mathrm{F}} + C_{\mathbf{1}_\mathrm{F}}$

$$\begin{pmatrix}\Lambda_b\\ \Xi_b\end{pmatrix} \to \begin{pmatrix}\Lambda_b \eta'\\ \Xi_b \eta'\end{pmatrix} = \begin{pmatrix}\frac{1}{9}\\ \frac{1}{9}\end{pmatrix} \tag{D5}$$

(v) $A_{\mathbf{6}_\mathrm{F}} \to B_{\mathbf{6}_\mathrm{F}} + C_{\mathbf{8}_\mathrm{F}}$

$$\begin{pmatrix}\Omega_b\\ \Sigma_b\\ \Xi_b'\end{pmatrix} \to \begin{pmatrix} & \Xi_b' K & \Omega_b \eta\\ \Xi_b' K & \Sigma_b \pi & \Sigma_b \eta\\ \Sigma_b K & \Xi_b' \pi & \Xi_b' \eta\end{pmatrix} = \begin{pmatrix} & \frac{1}{3} & \frac{2}{9}\\ \frac{1}{6} & \frac{1}{3} & \frac{1}{18}\\ \frac{1}{4} & \frac{1}{8} & \frac{1}{72}\end{pmatrix} \tag{D6}$$

(vi) $A_{\mathbf{6}_\mathrm{F}} \to B_{\mathbf{6}_\mathrm{F}} + C_{\mathbf{1}_\mathrm{F}}$

$$\begin{pmatrix}\Omega_b\\ \Sigma_b\\ \Xi_b'\end{pmatrix} \to \begin{pmatrix}\Omega_b \eta'\\ \Sigma_b \eta'\\ \Xi_b' \eta'\end{pmatrix} = \begin{pmatrix}\frac{1}{3}\\ \frac{1}{9}\\ \frac{1}{9}\end{pmatrix} \tag{D7}$$

(vii) $A_{\mathbf{6}_\mathrm{F}} \to B_{\bar{\mathbf{3}}_\mathrm{F}} + C_{\mathbf{8}_\mathrm{F}}$

$$\begin{pmatrix}\Omega_b\\ \Sigma_b\\ \Xi_b'\end{pmatrix} \to \begin{pmatrix} & \Xi_b K & \\ \Xi_b K & \Lambda_b \pi & \\ \Lambda_b K & \Xi_b \pi & \Xi_b \eta\end{pmatrix} = \begin{pmatrix} & \frac{1}{3} & \\ \frac{1}{6} & \frac{1}{2} & \\ \frac{1}{12} & \frac{1}{8} & \frac{1}{72}\end{pmatrix} \tag{D8}$$

(viii) $A_{\mathbf{6}_\mathrm{F}} \to B_{\bar{\mathbf{3}}_\mathrm{F}} + C_{\mathbf{1}_\mathrm{F}}$

$$(\Xi_b') \to (\Xi_b \eta') = \left(\frac{1}{9}\right) \tag{D9}$$

2. Bottom-baryon and vector-meson flavor couplings

We give the squared flavor-coupling coefficients, $\mathcal{F}^2_{A\to BC}$ when the final states have a vector-light meson. Here A and B are bottom baryons, and the subindexes $\bar{\mathbf{3}}_\mathrm{F}$ and $\mathbf{6}_\mathrm{F}$ refer to the antitriplet and the sextet baryon multiplets. The C is a vector meson and the subindexes $\mathbf{8}_\mathrm{F}$ and $\mathbf{1}_\mathrm{F}$ refer to the octet and singlet meson multiplets, respectively.

(i) $A_{\bar{\mathbf{3}}_\mathrm{F}} \to B_{\mathbf{6}_\mathrm{F}} + C_{\mathbf{8}_\mathrm{F}}$

$$\begin{pmatrix}\Lambda_b\\ \Xi_b\end{pmatrix} \to \begin{pmatrix}\Xi_b' K^* & \Sigma_b \rho & \\ \Sigma_b K^* & \Xi_b' \rho & \Xi_b' \omega\end{pmatrix} = \begin{pmatrix}\frac{1}{6} & \frac{1}{2} & \\ \frac{1}{4} & \frac{1}{8} & \frac{1}{24}\end{pmatrix} \tag{D10}$$

(ii) $A_{\bar{\mathbf{3}}_F} \to B_{\mathbf{6}_F} + C_{\mathbf{1}_F}$

$$(\Xi_b) \to (\Xi_c' \phi) = \begin{pmatrix} \frac{1}{12} \end{pmatrix} \tag{D11}$$

(iii) $A_{\bar{\mathbf{3}}_F} \to B_{\bar{\mathbf{3}}_F} + C_{\mathbf{8}_F}$

$$\begin{pmatrix} \Lambda_b \\ \Xi_b \end{pmatrix} \to \begin{pmatrix} \Xi_b K^* & \Lambda_b \omega & \\ \Lambda_b K^* & \Xi_b \rho & \Xi_b \omega \end{pmatrix} = \begin{pmatrix} \frac{1}{6} & \frac{1}{6} & \\ \frac{1}{12} & \frac{1}{8} & \frac{1}{24} \end{pmatrix} \tag{D12}$$

(iv) $A_{\bar{\mathbf{3}}_F} \to B_{\bar{\mathbf{3}}_F} + C_{\mathbf{1}_F}$

$$\begin{pmatrix} \Lambda_b \\ \Xi_b \end{pmatrix} \to \begin{pmatrix} \Lambda_b \phi \\ \Xi_b \phi \end{pmatrix} = \begin{pmatrix} 0 \\ \frac{1}{12} \end{pmatrix} \tag{D13}$$

(v) $A_{\mathbf{6}_F} \to B_{\mathbf{6}_F} + C_{\mathbf{8}_F}$

$$\begin{pmatrix} \Omega_b \\ \Sigma_b \\ \Xi_b' \end{pmatrix} \to \begin{pmatrix} & \Xi_b' K^* & \\ \Xi_b' K^* & \Sigma_b \rho & \Sigma_b \omega \\ \Sigma_b K^* & \Xi_b' \rho & \Xi_b' \omega \end{pmatrix} = \begin{pmatrix} & \frac{1}{3} & \\ \frac{1}{6} & \frac{1}{3} & \frac{1}{6} \\ \frac{1}{4} & \frac{1}{8} & \frac{1}{24} \end{pmatrix} \tag{D14}$$

(vi) $A_{\mathbf{6}_F} \to B_{\mathbf{6}_F} + C_{\mathbf{1}_F}$

$$\begin{pmatrix} \Omega_b \\ \Sigma_b \\ \Xi_b' \end{pmatrix} \to \begin{pmatrix} \Omega_b \phi \\ \Sigma_b \phi \\ \Xi_b' \phi \end{pmatrix} = \begin{pmatrix} \frac{1}{9} \\ 0 \\ \frac{1}{2} \end{pmatrix} \tag{D15}$$

(vii) $A_{\mathbf{6}_F} \to B_{\bar{\mathbf{3}}_F} + C_{\mathbf{8}_F}$

$$\begin{pmatrix} \Omega_b \\ \Sigma_b \\ \Xi_b' \end{pmatrix} \to \begin{pmatrix} & \Xi_b K^* & \\ \Xi_b K^* & \Lambda_b \rho & \\ \Lambda_b K^* & \Xi_b \rho & \Xi_b \omega \end{pmatrix} = \begin{pmatrix} & \frac{1}{3} & \\ \frac{1}{6} & \frac{1}{3} & \\ \frac{1}{12} & \frac{1}{8} & \frac{1}{24} \end{pmatrix} \tag{D16}$$

(viii) $A_{\mathbf{6}_F} \to B_{\bar{\mathbf{3}}_F} + C_{\mathbf{1}_F}$

$$(\Xi_b') \to (\Xi_b \phi) = \begin{pmatrix} \frac{1}{12} \end{pmatrix} \tag{D17}$$

3. Light baryon and bottom-(pseudoscalar/vector) meson flavor coupling

We give the $\mathcal{F}^2_{A\to BC}$ when the final states have a light baryon and a bottom-(pseudoscalar/vector) meson. Since the B mesons form an isospin doublet, both are treated as B in the tables; whereas the bottom strange are denoted as B_s. The subindexes $\bar{\mathbf{3}}_F$ and $\mathbf{6}_F$ refer to the antitriplet and the sextet baryon multiplets for the initial bottom baryon A, whereas the final B baryons can have subindexes 8 or 10, according to whether the final light baryon belongs to the octet or decuplet baryon multiplet. Additionally, owing to the symmetry of the wave functions of the octet-light baryons, we can have only ρ or λ contributions in the final states, as indicated by a superindex.

(i) $A_{\bar{\mathbf{3}}_F} \to B_{\mathbf{8}_F} + C$

$$\begin{pmatrix} \Lambda_b \\ \Xi_b \end{pmatrix} \to \begin{pmatrix} N^\rho B & \Lambda_8^\rho B_s & \\ \Sigma_8^\rho B & \Xi_8^\rho B_s & \Lambda_8^\rho B \end{pmatrix} = \begin{pmatrix} \frac{2}{3} & \frac{2}{9} & \\ \frac{1}{2} & \frac{1}{3} & \frac{1}{18} \end{pmatrix} \tag{D18}$$

(ii) $A_{\mathbf{6}_F} \to B_{\mathbf{10}_F} + C$

$$\begin{pmatrix} \Omega_b \\ \Sigma_b \\ \Xi_b' \end{pmatrix} \to \begin{pmatrix} \Xi_{10}^* B & \Omega_{10} B_s \\ \Delta B & \Sigma_{10}^* B_s \\ \Sigma_{10}^* B & \Xi_{10}^* B_s \end{pmatrix} = \begin{pmatrix} \frac{2}{9} & \frac{1}{3} \\ \frac{4}{9} & \frac{1}{9} \\ \frac{1}{3} & \frac{2}{9} \end{pmatrix} \tag{D19}$$

(iii) $A_{\mathbf{6}_F} \to B_{\mathbf{8}_F} + C$

$$\begin{pmatrix} \Omega_b \\ \Sigma_b \\ \Xi_b' \end{pmatrix} \to \begin{pmatrix} & \Xi_8^\lambda B \\ N^\lambda B & \Sigma_8^\lambda B_s \\ \Sigma_8^\lambda B & \Xi_8^\lambda B_s \end{pmatrix} = \begin{pmatrix} & \frac{4}{9} \\ \frac{2}{9} & \frac{2}{9} \\ \frac{1}{6} & \frac{1}{9} \end{pmatrix} \tag{D20}$$

APPENDIX E: STRONG PARTIAL DECAY WIDTHS

The calculated strong partial decay widths, $\Gamma_{\text{Strong}}(A \to BC)$, are shown in Tables XXII–XXVI. The charge channel decay width for a baryon A with isospin I_A and isospin projection M_{I_A}, $|A, I_A, M_{I_A}\rangle$, decaying into a baryon B with isospin I_B and isospin projection M_{I_B}, $|B, I_B, M_{I_B}\rangle$, and a meson C with isospin I_C and isospin projection M_{I_C}, $|C, I_C, M_{I_C}\rangle$, can be obtained as follows

$$\Gamma^{M_{I_A}, M_{I_B}, M_{I_C}}_{\text{Strong}}(A \to BC) = \langle I_B, M_{I_B}, I_C, M_{I_C} | I_A, M_{I_A}\rangle^2 \Gamma_{\text{Strong}}(A \to BC), \tag{E1}$$

where $\langle I_B, M_{I_B}, I_C, M_{I_C} | I_A, M_{I_A}\rangle$ is the Clebsch-Gordan coefficient in the isospin space; the partial decay width $\Gamma_{\text{Strong}}(A \to BC)$ can be extracted from Tables XXII–XXVI.

APPENDIX F: DECAY PRODUCTS

TABLE XXII. Predicted $\Lambda_b(nnb)$ strong partial decay widths (in MeV). The flavor multiplet is denoted by the symbol $\mathcal{F}$. The first column reports the baryon name with its predicted mass, calculated using the three-quark model Hamiltonian given by Eqs. (1) and (2). The second column displays $\mathbf{J}^{\mathrm{P}}$, the third column shows the three-quark model state, $|l_\lambda, l_\rho, k_\lambda, k_\rho\rangle$, where $l_{\lambda,\rho}$ represent the orbital angular momenta and $k_{\lambda,\rho}$ denote the number of nodes of the λ and ρ oscillators. The fourth column presents the spectroscopic notation $^{2S+1}L_J$. The value of $N = n_\rho + n_\lambda$ distinguishes the $N = 0$, 1, 2 energy bands. Starting from the fifth column, we provide the strong partial decay widths calculated by means of Eq. (17). Each column corresponds to an open-flavor strong decay channel, and the specific decay channels are indicated at the top of each column. The masses of the decay products are given in Table XXVII. The values for the strong decay widths are given in MeV. The decay widths denoted by 0 are either too small to be shown on this scale or forbidden by phase space, while the decay widths denoted by ⋯ are forbidden by selection rules. Finally, the last column represents the sum of the strong partial decay widths over all the decay channels.

$\mathcal{F} = \bar{\mathbf{3}}_{\mathrm{F}}$				$\Sigma_b\pi$	$\Sigma_b^*\pi$	$\Lambda_b\eta$	$\Sigma_b\rho$	$\Sigma_b^*\rho$	$\Lambda_b\eta'$	$\Lambda_b\omega$	$\Xi_b K$	$\Xi_b' K$	$\Xi_b^* K$	$\Xi_b K^*$	$\Xi_b' K^*$	$\Xi_b^* K^*$	NB	Γ^{Strong}
$\Lambda_b(nnb)$	$\mathbf{J}^P$	$\lvert l_\lambda, l_\rho, k_\lambda, k_\rho\rangle$	$^{2S+1}L_J$	MeV	MeV	MeV	MeV	MeV	MeV	MeV	MeV	MeV	MeV	MeV	MeV	MeV	MeV	MeV
$N = 0$																		
$\Lambda_b(5613)$	$\frac{1}{2}^+$	$\lvert 0,0,0,0\rangle$	$^2S_{1/2}$	0	0	0	0	0	0	0	0	0	0	0	0	0	0	0
$N = 1$																		
$\Lambda_b(5918)$	$\frac{1}{2}^-$	$\lvert 1,0,0,0\rangle$	$^2P_{1/2}$	0	0	0	0	0	0	0	0	0	0	0	0	0	0	0
$\Lambda_b(5924)$	$\frac{3}{2}^-$	$\lvert 1,0,0,0\rangle$	$^2P_{3/2}$	0	0	0	0	0	0	0	0	0	0	0	0	0	0	0
$\Lambda_b(6114)$	$\frac{1}{2}^-$	$\lvert 0,1,0,0\rangle$	$^2P_{1/2}$	9.3	57.5	0	0	0	0	0	0	0	0	0	0	0	0	66.8
$\Lambda_b(6137)$	$\frac{1}{2}^-$	$\lvert 0,1,0,0\rangle$	$^4P_{1/2}$	4.2	31.3	0	0	0	0	0	0	0	0	0	0	0	0	35.5
$\Lambda_b(6121)$	$\frac{3}{2}^-$	$\lvert 0,1,0,0\rangle$	$^2P_{3/2}$	76.9	7.8	0	0	0	0	0	0	0	0	0	0	0	0	84.7
$\Lambda_b(6143)$	$\frac{3}{2}^-$	$\lvert 0,1,0,0\rangle$	$^4P_{3/2}$	4.2	123.6	0	0	0	0	0	0	0	0	0	0	0	0	127.8
$\Lambda_b(6153)$	$\frac{5}{2}^-$	$\lvert 0,1,0,0\rangle$	$^4P_{5/2}$	26.4	47.9	0	0	0	0	0	0	0	0	0	0	0	0	74.3
$N = 2$																		
$\Lambda_b(6225)$	$\frac{3}{2}^+$	$\lvert 2,0,0,0\rangle$	$^2D_{3/2}$	1.4	8.3	⋯	0	0	0	0	0	0	0	0	0	0	3.3	13.0
$\Lambda_b(6235)$	$\frac{5}{2}^+$	$\lvert 2,0,0,0\rangle$	$^2D_{5/2}$	3.1	1.2	⋯	0	0	0	0	0	0	0	0	0	0	13.2	17.5
$\Lambda_b(6231)$	$\frac{1}{2}^+$	$\lvert 0,0,1,0\rangle$	$^2S_{1/2}$	6.2	11.1	⋯	0	0	0	0	0	0	0	0	0	0	11.5	28.9
$\Lambda_b(6624)$	$\frac{1}{2}^+$	$\lvert 0,0,0,1\rangle$	$^2S_{1/2}$	9.3	24.2	⋯	27.0	2.6	⋯	48.7	⋯	13.0	5.6	0	0	0	⋯	130.5
$\Lambda_b(6421)$	$\frac{3}{2}^+$	$\lvert 1,1,0,0\rangle$	$^2D_{3/2}$	11.4	48.7	1.3	0	0	0	3.2	2.5	0	0	0	0	0	⋯	67.1
$\Lambda_b(6431)$	$\frac{5}{2}^+$	$\lvert 1,1,0,0\rangle$	$^2D_{5/2}$	81.4	8.0	8.3	0	0	0	0.7	9.4	0.3	0	0	0	0	⋯	108.1
$\Lambda_b(6438)$	$\frac{1}{2}^+$	$\lvert 1,1,0,0\rangle$	$^4D_{1/2}$	2.2	23.5	1.1	0	0	0	3.3	4.3	0.1	0	0	0	0	⋯	34.5
$\Lambda_b(6444)$	$\frac{3}{2}^+$	$\lvert 1,1,0,0\rangle$	$^4D_{3/2}$	2.8	75.5	1.2	0	0	0	12.5	2.9	0.1	0	0	0	0	⋯	95.0
$\Lambda_b(6454)$	$\frac{5}{2}^+$	$\lvert 1,1,0,0\rangle$	$^4D_{5/2}$	9.0	95.1	3.7	0	0	0	15.6	4.5	0.1	0	0	0	0	⋯	128.0
$\Lambda_b(6468)$	$\frac{7}{2}^+$	$\lvert 1,1,0,0\rangle$	$^4D_{7/2}$	29.1	59.4	12.1	0	0	0	4.8	16.3	0.7	0	0	0	0	⋯	122.4
$\Lambda_b(6423)$	$\frac{1}{2}^-$	$\lvert 1,1,0,0\rangle$	$^2P_{1/2}$	0	0.5	0	0	0	0	0	0	0	0	0	0	0	⋯	0.5
$\Lambda_b(6429)$	$\frac{3}{2}^-$	$\lvert 1,1,0,0\rangle$	$^2P_{3/2}$	1.2	0.3	0.1	0	0	0	0	0.1	0	0	0	0	0	⋯	1.7
$\Lambda_b(6446)$	$\frac{1}{2}^-$	$\lvert 1,1,0,0\rangle$	$^4P_{1/2}$	0	0.3	0	0	0	0	0	0	0	0	0	0	0	⋯	0.3
$\Lambda_b(6452)$	$\frac{3}{2}^-$	$\lvert 1,1,0,0\rangle$	$^4P_{3/2}$	0.1	1.0	0	0	0	0	0.1	0	0	0	0	0	0	⋯	1.2
$\Lambda_b(6462)$	$\frac{5}{2}^-$	$\lvert 1,1,0,0\rangle$	$^4P_{5/2}$	0.4	1.3	0.2	0	0	0	0.2	0.2	0	0	0	0	0	⋯	2.3
$\Lambda_b(6456)$	$\frac{3}{2}^+$	$\lvert 1,1,0,0\rangle$	$^4S_{3/2}$	2.3	14.1	1.1	0	0	0	8.2	5.8	0.3	0	0	0	0	⋯	31.8
$\Lambda_b(6427)$	$\frac{1}{2}^+$	$\lvert 1,1,0,0\rangle$	$^2S_{1/2}$	12.2	7.0	1.5	0	0	0	3.5	5.2	0	0	0	0	0	⋯	29.4
$\Lambda_b(6618)$	$\frac{3}{2}^+$	$\lvert 0,2,0,0\rangle$	$^2D_{3/2}$	21.5	53.1	⋯	9.3	0.1	⋯	40.7	⋯	3.1	3.6	0	0	0	⋯	131.4
$\Lambda_b(6628)$	$\frac{5}{2}^+$	$\lvert 0,2,0,0\rangle$	$^2D_{5/2}$	52.9	93.0	⋯	1.0	1.1	⋯	29.2	⋯	7.5	0.5	0	0	0	⋯	185.2

TABLE XXIII. Same as XXII, but for $\Xi_b(snb)$ states.

$\mathcal{F}=\bar{\mathbf{3}}_{\mathrm{F}}$				$\Lambda_b K$	$\Xi_b\pi$	$\Xi_b'\pi$	$\Xi_b^*\pi$	$\Sigma_b K$	$\Sigma_b^* K$	$\Xi_b\eta$	$\Lambda_b K^*$	$\Xi_b\rho$	$\Xi_b'\rho$	$\Xi_b^*\rho$	$\Sigma_b K^*$	$\Sigma_b^* K^*$	$\Xi_b'\eta$	$\Xi_b^*\eta$	$\Xi_b\eta'$	$\Xi_b'\eta'$	$\Xi_b^*\eta'$	$\Xi_b\omega$	$\Xi_b'\omega$	$\Xi_b^*\omega$	$\Xi_b\phi$	$\Xi_b'\phi$	$\Xi_b^*\phi$	$\Lambda_8 B$	$\Lambda_8 B^*$	$\Sigma_8 B$	$\Lambda_8^* B$	Γ^{Strong}
$\Xi_b(snb)$	$\mathbf{J}^P$	$\lvert l_\lambda, l_\rho, k_\lambda, k_\rho\rangle$	$^{2S+1}L_J$	MeV	MeV	MeV	MeV	MeV	MeV	MeV	MeV	MeV	MeV	MeV	MeV	MeV	MeV	MeV	MeV	MeV	MeV	MeV	MeV	MeV	MeV	MeV	MeV	MeV	MeV	MeV	MeV	MeV
$N=0$																																
$\Xi_b(5806)$	$\frac{1}{2}^+$	$\lvert 0,0,0,0\rangle$	$^2S_{1/2}$	0	0	0	0	0	0	0	0	0	0	0	0	0	0	0	0	0	0	0	0	0	0	0	0	0	0	0	0	0
$N=1$																																
$\Xi_b(6079)$	$\frac{1}{2}^-$	$\lvert 1,0,0,0\rangle$	$^2P_{1/2}$	0	0	0.2	0	0	0	0	0	0	0	0	0	0	0	0	0	0	0	0	0	0	0	0	0	0	0	0	0	0.2
$\Xi_b(6085)$	$\frac{3}{2}^-$	$\lvert 1,0,0,0\rangle$	$^2P_{3/2}$	0	0	1.1	0	0	0	0	0	0	0	0	0	0	0	0	0	0	0	0	0	0	0	0	0	0	0	0	0	1.1
$\Xi_b(6248)$	$\frac{1}{2}^-$	$\lvert 0,1,0,0\rangle$	$^2P_{1/2}$	1.0	0.4	2.5	4.8	0	0	0	0	0	0	0	0	0	0	0	0	0	0	0	0	0	0	0	0	0	0	0	0	8.7
$\Xi_b(6271)$	$\frac{1}{2}^-$	$\lvert 0,1,0,0\rangle$	$^4P_{1/2}$	1.1	0.3	1.1	3.5	0	0	0	0	0	0	0	0	0	0	0	0	0	0	0	0	0	0	0	0	0	0	0	0	6.0
$\Xi_b(6255)$	$\frac{3}{2}^-$	$\lvert 0,1,0,0\rangle$	$^2P_{3/2}$	21.1	23.7	20.5	0.6	0	0	0	0	0	0	0	0	0	0	0	0	0	0	0	0	0	0	0	0	0	0	0	0	65.9
$\Xi_b(6277)$	$\frac{3}{2}^-$	$\lvert 0,1,0,0\rangle$	$^4P_{3/2}$	4.4	5.0	1.1	15.6	0	0	0	0	0	0	0	0	0	0	0	0	0	0	0	0	0	0	0	0	0	0	0	0	0	26.1
$\Xi_b(6287)$	$\frac{5}{2}^-$	$\lvert 0,1,0,0\rangle$	$^4P_{5/2}$	26.9	30.5	7.0	4.1	0	0	0	0	0	0	0	0	0	0	0	0	0	0	0	0	0	0	0	0	0	0	0	0	0	68.5
$N=2$																																
$\Xi_b(6354)$	$\frac{3}{2}^+$	$\lvert 2,0,0,0\rangle$	$^2D_{3/2}$	⋯	⋯	0.3	0.5	0.2	0.8	⋯	0	0	0	0	0	0	0	0	0	0	0	0	0	0	0	0	0	0	0	0	0	1.8
$\Xi_b(6364)$	$\frac{5}{2}^+$	$\lvert 2,0,0,0\rangle$	$^2D_{5/2}$	⋯	⋯	0.8	0.1	0.6	0.1	⋯	0	0	0	0	0	0	0	0	0	0	0	0	0	0	0	0	0	0	0	0	0	1.6
$\Xi_b(6360)$	$\frac{1}{2}^+$	$\lvert 0,0,1,0\rangle$	$^2S_{1/2}$	⋯	⋯	1.7	0.9	1.4	1.4	⋯	0	0	0	0	0	0	0	0	0	0	0	0	0	0	0	0	0	0	0	0	0	5.4
$\Xi_b(6699)$	$\frac{1}{2}^+$	$\lvert 0,0,0,1\rangle$	$^2S_{1/2}$	⋯	⋯	7.2	20.6	18.9	41.8	⋯	34.8	40.1	0	0	0	0	1.4	0.9	0	0	0	12.9	0	0	0	0	0	⋯	⋯	⋯	0	178.8
$\Xi_b(6524)$	$\frac{3}{2}^+$	$\lvert 1,1,0,0\rangle$	$^2D_{3/2}$	1.6	2.1	3.1	6.4	7.7	23.6	0.3	1.0	0	0	0	0	0	0.1	0	0	0	0	0	0	0	0	0	0	⋯	⋯	⋯	0	45.9
$\Xi_b(6534)$	$\frac{5}{2}^+$	$\lvert 1,1,0,0\rangle$	$^2D_{5/2}$	21.2	24.4	19.3	0.6	37.6	2.3	1.4	0.3	0	0	0	0	0	0.3	0	0	0	0	0	0	0	0	0	0	⋯	⋯	⋯	0	107.4
$\Xi_b(6540)$	$\frac{1}{2}^+$	$\lvert 1,1,0,0\rangle$	$^4D_{1/2}$	0.1	0.5	0.9	3.1	2.7	11.1	0.5	1.3	0	0	0	0	0	0.1	0	0	0	0	0	0	0	0	0	0	⋯	⋯	⋯	0	20.3
$\Xi_b(6546)$	$\frac{3}{2}^+$	$\lvert 1,1,0,0\rangle$	$^4D_{3/2}$	1.6	2.0	0.8	12.2	2.0	42.7	0.3	5.3	0	0	0	0	0	0	0	0	0	0	0	0	0	0	0	0	⋯	⋯	⋯	0	66.9
$\Xi_b(6556)$	$\frac{5}{2}^+$	$\lvert 1,1,0,0\rangle$	$^4D_{5/2}$	8.9	10.2	2.0	14.8	4.0	52.3	0.6	7.3	0	0	0	0	0	0	0	0	0	0	0	0	0	0	0	0	⋯	⋯	⋯	0	100.1
$\Xi_b(6570)$	$\frac{7}{2}^+$	$\lvert 1,1,0,0\rangle$	$^4D_{7/2}$	29.8	34.2	7.0	4.3	14.4	19.5	2.2	2.2	0	0	0	0	0	0.2	0	0	0	0	0	0	0	0	0	0	⋯	⋯	⋯	0	113.8
$\Xi_b(6526)$	$\frac{1}{2}^-$	$\lvert 1,1,0,0\rangle$	$^2P_{1/2}$	0	0	0	0.1	0	0.2	0	0	0	0	0	0	0	0	0	0	0	0	0	0	0	0	0	0	⋯	⋯	⋯	0	0.3
$\Xi_b(6532)$	$\frac{3}{2}^-$	$\lvert 1,1,0,0\rangle$	$^2P_{3/2}$	0.4	0.5	0.3	0	0.6	0.1	0	0	0	0	0	0	0	0	0	0	0	0	0	0	0	0	0	0	⋯	⋯	⋯	0	1.9
$\Xi_b(6548)$	$\frac{1}{2}^-$	$\lvert 1,1,0,0\rangle$	$^4P_{1/2}$	0	0	0	0	0	0.1	0	0	0	0	0	0	0	0	0	0	0	0	0	0	0	0	0	0	⋯	⋯	⋯	0	0.1
$\Xi_b(6554)$	$\frac{3}{2}^-$	$\lvert 1,1,0,0\rangle$	$^4P_{3/2}$	0.1	0.1	0	0.1	0	0.5	0	0.1	0	0	0	0	0	0	0	0	0	0	0	0	0	0	0	0	⋯	⋯	⋯	0	0.9
$\Xi_b(6564)$	$\frac{5}{2}^-$	$\lvert 1,1,0,0\rangle$	$^4P_{5/2}$	0.5	0.6	0.1	0.2	0.2	0.7	0	0.1	0	0	0	0	0	0	0	0	0	0	0	0	0	0	0	0	⋯	⋯	⋯	0	2.4
$\Xi_b(6558)$	$\frac{3}{2}^+$	$\lvert 1,1,0,0\rangle$	$^4S_{3/2}$	0	0.3	1.1	6.1	3.3	17.2	0.6	4.0	0	0	0	0	0	0.1	0	0	0	0	0	0	0	0	0	0	⋯	⋯	⋯	0	32.7
$\Xi_b(6530)$	$\frac{1}{2}^+$	$\lvert 1,1,0,0\rangle$	$^2S_{1/2}$	0.2	0.9	4.8	2.2	13.9	7.0	0.6	1.3	0	0	0	0	0	0.2	0	0	0	0	0	0	0	0	0	0	⋯	⋯	⋯	0	31.1
$\Xi_b(6693)$	$\frac{3}{2}^+$	$\lvert 0,2,0,0\rangle$	$^2D_{3/2}$	⋯	⋯	4.2	17.3	9.1	42.9	⋯	22.8	22.9	0	0	0	0	0.3	0.6	0	0	0	7.3	0	0	0	0	0	⋯	⋯	⋯	0	127.4
$\Xi_b(6703)$	$\frac{5}{2}^+$	$\lvert 0,2,0,0\rangle$	$^2D_{5/2}$	⋯	⋯	11.3	6.3	24.9	30.4	⋯	12.6	8.4	0	0	0	0	0.8	0.1	0	0	0	2.6	0	0	0	0	0	⋯	⋯	⋯	0	97.4

TABLE XXIV. Predicted $\Sigma_b(nnb)$ strong partial decay widths (in MeV). The flavor multiplet is denoted by the symbol $\mathcal{F}$. The first column reports the baryon name with its predicted mass, calculated by using the three-quark model Hamiltonian given in Eqs. (1) and (2). The second column displays $\mathbf{J}^{\mathrm{P}}$, the third column shows the three-quark model state, $|l_\lambda, l_\rho, k_\lambda, k_\rho\rangle$, where $l_{\lambda,\rho}$ represent the orbital angular momenta and $k_{\lambda,\rho}$ denote the number of nodes of the λ and ρ oscillators. The fourth column presents the spectroscopic notation $^{2S+1}L_J$. The value of $N = n_\rho + n_\lambda$ distinguishes the $N = 0, 1, 2$ energy bands. Starting from the fifth column, we provide the strong partial decay widths calculated using Eq. (17). Each column corresponds to an open flavor strong decay channel, and the specific decay channels are indicated at the top of each column. The masses of the decay products are given in Table XXVII. The values for the strong decay widths are given in MeV. The decay widths denoted by 0 are either too small to be shown in this scale or forbidden by phase space, while the decay widths denoted by $\cdots$ are forbidden by selection rules. Finally, the last column represents the sum of the strong partial decay widths over all the decay channels. N_1^*, N_2^*, N_3^*, and N_4^* represent $N(1520)$, $N(1535)$, $N(1680)$, and $N(1720)$, respectively.

$\mathcal{F} = \mathbf{6}_{\mathrm{F}}$				$\Sigma_b\pi$	$\Sigma_b^*\pi$	$\Lambda_b\pi$	$\Sigma_b\eta$	Ξ_bK	$\Sigma_b\rho$	$\Sigma_b^*\rho$	$\Lambda_b\rho$	$\Sigma_b^*\eta$	$\Sigma_b\eta'$	$\Sigma_b^*\eta'$	$\Xi_b'K$	Ξ_b^*K	Ξ_bK^*	$\Xi_b'K^*$	$\Xi_b^*K^*$	$\Sigma_b\omega$	$\Sigma_b^*\omega$	NB	Σ_8B_s	NB^*	ΔB	N_1^*B	N_2^*B	N_3^*B	N_4^*B	Γ^{Strong}
$\Sigma_b(nnb)$	$\mathbf{J}^P$	$\lvert l_\lambda, l_\rho, k_\lambda, k_\rho\rangle$	$^{2S+1}L_J$	MeV	MeV	MeV	MeV	MeV	MeV	MeV	MeV	MeV	MeV	MeV	MeV	MeV	MeV	MeV	MeV	MeV	MeV	MeV	MeV	MeV	MeV	MeV	MeV	MeV	MeV	MeV
$N = 0$																														
$\Sigma_b(5804)$	$\frac{1}{2}^+$	$\lvert 0,0,0,0\rangle$	$^2S_{1/2}$	0	0	3.9	0	0	0	0	0	0	0	0	0	0	0	0	0	0	0	0	0	0	0	0	0	0	0	3.9
$\Sigma_b(5832)$	$\frac{3}{2}^+$	$\lvert 0,0,0,0\rangle$	$^4S_{3/2}$	0	0	10.0	0	0	0	0	0	0	0	0	0	0	0	0	0	0	0	0	0	0	0	0	0	0	0	10.0
$N = 1$																														
$\Sigma_b(6108)$	$\frac{1}{2}^-$	$\lvert 1,0,0,0\rangle$	$^2P_{1/2}$	3.4	20.1	0	0	0	0	0	0	0	0	0	0	0	0	0	0	0	0	0	0	0	0	0	0	0	0	23.5
$\Sigma_b(6131)$	$\frac{1}{2}^-$	$\lvert 1,0,0,0\rangle$	$^4P_{1/2}$	1.6	11.1	0.5	0	0	0	0	0	0	0	0	0	0	0	0	0	0	0	0	0	0	0	0	0	0	0	0	13.2
$\Sigma_b(6114)$	$\frac{3}{2}^-$	$\lvert 1,0,0,0\rangle$	$^2P_{3/2}$	27.2	2.7	54.0	0	0	0	0	0	0	0	0	0	0	0	0	0	0	0	0	0	0	0	0	0	0	0	0	83.9
$\Sigma_b(6137)$	$\frac{3}{2}^-$	$\lvert 1,0,0,0\rangle$	$^4P_{3/2}$	1.5	44.1	11.3	0	0	0	0	0	0	0	0	0	0	0	0	0	0	0	0	0	0	0	0	0	0	0	0	56.9
$\Sigma_b(6147)$	$\frac{5}{2}^-$	$\lvert 1,0,0,0\rangle$	$^4P_{5/2}$	9.4	16.7	69.8	0	0	0	0	0	0	0	0	0	0	0	0	0	0	0	0	0	0	0	0	0	0	0	0	95.9
$\Sigma_b(6304)$	$\frac{1}{2}^-$	$\lvert 0,1,0,0\rangle$	$^2P_{1/2}$	0.1	134.1	$\cdots$	0	$\cdots$	0	0	0	0	0	0	0	0	0	0	0	0	0	0	$\cdots$	0	$\cdots$	0	0	0	0	0	134.2
$\Sigma_b(6311)$	$\frac{3}{2}^-$	$\lvert 0,1,0,0\rangle$	$^2P_{3/2}$	67.1	62.2	$\cdots$	0	$\cdots$	0	0	0	0	0	0	0	0	0	0	0	0	0	0	$\cdots$	0	$\cdots$	0	0	0	0	0	129.3
$N = 2$																														
$\Sigma_b(6415)$	$\frac{3}{2}^+$	$\lvert 2,0,0,0\rangle$	$^2D_{3/2}$	2.7	4.2	6.0	0.1	0.6	0	0	1.0	0.1	0	0	0	0	0	0	0	0	0	0	0	4.3	0	38.6	0	0	0	0	57.6
$\Sigma_b(6425)$	$\frac{5}{2}^+$	$\lvert 2,0,0,0\rangle$	$^2D_{5/2}$	7.3	1.5	15.1	0.3	1.3	0	0	0.1	0	0	0	0	0	0	0	0	0	0	0	11.0	0	93.3	0	0	0	0	0	129.9
$\Sigma_b(6431)$	$\frac{1}{2}^+$	$\lvert 2,0,0,0\rangle$	$^4D_{1/2}$	0.1	6.7	2.2	0	0.5	0	0	2.3	0.2	0	0	0	0	0	0	0	0	0	0	4.5	0	61.3	0	0	0	0	0	77.8
$\Sigma_b(6437)$	$\frac{3}{2}^+$	$\lvert 2,0,0,0\rangle$	$^4D_{3/2}$	0.7	7.3	6.6	0	0.7	0	0	5.0	0.4	0	0	0	0	0	0	0	0	0	0	18.7	0	66.5	0	0	0	0	0	105.9
$\Sigma_b(6448)$	$\frac{5}{2}^+$	$\lvert 2,0,0,0\rangle$	$^4D_{5/2}$	1.6	6.6	12.5	0.1	1.2	0	0	4.1	0.4	0	0	0	0	0	0	0	0	0	0	39.1	0	67.1	0	0	0	0	0	132.7
$\Sigma_b(6462)$	$\frac{7}{2}^+$	$\lvert 2,0,0,0\rangle$	$^4D_{7/2}$	2.2	7.8	18.5	0.1	2.0	0	0	2.5	0.2	0	0	0.1	0	0	0	0	0	0	0	55.8	0	56.0	0	0	0	0	0	145.2
$\Sigma_b(6421)$	$\frac{1}{2}^+$	$\lvert 0,0,1,0\rangle$	$^2S_{1/2}$	8.5	4.3	3.2	0.6	2.8	0	0	3.3	0.2	0	0	0	0	0	0	0	0	0	0	7.9	0	88.4	0	0	0	0	0	119.2
$\Sigma_b(6450)$	$\frac{3}{2}^+$	$\lvert 0,0,1,0\rangle$	$^4S_{3/2}$	2.0	10.5	2.0	0.2	3.4	0	0	8.6	0.9	0	0	0.1	0	0	0	0	0	0	0	28.6	0	64.8	0	0	0	0	0	121.2
$\Sigma_b(6813)$	$\frac{1}{2}^+$	$\lvert 0,0,0,1\rangle$	$^2S_{1/2}$	5.5	1.5	81.7	0.9	0.4	357.9	6.0	1.3	0.7	7.4	1.8	11.1	9.4	36.4	0	0	184.2	3.1	$\cdots$	$\cdots$	$\cdots$	$\cdots$	$\cdots$	$\cdots$	0	0	709.8
$\Sigma_b(6842)$	$\frac{3}{2}^+$	$\lvert 0,0,0,1\rangle$	$^4S_{3/2}$	2.7	8.7	100.0	0.1	0	18.1	497.3	0.1	0.9	3.1	11.4	2.1	23.2	38.7	0.8	0	9.4	256.9	$\cdots$	$\cdots$	$\cdots$	$\cdots$	$\cdots$	$\cdots$	0	0	973.5
$\Sigma_b(6611)$	$\frac{3}{2}^+$	$\lvert 1,1,0,0\rangle$	$^2D_{3/2}$	7.0	117.8	$\cdots$	1.3	$\cdots$	9.0	0.1	209.2	20.1	0	0	3.3	5.1	0	0	0	3.3	0	$\cdots$	$\cdots$	$\cdots$	$\cdots$	0	0	0	0	376.2
$\Sigma_b(6621)$	$\frac{5}{2}^+$	$\lvert 1,1,0,0\rangle$	$^2D_{5/2}$	77.8	77.0	$\cdots$	8.3	$\cdots$	1.7	1.1	66.6	2.9	0	0	14.6	0.5	0	0	0	0.7	0.4	$\cdots$	$\cdots$	$\cdots$	$\cdots$	0	0	0	0	251.6
$\Sigma_b(6613)$	$\frac{1}{2}^-$	$\lvert 1,1,0,0\rangle$	$^2P_{1/2}$	0	2.2	$\cdots$	0	$\cdots$	0	0	1.8	0.2	0	0	0	0	0	0	0	0	0	$\cdots$	$\cdots$	$\cdots$	$\cdots$	0	0	0	0	4.2
$\Sigma_b(6619)$	$\frac{3}{2}^-$	$\lvert 1,1,0,0\rangle$	$^2P_{3/2}$	1.2	1.1	$\cdots$	0.1	$\cdots$	0	0	1.9	0.1	0	0	0.2	0	0	0	0	0	0	$\cdots$	$\cdots$	$\cdots$	$\cdots$	0	0	0	0	4.6
$\Sigma_b(6617)$	$\frac{1}{2}^+$	$\lvert 1,1,0,0\rangle$	$^2S_{1/2}$	2.0	1.5	$\cdots$	1.5	$\cdots$	9.0	1.0	26.2	3.5	0	0	6.1	2.9	0	0	0	3.5	0.3	$\cdots$	$\cdots$	$\cdots$	$\cdots$	0	0	0	0	57.5
$\Sigma_b(6807)$	$\frac{3}{2}^+$	$\lvert 0,2,0,0\rangle$	$^2D_{3/2}$	49.8	3.7	120.5	4.3	11.8	213.3	0.4	2.2	2.1	1.4	1.2	8.0	8.4	13.6	0	0	108.3	0.2	$\cdots$	$\cdots$	$\cdots$	$\cdots$	$\cdots$	0	0	0	549.2
$\Sigma_b(6817)$	$\frac{5}{2}^+$	$\lvert 0,2,0,0\rangle$	$^2D_{5/2}$	85.6	54.0	160.6	10.1	25.4	116.2	1.4	73.8	4.7	3.6	0.2	21.8	2.4	0.9	0	0	54.9	0.7	$\cdots$	$\cdots$	$\cdots$	$\cdots$	$\cdots$	$\cdots$	0	0	616.3
$\Sigma_b(6824)$	$\frac{1}{2}^+$	$\lvert 0,2,0,0\rangle$	$^4D_{1/2}$	17.2	15.6	213.5	0.7	10.6	13.2	676.3	13.9	5.0	0.4	2.8	0.2	13.4	18.5	0	0	6.6	340.9	$\cdots$	$\cdots$	$\cdots$	$\cdots$	$\cdots$	$\cdots$	0	0	1348.8
$\Sigma_b(6830)$	$\frac{3}{2}^+$	$\lvert 0,2,0,0\rangle$	$^4D_{3/2}$	14.0	4.2	130.3	1.2	13.5	25.2	291.0	38.8	2.4	0.6	4.9	2.2	15.4	35.7	0	0	12.7	148.4	$\cdots$	$\cdots$	$\cdots$	$\cdots$	$\cdots$	$\cdots$	0	0	740.5
$\Sigma_b(6840)$	$\frac{5}{2}^+$	$\lvert 0,2,0,0\rangle$	$^4D_{5/2}$	13.6	75.2	77.8	2.0	19.0	15.4	29.5	66.0	6.9	1.0	5.1	4.7	13.4	22.1	0.7	0	7.7	15.6	$\cdots$	$\cdots$	$\cdots$	$\cdots$	$\cdots$	$\cdots$	0	0	375.7
$\Sigma_b(6854)$	$\frac{7}{2}^+$	$\lvert 0,2,0,0\rangle$	$^4D_{7/2}$	27.8	173.6	211.6	3.2	32.3	32.3	235.6	267.6	18.6	1.9	2.5	6.6	14.1	24.8	0.6	0	15.6	109.8	$\cdots$	$\cdots$	$\cdots$	$\cdots$	$\cdots$	$\cdots$	0	0	1178.5

TABLE XXV. Same as XXII, but for $\Xi_b'(snb)$ states.

$\mathcal{F}=\mathbf{6}_{\mathrm{F}}$				$\Lambda_b K$	$\Xi_b\pi$	$\Xi_b'\pi$	$\Xi_b^*\pi$	$\Sigma_b K$	$\Sigma_b^* K$	$\Xi_b\eta$	$\Lambda_b K^*$	$\Xi_b\rho$	$\Xi_b'\rho$	$\Xi_b^*\rho$	$\Sigma_b K^*$	$\Sigma_b^* K^*$	$\Xi_b'\eta$	$\Xi_b^*\eta$	$\Xi_b\eta'$	$\Xi_b'\eta'$	$\Xi_b^*\eta'$	$\Xi_b\omega$	$\Xi_b'\omega$	$\Xi_b^*\omega$	$\Xi_b\phi$	$\Xi_b'\phi$	$\Xi_b^*\phi$	$\Sigma_8 B$	$\Xi_8 B_s$	$\Sigma_8 B^*$	$\Sigma_{10} B$	Γ^{Strong}
$\Xi_b'(snb)$	$\mathbf{J}^P$	$\lvert l_\lambda, l_\rho, k_\lambda, k_\rho\rangle$	$^{2S+1}L_J$	MeV	MeV	MeV	MeV	MeV	MeV	MeV	MeV	MeV	MeV	MeV	MeV	MeV	MeV	MeV	MeV	MeV	MeV	MeV	MeV	MeV	MeV	MeV	MeV	MeV	MeV	MeV	MeV	MeV	MeV
$N=0$																																	
$\Xi_b'(5925)\,\frac{1}{2}^+$		$\lvert 0,0,0,0\rangle$	$^2S_{1/2}$	0	0	0	0	0	0	0	0	0	0	0	0	0	0	0	0	0	0	0	0	0	0	0	0	0	0	0	0	0	0
$\Xi_b'(5953)\,\frac{3}{2}^+$		$\lvert 0,0,0,0\rangle$	$^4S_{3/2}$	0	0.2	0	0	0	0	0	0	0	0	0	0	0	0	0	0	0	0	0	0	0	0	0	0	0	0	0	0	0	0	0.2
$N=1$																																	
$\Xi_b'(6198)\,\frac{1}{2}^-$		$\lvert 1,0,0,0\rangle$	$^2P_{1/2}$	1.1	0.5	1.4	0	0	0	0	0	0	0	0	0	0	0	0	0	0	0	0	0	0	0	0	0	0	0	0	0	0	0	3.0
$\Xi_b'(6220)\,\frac{1}{2}^-$		$\lvert 1,0,0,0\rangle$	$^4P_{1/2}$	1.8	0.8	0.7	0.4	0	0	0	0	0	0	0	0	0	0	0	0	0	0	0	0	0	0	0	0	0	0	0	0	0	0	3.7
$\Xi_b'(6204)\,\frac{3}{2}^-$		$\lvert 1,0,0,0\rangle$	$^2P_{3/2}$	9.9	11.2	8.4	0	0	0	0	0	0	0	0	0	0	0	0	0	0	0	0	0	0	0	0	0	0	0	0	0	0	0	29.5
$\Xi_b'(6226)\,\frac{3}{2}^-$		$\lvert 1,0,0,0\rangle$	$^4P_{3/2}$	2.1	2.4	0.5	2.6	0	0	0	0	0	0	0	0	0	0	0	0	0	0	0	0	0	0	0	0	0	0	0	0	0	0	7.6
$\Xi_b'(6237)\,\frac{5}{2}^-$		$\lvert 1,0,0,0\rangle$	$^4P_{5/2}$	13.0	14.6	3.0	0.8	0	0	0	0	0	0	0	0	0	0	0	0	0	0	0	0	0	0	0	0	0	0	0	0	0	0	31.4
$\Xi_b'(6367)\,\frac{1}{2}^-$		$\lvert 0,1,0,0\rangle$	$^2P_{1/2}$	⋯	⋯	0.6	44.8	7.2	144.0	⋯	0	0	0	0	0	0	0	0	0	0	0	0	0	0	0	0	0	0	0	0	0	0	0	196.6
$\Xi_b'(6374)\,\frac{3}{2}^-$		$\lvert 0,1,0,0\rangle$	$^2P_{3/2}$	⋯	⋯	22.8	6.1	50.1	18.2	⋯	0	0	0	0	0	0	0	0	0	0	0	0	0	0	0	0	0	0	0	0	0	0	0	97.2
$N=2$																																	
$\Xi_b'(6473)\,\frac{3}{2}^+$		$\lvert 2,0,0,0\rangle$	$^2D_{3/2}$	0.8	0.9	0.8	0.7	1.6	2.4	0.1	0	0	0	0	0	0	0	0	0	0	0	0	0	0	0	0	0	0	1.6	0	4.8	0	13.7
$\Xi_b'(6483)\,\frac{5}{2}^+$		$\lvert 2,0,0,0\rangle$	$^2D_{5/2}$	2.2	2.5	2.0	0.1	3.6	0.4	0.1	0	0	0	0	0	0	0	0	0	0	0	0	0	0	0	0	0	0	3.6	0	15.7	0	30.2
$\Xi_b'(6489)\,\frac{1}{2}^+$		$\lvert 2,0,0,0\rangle$	$^4D_{1/2}$	0	0	0.1	1.0	0.3	3.6	0	0	0	0	0	0	0	0	0	0	0	0	0	0	0	0	0	0	0	6.2	0	13.5	0	24.7
$\Xi_b'(6495)\,\frac{3}{2}^+$		$\lvert 2,0,0,0\rangle$	$^4D_{3/2}$	0.9	1.0	0.2	1.4	0.5	5.1	0.1	0	0	0	0	0	0	0	0	0	0	0	0	0	0	0	0	0	0	8.5	0	17.7	0	35.4
$\Xi_b'(6506)\,\frac{5}{2}^+$		$\lvert 2,0,0,0\rangle$	$^4D_{5/2}$	1.9	2.2	0.4	1.3	0.8	4.5	0.1	0	0	0	0	0	0	0	0	0	0	0	0	0	0	0	0	0	0	14.2	0	20.9	0	46.3
$\Xi_b'(6520)\,\frac{7}{2}^+$		$\lvert 2,0,0,0\rangle$	$^4D_{7/2}$	2.6	3.0	0.6	0.6	1.3	2.4	0.2	0.1	0	0	0	0	0	0	0	0	0	0	0	0	0	0	0	0	0	24.6	0	11.4	0	46.8
$\Xi_b'(6479)\,\frac{1}{2}^+$		$\lvert 0,0,1,0\rangle$	$^2S_{1/2}$	2.1	2.8	3.7	0.9	7.8	3.5	0.3	0	0	0	0	0	0	0	0	0	0	0	0	0	0	0	0	0	0	5.0	0	21.2	0	47.4
$\Xi_b'(6508)\,\frac{3}{2}^+$		$\lvert 0,0,1,0\rangle$	$^4S_{3/2}$	1.8	2.6	0.9	2.9	2.2	10.2	0.3	0	0	0	0	0	0	0	0	0	0	0	0	0	0	0	0	0	0	26.2	0	31.7	0	79
$\Xi_b'(6818)\,\frac{1}{2}^+$		$\lvert 0,0,0,1\rangle$	$^2S_{1/2}$	1.9	0.2	3.0	5.4	7.4	5.1	0.4	12.7	29.7	133.6	0	331.3	4.5	1.7	0.9	8.5	0	0	10.1	42.3	0	0.1	0	0	⋯	⋯	⋯	⋯	599
$\Xi_b'(6847)\,\frac{3}{2}^+$		$\lvert 0,0,0,1\rangle$	$^4S_{3/2}$	3.4	0.9	0.4	11.7	1.0	7.8	0.2	9.0	26.5	9.4	0	22.2	504.4	0.4	2.4	12.2	0	0	9.1	3.1	0	5.8	0	0	⋯	⋯	⋯	⋯	630.2
$\Xi_b'(6642)\,\frac{3}{2}^+$		$\lvert 1,1,0,0\rangle$	$^2D_{3/2}$	⋯	⋯	2.1	35.8	5.4	113.8	⋯	43.4	25.7	0	0	0	0	0.3	0.2	0	0	0	7.5	0	0	0	0	0	⋯	0	⋯	0	234.2
$\Xi_b'(6653)\,\frac{5}{2}^+$		$\lvert 1,1,0,0\rangle$	$^2D_{5/2}$	⋯	⋯	22.9	4.4	49.4	21.7	⋯	9.1	5.3	0	0	0	0	1.2	0	0	0	0	1.6	0	0	0	0	0	⋯	0	⋯	0	115.6
$\Xi_b'(6644)\,\frac{1}{2}^-$		$\lvert 1,1,0,0\rangle$	$^2P_{1/2}$	⋯	⋯	0	0.4	0	1.6	⋯	0.3	0.2	0	0	0	0	0	0	0	0	0	0.1	0	0	0	0	0	⋯	0	⋯	0	2.6
$\Xi_b'(6651)\,\frac{3}{2}^-$		$\lvert 1,1,0,0\rangle$	$^2P_{3/2}$	⋯	⋯	0.4	0.2	0.9	0.8	⋯	0.4	0.2	0	0	0	0	0	0	0	0	0	0.1	0	0	0	0	0	⋯	0	⋯	0	3.0
$\Xi_b'(6649)\,\frac{1}{2}^+$		$\lvert 1,1,0,0\rangle$	$^2S_{1/2}$	⋯	⋯	1.3	7.7	4.9	12.6	⋯	14.5	13.2	0	0	0	0	0.6	0.1	0	0	0	4.0	0	0	0	0	0	⋯	0	⋯	0	58.9
$\Xi_b'(6812)\,\frac{3}{2}^+$		$\lvert 0,2,0,0\rangle$	$^2D_{3/2}$	13.5	13.7	9.3	5.9	20.4	10.0	0.8	4.1	10.0	57.7	0	145.2	0.1	0.6	0.7	1.5	0	0	3.4	18.1	0	0	0	0	⋯	⋯	⋯	⋯	315.0
$\Xi_b'(6822)\,\frac{5}{2}^+$		$\lvert 0,2,0,0\rangle$	$^2D_{5/2}$	22.0	24.8	21.8	5.0	48.6	23.0	2.0	6.9	2.8	11.1	0	29.8	1.0	1.7	0.1	3.7	0	0	0.9	3.4	0	0.1	0	0	⋯	⋯	⋯	⋯	208.7
$\Xi_b'(6828)\,\frac{1}{2}^+$		$\lvert 0,2,0,0\rangle$	$^4D_{1/2}$	20.2	17.4	1.5	11.0	3.1	23.6	0.4	9.1	15.7	3.5	0	8.7	404.9	0	1.0	1.6	0	0	5.3	1.1	0	1.1	0	0	⋯	⋯	⋯	⋯	529.2
$\Xi_b'(6834)\,\frac{3}{2}^+$		$\lvert 0,2,0,0\rangle$	$^4D_{3/2}$	15.2	15.4	2.6	8.7	5.8	11.3	0.9	18.5	30.4	6.9	0	17.0	212.1	0.2	1.3	2.2	0	0	10.2	2.2	0	2.7	0	0	⋯	⋯	⋯	⋯	363.6
$\Xi_b'(6845)\,\frac{5}{2}^+$		$\lvert 0,2,0,0\rangle$	$^4D_{5/2}$	13.2	16.4	4.3	10.7	9.6	33.0	1.6	13.8	18.5	4.5	0	10.9	41.8	0.4	1.1	3.8	0	0	6.2	1.4	0	2.6	0	0	⋯	⋯	⋯	⋯	193.8
$\Xi_b'(6859)\,\frac{7}{2}^+$		$\lvert 0,2,0,0\rangle$	$^4D_{7/2}$	28.8	32.0	6.7	22.3	15.1	89.3	2.5	46.1	38.1	3.7	0.2	10.2	31.2	0.5	0.8	6.7	0	0	12.3	1.1	0	1.8	0	0	⋯	⋯	⋯	⋯	349.4

TABLE XXVI. Same as XXII, but for $\Omega_b(snb)$ states.

$\mathcal{F}=\mathbf{6}_{\mathrm{F}}$				$\Xi_b K$	$\Xi_b' K$	$\Xi_b^* K$	$\Xi_b K^*$	$\Xi_b' K^*$	$\Xi_b^* K^*$	$\Omega_b \eta$	$\Omega_b^* \eta$	$\Omega_b \phi$	$\Omega_b^* \phi$	$\Omega_b \eta'$	$\Omega_b^* \eta'$	$\Xi_8 B$	$\Xi_{10} B$	Γ^{Strong}
$\Omega_b(ssb)$	$\mathbf{J}^P$	$\lvert l_\lambda, l_\rho, k_\lambda, k_\rho\rangle$	$^{2S+1}L_J$	MeV	MeV	MeV	MeV	MeV	MeV	MeV	MeV	MeV	MeV	MeV	MeV	MeV	MeV	MeV
$N=0$																		
$\Omega_b(6064)$	$\frac{1}{2}^+$	$\lvert 0,0,0,0\rangle$	$^2S_{1/2}$	0	0	0	0	0	0	0	0	0	0	0	0	0	0	0
$\Omega_b(6093)$	$\frac{3}{2}^+$	$\lvert 0,0,0,0\rangle$	$^4S_{3/2}$	0	0	0	0	0	0	0	0	0	0	0	0	0	0	0
$N=1$																		
$\Omega_b(6315)$	$\frac{1}{2}^-$	$\lvert 1,0,0,0\rangle$	$^2P_{1/2}$	4.6	0	0	0	0	0	0	0	0	0	0	0	0	0	4.6
$\Omega_b(6337)$	$\frac{1}{2}^-$	$\lvert 1,0,0,0\rangle$	$^4P_{1/2}$	10.7	0	0	0	0	0	0	0	0	0	0	0	0	0	10.7
$\Omega_b(6321)$	$\frac{3}{2}^-$	$\lvert 1,0,0,0\rangle$	$^2P_{3/2}$	24.0	0	0	0	0	0	0	0	0	0	0	0	0	0	24.0
$\Omega_b(6343)$	$\frac{3}{2}^-$	$\lvert 1,0,0,0\rangle$	$^4P_{3/2}$	6.3	0	0	0	0	0	0	0	0	0	0	0	0	0	6.3
$\Omega_b(6353)$	$\frac{5}{2}^-$	$\lvert 1,0,0,0\rangle$	$^4P_{5/2}$	40.5	0	0	0	0	0	0	0	0	0	0	0	0	0	40.5
$\Omega_b(6465)$	$\frac{1}{2}^-$	$\lvert 0,1,0,0\rangle$	$^2P_{1/2}$	⋯	9.8	0	0	0	0	0	0	0	0	0	0	0	0	9.8
$\Omega_b(6471)$	$\frac{3}{2}^-$	$\lvert 0,1,0,0\rangle$	$^2P_{3/2}$	⋯	53.5	0	0	0	0	0	0	0	0	0	0	0	0	53.5
$N=2$																		
$\Omega_b(6568)$	$\frac{3}{2}^+$	$\lvert 2,0,0,0\rangle$	$^2D_{3/2}$	2.4	1.6	0	0	0	0	0	0	0	0	0	0	0	0	4.0
$\Omega_b(6578)$	$\frac{5}{2}^+$	$\lvert 2,0,0,0\rangle$	$^2D_{5/2}$	6.2	3.5	0	0	0	0	0	0	0	0	0	0	0	0	9.7
$\Omega_b(6584)$	$\frac{1}{2}^+$	$\lvert 2,0,0,0\rangle$	$^4D_{1/2}$	0.5	0.3	0.1	0	0	0	0	0	0	0	0	0	0	0	0.9
$\Omega_b(6590)$	$\frac{3}{2}^+$	$\lvert 2,0,0,0\rangle$	$^4D_{3/2}$	2.6	0.5	0.3	0	0	0	0	0	0	0	0	0	0	0	3.4
$\Omega_b(6600)$	$\frac{5}{2}^+$	$\lvert 2,0,0,0\rangle$	$^4D_{5/2}$	5.5	0.8	0.4	0	0	0	0	0	0	0	0	0	1.0	0	7.7
$\Omega_b(6614)$	$\frac{7}{2}^+$	$\lvert 2,0,0,0\rangle$	$^4D_{7/2}$	7.7	1.3	0.2	0	0	0	0.1	0	0	0	0	0	8.2	0	17.5
$\Omega_b(6574)$	$\frac{1}{2}^+$	$\lvert 0,0,1,0\rangle$	$^2S_{1/2}$	11.3	8.9	0	0	0	0	0	0	0	0	0	0	0	0	20.3
$\Omega_b(6602)$	$\frac{3}{2}^+$	$\lvert 0,0,1,0\rangle$	$^4S_{3/2}$	11.4	2.7	1.2	0	0	0	0	0	0	0	0	0	1.44	0	16.8
$\Omega_b(6874)$	$\frac{1}{2}^+$	$\lvert 0,0,0,1\rangle$	$^2S_{1/2}$	5.2	36.1	27.1	107.6	166.8	0	37.5	17.9	0	0	0	0	⋯	⋯	398.3
$\Omega_b(6902)$	$\frac{3}{2}^+$	$\lvert 0,0,0,1\rangle$	$^4S_{3/2}$	2.2	7.4	66.5	107.1	18.2	0	9.2	46.6	0	0	0	0	⋯	⋯	257.3
$\Omega_b(6718)$	$\frac{3}{2}^+$	$\lvert 1,1,0,0\rangle$	$^2D_{3/2}$	⋯	8.5	61.6	22.3	0	0	3.7	19.8	0	0	0	0	⋯	0	115.9
$\Omega_b(6728)$	$\frac{5}{2}^+$	$\lvert 1,1,0,0\rangle$	$^2D_{5/2}$	⋯	55.3	5.4	6.0	0	0	13.8	1.8	0	0	0	0	⋯	0	82.3
$\Omega_b(6720)$	$\frac{1}{2}^-$	$\lvert 1,1,0,0\rangle$	$^2P_{1/2}$	⋯	0	0.7	0.2	0	0	0	0.2	0	0	0	0	⋯	0	1.1
$\Omega_b(6726)$	$\frac{3}{2}^-$	$\lvert 1,1,0,0\rangle$	$^2P_{3/2}$	⋯	1.1	0.4	0.2	0	0	0.2	0.1	0	0	0	0	⋯	0	2.0
$\Omega_b(6724)$	$\frac{1}{2}^+$	$\lvert 1,1,0,0\rangle$	$^2S_{1/2}$	⋯	13.7	24.7	16.0	0	0	8.2	9.9	0	0	0	0	⋯	0	72.5
$\Omega_b(6868)$	$\frac{3}{2}^+$	$\lvert 0,2,0,0\rangle$	$^2D_{3/2}$	27.3	19.1	20.1	33.1	59.4	0	8.5	12.4	0	0	0	0	⋯	⋯	179.9
$\Omega_b(6878)$	$\frac{5}{2}^+$	$\lvert 0,2,0,0\rangle$	$^2D_{5/2}$	58.4	51.2	6.8	3.1	12.1	0	22.0	3.0	0	0	0	0	⋯	⋯	156.6
$\Omega_b(6884)$	$\frac{1}{2}^+$	$\lvert 0,2,0,0\rangle$	$^4D_{1/2}$	23.1	0.6	32.1	46.2	4.7	0	0.3	19.1	0	0	0	0	⋯	⋯	126.1
$\Omega_b(6890)$	$\frac{3}{2}^+$	$\lvert 0,2,0,0\rangle$	$^4D_{3/2}$	30.7	5.2	35.2	88.4	9.8	0	2.3	23.4	0	0	0	0	⋯	⋯	195.0
$\Omega_b(6900)$	$\frac{5}{2}^+$	$\lvert 0,2,0,0\rangle$	$^4D_{5/2}$	44.2	11.0	31.1	53.0	7.4	0	4.9	19.9	0	0	0	0	⋯	⋯	171.5
$\Omega_b(6914)$	$\frac{7}{2}^+$	$\lvert 0,2,0,0\rangle$	$^4D_{7/2}$	74.1	15.6	37.0	74.7	4.6	0	6.8	17.7	0	0	0	0	⋯	⋯	230.5

TABLE XXVII. Masses as from PDG [1] of the final baryon and meson states used in the calculation of the decay widths.

	Mass in GeV
m_π	0.13725 ± 0.00295
m_K	0.49564 ± 0.00279
m_η	0.54786 ± 0.00002
$m_{\eta'}$	0.95778 ± 0.00006
m_ρ	0.77518 ± 0.00045
m_{K^*}	0.89555 ± 0.00100
m_ω	0.78266 ± 0.00002
m_ϕ	1.01946 ± 0.00002
m_B	5.27966 ± 0.00012
m_{B_s}	5.36692 ± 0.00010
m_{B^*}	5.32471 ± 0.00021
m_N	0.93891 ± 0.00091
$m_{N(1520)}$	1.51500 ± 0.00500
$m_{N(1535)}$	1.53000 ± 0.01500
$m_{N(1680)}$	1.68500 ± 0.00500
$m_{N(1720)}$	1.72000 ± 0.03500
m_Δ	1.23200 ± 0.00200
m_Λ	1.11568 ± 0.00001
$m_{\Lambda(1520)}$	1.51900 ± 0.00010
m_{Ξ_8}	1.31820 ± 0.00360
$m_{\Xi_{10}}$	1.53370 ± 0.00250
m_{Σ_8}	1.11932 ± 0.00340
$m_{\Sigma_{10}}$	1.38460 ± 0.00460
m_{Λ_b}	5.61960 ± 0.00010
m_{Ξ_b}	5.79700 ± 0.00060
$m_{\Xi'_b}$	5.93502 ± 0.00005
$m_{\Xi^*_b}$	6.07800 ± 0.00006
m_{Σ_b}	5.81056 ± 0.00025
$m_{\Sigma^*_b}$	5.83032 ± 0.00030
m_{Ω_b}	6.04520 ± 0.00120
$m_{\Omega^*_b}$	6.09300 ± 0.00060

APPENDIX G: ELECTROMAGNETIC TRANSITION AMPLITUDES

In the nonrelativistic approximation, the transition operator describing an electromagnetic decay is given by the following electromagnetic Hamiltonian, as shown in Sec. IV:

$$\mathcal{H}_{\rm em} = 2\sqrt{\frac{\pi}{\rm k}}\sum_{j=1}^{3}\mu_j\left[{\rm k}\mathbf{s}_{j,-}\hat{U}_j - \frac{1}{2}\hat{T}_{j,-}\right], \tag{G1}$$

where $\hat{U}_j = e^{-i\vec{\rm k}\cdot\vec{r}_j}$ and $\hat{T}_{j,-} = \mathbf{p}_{j,-}\hat{U}_j + \hat{U}_j\mathbf{p}_{j,-}$.

1. Evaluation of the $\hat{T}_{j,-}$ matrix elements

The matrix elements of the tensor operators, $\hat{T}_{j,-}$, can be expressed as a sum of the matrix elements of the $\hat{U}_j$ operators, as we will show in the following.

In order to achieve it, we have to calculate the action of the $\mathbf{p}_{\rho,\pm}$ and $\mathbf{p}_{\lambda,\pm}$ ladder operators on the states. In the following subsection, we will calculate the action of these two operators.

2. Ladder operators

In coordinate representation, the $\mathbf{p}_{j,\pm}$ ladder operators of the jth quark are

$$\begin{aligned}\langle\vec{r}'|\mathbf{p}_{j,\pm}|\vec{r}\rangle &= \langle\vec{r}'|\mathbf{p}_{j,x} \pm i\mathbf{p}_{j,y}|\vec{r}\rangle \\ &= \left[-i\frac{\partial}{\partial x} \pm i\left(-i\frac{\partial}{\partial y}\right)\right]_j \delta^3(\vec{r}' - \vec{r}) \\ &= -i\left[\frac{\partial}{\partial x} \pm i\frac{\partial}{\partial y}\right]_j \delta^3(\vec{r}' - \vec{r}),\end{aligned} \tag{G2}$$

which can be written in spherical coordinates as

$$\langle\vec{r}'|\mathbf{p}_{j,\pm}|\vec{r}\rangle = \left[-i\frac{e^{-i\varphi}\cos\theta}{r}\frac{\partial}{\partial\theta} \pm \frac{e^{-i\varphi}}{r\sin\theta}\frac{\partial}{\partial\varphi} - ie^{-i\varphi}\sin\theta\frac{\partial}{\partial r}\right]_j \delta^3(\vec{r}' - \vec{r}). \tag{G3}$$

The previous equation imply for the $\mathbf{p}_{\rho,\pm}$ and $\mathbf{p}_{\lambda,\pm}$ ladder operators

$$\langle\vec{\rho}'|\mathbf{p}_{\rho,\pm}|\vec{\rho}\rangle = \left[-i\frac{e^{-i\varphi}\cos\theta}{\rho}\frac{\partial}{\partial\theta} \pm \frac{e^{-i\varphi}}{\rho\sin\theta}\frac{\partial}{\partial\varphi} - ie^{-i\varphi}\sin\theta\frac{\partial}{\partial\rho}\right]\delta^3(\vec{\rho}' - \vec{\rho}), \tag{G4}$$

$$\langle\vec{\lambda}'|\mathbf{p}_{\lambda,\pm}|\vec{\lambda}\rangle = \left[-i\frac{e^{-i\varphi}\cos\theta}{\lambda}\frac{\partial}{\partial\theta} \pm \frac{e^{-i\varphi}}{\lambda\sin\theta}\frac{\partial}{\partial\varphi} - ie^{-i\varphi}\sin\theta\frac{\partial}{\partial\lambda}\right]\delta^3(\vec{\lambda}' - \vec{\lambda}). \tag{G5}$$

As an example, we evaluate the action of the p_ρ operators on the ground state $\langle\vec{\rho},\vec{\lambda}|\mathbf{p}_{\rho,\pm}|0,0,0,0,0,0\rangle$ as follows

$$\begin{aligned}\langle\vec{\rho},\vec{\lambda}|\mathbf{p}_{\rho,\pm}|0,0,0,0,0,0\rangle &= \int d^3\vec{\rho}'d^3\vec{\lambda}'\langle\vec{\rho},\vec{\lambda}|\mathbf{p}_{\rho,\pm}|\vec{\rho}',\vec{\lambda}'\rangle\langle\vec{\rho}',\vec{\lambda}'|0,0,0,0,0,0\rangle \\ &= \left[-i\frac{e^{-i\varphi}\cos\theta}{\rho}\frac{\partial}{\partial\theta}\pm\frac{e^{-i\varphi}}{\rho\sin\theta}\frac{\partial}{\partial\varphi}-ie^{-i\varphi}\sin\theta\frac{\partial}{\partial\rho}\right]\frac{1}{3^{3/4}}\left(\frac{\omega_\rho m_\rho}{\pi}\right)^{\frac{3}{4}}\left(\frac{\omega_\lambda m_\lambda}{\pi}\right)^{\frac{3}{4}}\exp\left[-\frac{\omega_\rho m_\rho\vec{\rho}^2}{2}-\frac{\omega_\lambda m_\lambda\vec{\lambda}^2}{2}\right] \\ &= \mp i(\omega_\rho m_\rho)^{1/2}\psi_{0,1,\pm1,0,0,0}(\vec{\rho},\vec{\lambda}),\end{aligned} \tag{G6}$$

where, in the second line, we use the fact that the $\mathbf{p}_{\rho,\pm}$ operators are diagonal in coordinate space, i.e.

$$\langle\vec{\rho},\vec{\lambda}|\mathbf{p}_{\rho,\pm}|\vec{\rho}',\vec{\lambda}'\rangle = \left[-i\frac{e^{-i\varphi}\cos\theta}{\rho}\frac{\partial}{\partial\theta}\pm\frac{e^{-i\varphi}}{\rho\sin\theta}\frac{\partial}{\partial\varphi}-ie^{-i\varphi}\sin\theta\frac{\partial}{\partial\rho}\right]\delta^3(\vec{\rho}-\vec{\rho}')\delta^3(\vec{\lambda}-\vec{\lambda}'). \tag{G7}$$

We have a similar expression for p_λ. The results for the other cases are reported below.

$$\langle\vec{\rho},\vec{\lambda}|\mathbf{p}_{\lambda,\pm}|0,0,0,0,0,0\rangle = \mp i(\omega_\lambda m_\lambda)^{1/2}\psi_{0,0,0,0,1,\pm1}(\vec{\rho},\vec{\lambda}), \tag{G8}$$

$$\langle\vec{\rho},\vec{\lambda}|\mathbf{p}_{\rho,\pm}|0,0,0,0,0,0\rangle = \mp i(\omega_\rho m_\rho)^{1/2}\psi_{0,1,\pm1,0,0,0}(\vec{\rho},\vec{\lambda}), \tag{G9}$$

$$\langle\vec{\rho},\vec{\lambda}|\mathbf{p}_{\lambda,\pm}|0,1,m_{l_\rho},0,0,0\rangle = \mp i(\omega_\lambda m_\lambda)^{1/2}\psi_{0,1,m_{l_\rho},0,1,\pm1}(\vec{\rho},\vec{\lambda}), \tag{G10}$$

$$\langle\vec{\rho},\vec{\lambda}|\mathbf{p}_{\rho,\pm}|0,0,0,0,1,m_{l_\lambda}\rangle = \mp i(\omega_\rho m_\rho)^{1/2}\psi_{0,1,\pm1,0,1,m_{l_\lambda}}(\vec{\rho},\vec{\lambda}), \tag{G11}$$

$$\begin{aligned}\langle\vec{\rho},\vec{\lambda}|\mathbf{p}_{\rho,-}|0,1,1,0,0,0\rangle &= \frac{i(\omega_\rho m_\rho)^{1/2}}{\sqrt{3}}\psi_{0,2,0,0,0,0}(\vec{\rho},\vec{\lambda}) \\ &+i(\omega_\rho m_\rho)^{1/2}\psi_{0,0,0,0,0,0}(\vec{\rho},\vec{\lambda})+i\sqrt{\frac{2}{3}}(\omega_\rho m_\rho)^{1/2}\psi_{1,0,0,0,0,0}(\vec{\rho},\vec{\lambda}),\end{aligned} \tag{G12}$$

$$\langle\vec{\rho},\vec{\lambda}|\mathbf{p}_{\rho,-}|0,1,-1,0,0,0\rangle = i\sqrt{2}(\omega_\rho m_\rho)^{1/2}\psi_{0,2,-2,0,0,0}(\vec{\rho},\vec{\lambda}), \tag{G13}$$

$$\langle\vec{\rho},\vec{\lambda}|\mathbf{p}_{\rho,-}|0,1,0,0,0,0\rangle = i(\omega_\rho m_\rho)^{1/2}\psi_{0,2,-1,0,0,0}(\vec{\rho},\vec{\lambda}), \tag{G14}$$

$$\begin{aligned}\langle\vec{\rho},\vec{\lambda}|\mathbf{p}_{\lambda,-}|0,0,0,0,1,1\rangle &= \frac{i(\omega_\lambda m_\lambda)^{1/2}}{\sqrt{3}}\psi_{0,0,0,0,2,0}(\vec{\rho},\vec{\lambda}) \\ &+i(\omega_\lambda m_\lambda)^{1/2}\psi_{0,0,0,0,0,0}(\vec{\rho},\vec{\lambda})+i\sqrt{\frac{2}{3}}(\omega_\lambda m_\lambda)^{1/2}\psi_{0,0,0,1,0,0}(\vec{\rho},\vec{\lambda}),\end{aligned} \tag{G15}$$

$$\langle\vec{\rho},\vec{\lambda}|\mathbf{p}_{\lambda,-}|0,0,0,0,1,-1\rangle = i\sqrt{2}(\omega_\lambda m_\lambda)^{1/2}\psi_{0,0,0,0,2,-2}(\vec{\rho},\vec{\lambda}), \tag{G16}$$

$$\langle\vec{\rho},\vec{\lambda}|\mathbf{p}_{\lambda,-}|0,0,0,0,1,0\rangle = i(\omega_\lambda m_\lambda)^{1/2}\psi_{0,0,0,0,2,-1}(\vec{\rho},\vec{\lambda}). \tag{G17}$$

3. Matrix elements of $\hat{T}_{j,-}$ operators

We apply the previous formulas to evaluate the matrix elements of the $\hat{T}_{1,-}$, $\hat{T}_{2,-}$, and $\hat{T}_{3,-}$ operators in the harmonic oscillator basis. We begin by evaluating the matrix elements for the ρ states. For the operator $\hat{T}_{1,-}$ we obtain

$$\begin{aligned}\langle 0,0,0,0,0,0|\hat{T}_{1,-}|0,1,m_{l\rho},0,0,0\rangle &= \sqrt{\frac{1}{2}}\langle 0,0,0,0,0,0|\mathbf{p}_{\rho,-}\hat{U}_1+\hat{U}_1\mathbf{p}_{\rho,-}|0,1,1,0,0,0\rangle \\ &+\sqrt{\frac{1}{6}}\langle 0,0,0,0,0,0|\mathbf{p}_{\lambda,-}\hat{U}_1+\hat{U}_1\mathbf{p}_{\lambda,-}|0,1,1,0,0,0\rangle \\ &= \sqrt{\frac{1}{2}}i(\omega_\rho m_\rho)^{1/2}[\langle 0,1,1,0,0,0|\hat{U}_1|0,1,1,0,0,0\rangle \\ &+\sqrt{\frac{1}{3}}\langle 0,0,0,0,0,0|\hat{U}_1|0,2,0,0,0,0\rangle+\langle 0,0,0,0,0,0|\hat{U}_1|0,0,0,0,0,0\rangle \\ &+\sqrt{\frac{2}{3}}\langle 0,0,0,0,0,0|\hat{U}_1|1,0,0,0,0,0\rangle]+\sqrt{\frac{1}{6}}i(\omega_\lambda m_\lambda)^{1/2} \\ &\times[\langle 0,0,0,0,1,1|\hat{U}_1|0,1,1,0,0,0\rangle+\langle 0,0,0,0,0,0|\hat{U}_1|0,1,1,0,1,-1\rangle] \\ &= i\sqrt{2}(\omega_\rho m_\rho)^{1/2}\exp\left[\frac{-\mathrm{k}^2}{8}\left(\frac{1}{\omega_\rho m_\rho}+\frac{3m_b^2}{\omega_\lambda m_\lambda(2m_\rho+m_b)^2}\right)\right]\delta_{m_{l_\rho},1}. \end{aligned} \tag{G18}$$

For $\hat{T}_{2,-}$ we obtain

$$\begin{aligned}\langle 0,0,0,0,0,0|\hat{T}_{2,-}|0,1,m_{l\rho},0,0,0\rangle &= -\sqrt{\frac{1}{2}}\langle 0,0,0,0,0,0|\mathbf{p}_{\rho,-}\hat{U}_2+\hat{U}_2\mathbf{p}_{\rho,-}|0,1,1,0,0,0\rangle \\ &+\sqrt{\frac{1}{6}}\langle 0,0,0,0,0,0|\mathbf{p}_{\lambda,-}\hat{U}_2+\hat{U}_2\mathbf{p}_{\lambda,-}|0,1,1,0,0,0\rangle \\ &= -\sqrt{\frac{1}{2}}i(\omega_\rho m_\rho)^{1/2}[\langle 0,1,1,0,0,0|\hat{U}_2|0,1,1,0,0,0\rangle \\ &+\sqrt{\frac{1}{3}}\langle 0,0,0,0,0,0|\hat{U}_2|0,2,0,0,0,0\rangle+\langle 0,0,0,0,0,0|\hat{U}_2|0,0,0,0,0,0\rangle \\ &+\sqrt{\frac{2}{3}}\langle 0,0,0,0,0,0|\hat{U}_2|1,0,0,0,0,0\rangle]+\sqrt{\frac{1}{6}}i(\omega_\lambda m_\lambda)^{1/2} \\ &\times[\langle 0,0,0,0,1,1|\hat{U}_2|0,1,1,0,0,0\rangle+\langle 0,0,0,0,0,0|\hat{U}_2|0,1,1,0,1,-1\rangle] \\ &= -i\sqrt{2}(\omega_\rho m_\rho)^{1/2}\exp\left[\frac{-\mathrm{k}^2}{8}\left(\frac{1}{\omega_\rho m_\rho}+\frac{3m_b^2}{\omega_\lambda m_\lambda(2m_\rho+m_b)^2}\right)\right]\delta_{m_{l_\rho},1}. \end{aligned} \tag{G19}$$

Finally, for $\hat{T}_{3,-}$ we obtain

$$\begin{aligned}\langle 0,0,0,0,0,0|\hat{T}_{3,-}|0,1,m_{l\rho},0,0,0\rangle &= -\sqrt{\frac{2}{3}}\langle 0,0,0,0,0,0|\mathbf{p}_{\lambda,-}\hat{U}_3+\hat{U}_3\mathbf{p}_{\lambda,-}|0,1,1,0,0,0\rangle \\ &= -\sqrt{\frac{2}{3}}[i(\omega_\lambda m_\lambda)^{1/2}\langle 0,0,0,0,1,1|\hat{U}_3|0,1,1,0,0,0\rangle \\ &+i(\omega_\lambda m_\lambda)^{1/2}\langle 0,0,0,0,0,0|\hat{U}_3|0,1,1,0,1,-1\rangle] \\ &= 0. \end{aligned} \tag{G20}$$

Analog computations are performed for the λ states. For $\hat{T}_{1,-}$ we obtain

$$\begin{aligned}\langle 0,0,0,0,0,0|\hat{T}_{1,-}|0,0,0,0,0,1,m_{l_\lambda}\rangle &= \sqrt{\frac{1}{6}}\langle 0,0,0,0,0,0|\mathbf{p}_{\lambda,-}\hat{U}_1+\hat{U}_1\mathbf{p}_{\lambda,-}|0,0,0,0,1,1\rangle\\ &+\sqrt{\frac{1}{2}}\langle 0,0,0,0,0,0|\mathbf{p}_{\rho,-}\hat{U}_1+\hat{U}_1\mathbf{p}_{\rho,-}|0,0,0,0,1,1\rangle\\ &=\sqrt{\frac{1}{6}}i(\omega_\lambda m_\lambda)^{1/2}[\langle 0,0,0,0,1,1|\hat{U}_1|0,0,0,0,1,1\rangle\\ &+\sqrt{\frac{1}{3}}\langle 0,0,0,0,0,0|\hat{U}_1|0,0,0,0,2,0\rangle+\langle 0,0,0,0,0,0|\hat{U}_1|0,0,0,0,0,0\rangle\\ &+\sqrt{\frac{2}{3}}\langle 0,0,0,0,0,0|\hat{U}_1|0,0,0,1,0,0\rangle]+\sqrt{\frac{1}{2}}i(\omega_\rho m_\rho)^{1/2}\\ &\times[\langle 0,1,1,0,0,0|\hat{U}_1|0,0,0,0,1,1\rangle+\langle 0,0,0,0,0,0|\hat{U}_1|0,1,-1,0,1,1\rangle]\\ &=i\sqrt{\frac{2}{3}}(\omega_\lambda m_\lambda)^{1/2}\exp\left[\frac{-\mathrm{k}^2}{8}\left(\frac{1}{\omega_\rho m_\rho}+\frac{3m_b^2}{\omega_\lambda m_\lambda(2m_\rho+m_b)^2}\right)\right]\delta_{m_{l_\lambda},1}.\end{aligned}\tag{G21}$$

Next, for $\hat{T}_{2,-}$ we obtain

$$\begin{aligned}\langle 0,0,0,0,0,0|\hat{T}_{2,-}|0,0,0,0,0,1,m_{l_\lambda}\rangle &= \sqrt{\frac{1}{6}}\langle 0,0,0,0,0,0|\mathbf{p}_{\lambda,-}\hat{U}_2+\hat{U}_2\mathbf{p}_{\lambda,-}|0,0,0,0,1,1\rangle\\ &-\sqrt{\frac{1}{2}}\langle 0,0,0,0,0,0|\mathbf{p}_{\rho,-}\hat{U}_2+\hat{U}_2\mathbf{p}_{\rho,-}|0,0,0,0,1,1\rangle\\ &=\sqrt{\frac{1}{6}}i(\omega_\lambda m_\lambda)^{1/2}[\langle 0,0,0,0,1,1|\hat{U}_2|0,0,0,0,1,1\rangle\\ &+\sqrt{\frac{1}{3}}\langle 0,0,0,0,0,0|\hat{U}_2|0,0,0,0,2,0\rangle+\langle 0,0,0,0,0,0|\hat{U}_2|0,0,0,0,0,0\rangle\\ &+\sqrt{\frac{2}{3}}\langle 0,0,0,0,0,0|\hat{U}_2|0,0,0,1,0,0\rangle]-\sqrt{\frac{1}{2}}i(\omega_\rho m_\rho)^{1/2}\\ &\times[\langle 0,1,1,0,0,0|\hat{U}_2|0,0,0,0,1,1\rangle+\langle 0,0,0,0,0,0|\hat{U}_2|0,1,-1,0,1,1\rangle]\\ &=i\sqrt{\frac{2}{3}}(\omega_\lambda m_\lambda)^{1/2}\exp\left[\frac{-\mathrm{k}^2}{8}\left(\frac{1}{\omega_\rho m_\rho}+\frac{3m_b^2}{\omega_\lambda m_\lambda(2m_\rho+m_b)^2}\right)\right]\delta_{m_{l_\lambda},1}.\end{aligned}\tag{G22}$$

Finally, for $\hat{T}_{3,-}$ we obtain

$$\begin{aligned}\langle 0,0,0,0,0,0|\hat{T}_{3,-}|0,0,0,0,0,1,m_{l_\lambda}\rangle &= -\sqrt{\frac{2}{3}}\langle 0,0,0,0,0,0|\mathbf{p}_{\lambda,-}\hat{U}_3+\hat{U}_3\mathbf{p}_{\lambda,-}|0,0,0,0,1,1\rangle\\ &=-\sqrt{\frac{2}{3}}i(\omega_\lambda m_\lambda)^{1/2}[\langle 0,0,0,0,1,1|\hat{U}_3|0,0,0,0,1,1\rangle\\ &+\frac{1}{\sqrt{3}}\langle 0,0,0,0,0,0|\hat{U}_3|0,0,0,0,2,0\rangle+\langle 0,0,0,0,0,0|\hat{U}_3|0,0,0,0,0,0\rangle\\ &+\sqrt{\frac{2}{3}}\langle 0,0,0,0,0,0|\hat{U}_3|0,0,0,1,0,0\rangle]\\ &=-2i\sqrt{\frac{2}{3}}(\omega_\lambda m_\lambda)^{1/2}\exp\left[\frac{-3\mathrm{k}^2m_\rho^2}{2\omega_\lambda m_\lambda(2m_\rho+m_b)^2}\right]\delta_{m_{l_\lambda},1}.\end{aligned}\tag{G23}$$

[1] R. L. Workman *et al.* (Particle Data Group), Prog. Theor. Exp. Phys. **2022**, 083C01 (2022).
[2] M. Basile *et al.*, Lett. Nuovo Cimento **31**, 97 (1981).
[3] G. Bari *et al.*, Nuovo Cimento Soc. Ital. Fis. **104A**, 1787 (1991).
[4] C. Albajar *et al.* (UA1 Collaboration), Phys. Lett. B **273**, 540 (1991).
[5] V. Abazov *et al.* (D0 Collaboration), Phys. Rev. Lett. **99**, 052001 (2007).
[6] T. Aaltonen *et al.* (CDF Collaboration), Phys. Rev. Lett. **99**, 052002 (2007).
[7] T. Aaltonen *et al.* (CDF Collaboration), Phys. Rev. Lett. **99**, 202001 (2007).
[8] T. Aaltonen *et al.* (CDF Collaboration), Phys. Rev. D **85**, 092011 (2012).
[9] V. Abazov *et al.* (D0 Collaboration), Phys. Rev. Lett. **101**, 232002 (2008).
[10] T. Aaltonen *et al.* (CDF Collaboration), Phys. Rev. D **80**, 072003 (2009).
[11] T. Aaltonen *et al.* (CDF Collaboration), Phys. Rev. Lett. **107**, 102001 (2011).
[12] S. Chatrchyan *et al.* (CMS Collaboration), Phys. Rev. Lett. **108**, 252002 (2012).
[13] R. Aaij *et al.* (LHCb Collaboration), Phys. Rev. Lett. **109**, 172003 (2012).
[14] T. A. Aaltonen *et al.* (CDF Collaboration), Phys. Rev. D **88**, 071101 (2013).
[15] R. Aaij *et al.* (LHCb Collaboration), Phys. Rev. Lett. **114**, 062004 (2015).
[16] R. Aaij *et al.* (LHCb Collaboration), Phys. Rev. Lett. **121**, 072002 (2018).
[17] R. Aaij *et al.* (LHCb Collaboration), Phys. Rev. Lett. **122**, 012001 (2019).
[18] R. Aaij *et al.* (LHCb Collaboration), Phys. Rev. Lett. **123**, 152001 (2019).
[19] R. Aaij *et al.* (LHCb Collaboration), Phys. Rev. Lett. **124**, 082002 (2020).
[20] A. M. Sirunyan *et al.* (CMS Collaboration), Phys. Lett. B **803**, 135345 (2020).
[21] R. Aaij *et al.* (LHCb Collaboration), J. High Energy Phys. 06 (2020) 136.
[22] A. M. Sirunyan *et al.* (CMS Collaboration), Phys. Rev. Lett. **126**, 252003 (2021).
[23] R. Aaij *et al.* (LHCb Collaboration), Phys. Rev. Lett. **128**, 162001 (2022).
[24] R. Aaij *et al.* (LHCb Collaboration), Phys. Rev. Lett. **131**, 171901 (2023).
[25] S. Capstick and N. Isgur, AIP Conf. Proc. **132**, 267 (1985).
[26] S. Capstick and N. Isgur, Phys. Rev. D **34**, 2809 (1986).
[27] E. Bagan, M. Chabab, H. G. Dosch, and S. Narison, Phys. Lett. B **287**, 176 (1992).
[28] R. Roncaglia, D. B. Lichtenberg, and E. Predazzi, Phys. Rev. D **52**, 1722 (1995).
[29] B. Silvestre-Brac, Few-Body Syst. **20**, 1 (1996).
[30] K. C. Bowler, R. D. Kenway, O. Oliveira, D. G. Richards, P. Ueberholz, L. Lellouch, J. Nieves, C. T. Sachrajda, N. Stella, and H. Wittig (UKQCD Collaboration), Phys. Rev. D **54**, 3619 (1996).
[31] E. E. Jenkins, Phys. Rev. D **54**, 4515 (1996).
[32] N. Mathur, R. Lewis, and R. M. Woloshyn, Phys. Rev. D **66**, 014502 (2002).
[33] C. Albertus, J. E. Amaro, E. Hernandez, and J. Nieves, Nucl. Phys. **A740**, 333 (2004).
[34] H. Garcilazo, J. Vijande, and A. Valcarce, J. Phys. G **34**, 961 (2007).
[35] A. Valcarce, H. Garcilazo, and J. Vijande, Eur. Phys. J. A **37**, 217 (2008).
[36] G. Yang, J. Ping, and J. Segovia, Few-Body Syst. **59**, 113 (2018).
[37] D. Ebert, R. N. Faustov, and V. O. Galkin, Phys. Lett. B **659**, 612 (2008).
[38] D. Ebert, R. N. Faustov, and V. O. Galkin, Phys. Rev. D **84**, 014025 (2011).
[39] W. Roberts and M. Pervin, Int. J. Mod. Phys. A **23**, 2817 (2008).
[40] M. Karliner, B. Keren-Zur, H. J. Lipkin, and J. L. Rosner, Ann. Phys. (Amsterdam) **324**, 2 (2009).
[41] T. Yoshida, E. Hiyama, A. Hosaka, M. Oka, and K. Sadato, Phys. Rev. D **92**, 114029 (2015).
[42] K. W. Wei, B. Chen, N. Liu, Q. Q. Wang, and X. H. Guo, Phys. Rev. D **95**, 116005 (2017).
[43] M. Ferraris, M. M. Giannini, M. Pizzo, E. Santopinto, and L. Tiator, Phys. Lett. B **364**, 231 (1995).
[44] E. Santopinto, F. Iachello, and M. M. Giannini, Nucl. Phys. **A623**, 100C (1997).
[45] E. Santopinto, F. Iachello, and M. M. Giannini, Eur. Phys. J. A **1**, 307 (1998).
[46] M. M. Giannini and E. Santopinto, Chin. J. Phys. (Taipei) **53**, 020301 (2015).
[47] H. Mutuk, Eur. Phys. J. A **56**, 146 (2020).
[48] H. X. Chen, Q. Mao, A. Hosaka, X. Liu, and S. L. Zhu, Phys. Rev. D **94**, 114016 (2016).
[49] Z. G. Wang, Eur. Phys. J. A **47**, 81 (2011).
[50] X. Liu, H. X. Chen, Y. R. Liu, A. Hosaka, and S. L. Zhu, Phys. Rev. D **77**, 014031 (2008).
[51] Q. Mao, H. X. Chen, W. Chen, A. Hosaka, X. Liu, and S. L. Zhu, Phys. Rev. D **92**, 114007 (2015).
[52] Guo-Liang Yu, Zhi-Gang Wang, and Xiu-Wu Wang, Chin. Phys. C **46**, 093102 (2022).
[53] L. X. Gutiérrez-Guerrero, A. Bashir, M. A. Bedolla, and E. Santopinto, Phys. Rev. D **100**, 114032 (2019).
[54] P. Hasenfratz, R. R. Horgan, J. Kuti, and J. M. Richard, Phys. Lett. B **94**, 401 (1980).
[55] Y. Kim, E. Hiyama, M. Oka, and K. Suzuki, Phys. Rev. D **102**, 014004 (2020).
[56] Y. Kim, Y. R. Liu, M. Oka, and K. Suzuki, Phys. Rev. D **104**, 054012 (2021).
[57] Y. Ma, L. Meng, Y. K. Chen, and S. L. Zhu, Phys. Rev. D **107**, 054035 (2023).
[58] J. Vijande, A. Valcarce, and H. Garcilazo, Phys. Rev. D **90**, 094004 (2014).
[59] P. Mohanta and S. Basak, Phys. Rev. D **101**, 094503 (2020).
[60] E. Klempt and J. M. Richard, Rev. Mod. Phys. **82**, 1095 (2010).
[61] J. G. Korner, M. Kramer, and D. Pirjol, Prog. Part. Nucl. Phys. **33**, 787 (1994).
[62] H. X. Chen, W. Chen, X. Liu, Y. R. Liu, and S. L. Zhu, Rep. Prog. Phys. **80**, 076201 (2017).

[63] V. Crede and W. Roberts, Rep. Prog. Phys. **76**, 076301 (2013).
[64] Y. S. Amhis *et al.* (HFLAV Collaboration), Eur. Phys. J. C **81**, 226 (2021).
[65] H. X. Chen, W. Chen, X. Liu, Y. R. Liu, and S. L. Zhu, Rep. Prog. Phys. **86**, 026201 (2023).
[66] A. Limphirat, C. Kobdaj, P. Suebka, and Y. Yan, Phys. Rev. C **82**, 055201 (2010).
[67] K. L. Wang, Y. X. Yao, X. H. Zhong, and Q. Zhao, Phys. Rev. D **96**, 116016 (2017).
[68] Y. X. Yao, K. L. Wang, and X. H. Zhong, Phys. Rev. D **98**, 076015 (2018).
[69] W. J. Wang, L. Y. Xiao, and X. H. Zhong, Phys. Rev. D **106**, 074020 (2022).
[70] L. Y. Xiao and X. H. Zhong, Phys. Rev. D **102**, 014009 (2020).
[71] W. Liang and Q. F. Lü, Eur. Phys. J. C **80**, 198 (2020).
[72] W. Liang and Q. F. Lü, Eur. Phys. J. C **80**, 690 (2020).
[73] H. Z. He, W. Liang, Q. F. Lü, and Y. B. Dong, Sci. China Phys. Mech. Astron. **64**, 261012 (2021).
[74] Q. F. Lü and X. H. Zhong, Phys. Rev. D **101**, 014017 (2020).
[75] B. Chen, K. W. Wei, X. Liu, and A. Zhang, Phys. Rev. D **98**, 031502 (2018).
[76] B. Chen and X. Liu, Phys. Rev. D **98**, 074032 (2018).
[77] W. J. Wang, Y. H. Zhou, L. Y. Xiao, and X. H. Zhong, Phys. Rev. D **105**, 074008 (2022).
[78] Y. H. Zhou, W. J. Wang, L. Y. Xiao, and X. H. Zhong, Phys. Rev. D **108**, 094032 (2023).
[79] C. W. Hwang, Eur. Phys. J. C **50**, 793 (2007).
[80] E. Hernandez and J. Nieves, Phys. Rev. D **84**, 057902 (2011).
[81] H. X. Chen, E. L. Cui, A. Hosaka, Q. Mao, and H. M. Yang, Eur. Phys. J. C **80**, 256 (2020).
[82] Y. Kim, M. Oka, D. Suenaga, and K. Suzuki, Phys. Rev. D **107**, 074015 (2023).
[83] R. Kokoski and N. Isgur, Phys. Rev. D **35**, 907 (1987).
[84] S. L. Zhu and Y. B. Dai, Phys. Rev. D **59**, 114015 (1999).
[85] Z. G. Wang, Eur. Phys. J. A **44**, 105 (2010).
[86] Z. G. Wang, Phys. Rev. D **81**, 036002 (2010).
[87] T. M. Aliev, K. Azizi, and H. Sundu, Eur. Phys. J. C **75**, 14 (2015).
[88] T. M. Aliev, K. Azizi, and A. Ozpineci, Phys. Rev. D **79**, 056005 (2009).
[89] T. M. Aliev, T. Barakat, and M. Savcı, Phys. Rev. D **93**, 056007 (2016).
[90] T. M. Aliev, M. Savcı, and V. S. Zamiralov, Mod. Phys. Lett. A **27**, 1250054 (2012).
[91] M. C. Banuls, A. Pich, and I. Scimemi, Phys. Rev. D **61**, 094009 (2000).
[92] H. Y. Cheng, C. Y. Cheung, G. L. Lin, Y. C. Lin, T. M. Yan, and H. L. Yu, Phys. Rev. D **47**, 1030 (1993).
[93] N. Jiang, X. L. Chen, and S. L. Zhu, Phys. Rev. D **92**, 054017 (2015).
[94] S. Tawfiq, J. G. Korner, and P. J. O'Donnell, Phys. Rev. D **63**, 034005 (2001).
[95] A. Bernotas and V. Šimonis, Phys. Rev. D **87**, 074016 (2013).
[96] C. K. Chow, Phys. Rev. D **54**, 3374 (1996).
[97] M. A. Ivanov, J. G. Korner, and V. E. Lyubovitskij, Phys. Lett. B **448**, 143 (1999).
[98] E. Santopinto, A. Giachino, J. Ferretti, H. García-Tecocoatzi, M. A. Bedolla, R. Bijker, and E. Ortiz-Pacheco, Eur. Phys. J. C **79**, 1012 (2019).
[99] R. Aaij *et al.* (LHCb Collaboration), Phys. Rev. Lett. **118**, 182001 (2017).
[100] R. Bijker, H. García-Tecocoatzi, A. Giachino, E. Ortiz-Pacheco, and E. Santopinto, Phys. Rev. D **105**, 074029 (2022).
[101] R. Aaij *et al.* (LHCb Collaboration), Phys. Rev. Lett. **124**, 222001 (2020).
[102] H. Garcia-Tecocoatzi, A. Giachino, J. Li, A. Ramirez-Morales, and E. Santopinto, Phys. Rev. D **107**, 034031 (2023).
[103] R. Aaij *et al.* (LHCb Collaboration), Phys. Rev. Lett. **131**, 131902 (2023).
[104] E. Ortiz-Pacheco and R. Bijker, Phys. Rev. D **108**, 054014 (2023).
[105] B. Efron and R. J. Tibshirani, *An Introduction to the Bootstrap*, Monographs on Statistics Applied Probability (Chapman and Hall, London, 1993), https://cds.cern.ch/record/526679.
[106] E. Santopinto, Phys. Rev. C **72**, 022201 (2005).
[107] D. Molina, M. De Sanctis, C. Fernández-Ramírez, and E. Santopinto, Eur. Phys. J. C **80**, 526 (2020).
[108] F. James and M. Roos, Comput. Phys. Commun. **10**, 343 (1975).
[109] C. R. Harris *et al.*, Nature (London) **585**, 357 (2020).
[110] J. Ferretti and E. Santopinto, Phys. Rev. D **97**, 114020 (2018).
[111] L. Micu, Nucl. Phys. **B10**, 521 (1969).
[112] A. Le Yaouanc, L. Oliver, O. Pene, and J. C. Raynal, Phys. Rev. D **8**, 2223 (1973).
[113] W. Roberts and B. Silvestre-Brac, Few-Body Syst. **11**, 171 (1992).
[114] R. Bijker, J. Ferretti, G. Galatà, H. García-Tecocoatzi, and E. Santopinto, Phys. Rev. D **94**, 074040 (2016).
[115] C. Chen, X. L. Chen, X. Liu, W. Z. Deng, and S. L. Zhu, Phys. Rev. D **75**, 094017 (2007).
[116] H. G. Blundell and S. Godfrey, Phys. Rev. D **53**, 3700 (1996).
[117] M. Artuso *et al.* (CLEO Collaboration), Phys. Rev. Lett. **86**, 4479 (2001).
[118] K. W. Edwards *et al.* (CLEO Collaboration), Phys. Rev. Lett. **74**, 3331 (1995).
[119] N. Isgur and M. B. Wise, Phys. Lett. B **232**, 113 (1989).
[120] N. Isgur and M. B. Wise, Phys. Lett. B **237**, 527 (1990).
[121] N. Isgur and M. B. Wise, Phys. Rev. Lett. **66**, 1130 (1991).
[122] S. Yasui, Phys. Rev. D **91**, 014031 (2015).
[123] V. Baru, C. Hanhart, Y. S. Kalashnikova, A. E. Kudryavtsev, and A. V. Nefediev, Eur. Phys. J. A **44**, 93 (2010).
[124] T. Barnes and E. S. Swanson, Phys. Rev. C **77**, 055206 (2008).
[125] J. X. Lu, Y. Zhou, H. X. Chen, J. J. Xie, and L. S. Geng, Phys. Rev. D **92**, 014036 (2015).
[126] W. H. Liang, C. W. Xiao, and E. Oset, Phys. Rev. D **89**, 054023 (2014).
[127] W. H. Liang and E. Oset, Phys. Rev. D **101**, 054033 (2020).

[128] Q. X. Yu, R. Pavao, V. R. Debastiani, and E. Oset, Eur. Phys. J. C **79**, 167 (2019).
[129] Y. Huang, C. j. Xiao, L. S. Geng, and J. He, Phys. Rev. D **99**, 014008 (2019).
[130] W. H. Liang, J. M. Dias, V. R. Debastiani, and E. Oset, Nucl. Phys. **B930**, 524 (2018).
[131] C. Garcia-Recio, J. Nieves, O. Romanets, L. L. Salcedo, and L. Tolos, Phys. Rev. D **87**, 034032 (2013).
[132] M. R. Pennington and D. J. Wilson, Phys. Rev. D **76**, 077502 (2007).
[133] J. Ferretti, G. Galatà, and E. Santopinto, Phys. Rev. C **88**, 015207 (2013).
[134] E. Cincioglu, J. Nieves, A. Ozpineci, and A. U. Yilmazer, Eur. Phys. J. C **76**, 576 (2016).
[135] J. Nieves, A. Feijoo, M. Albaladejo, and M. L. Du, Prog. Part. Nucl. Phys. **137**, 104118 (2024).